SERI/TP-211-3904
UC Category: 271
DE90000360

Basic Studies of III-V High Efficiency Cell Components

Annual Subcontract Report
15 August 1988 - 14 August 1989

M.S. Lundstrom
M.R. Melloch
R.F. Pierret
M.S. Carpenter
H.L. Chuang
A. Keshavarzi
M.E. Klausmeier-Brown
G.B. Lush
J.M. Morgan
T.B. Stellwag
School of Electrical Engineering
Purdue University
West Lafayette, Indiana

July 1990

SERI Technical Monitor: C. Leboeuf

Prepared under Subcontract No. XL-5-05018-1

Solar Energy Research Institute
A Division of Midwest Research Institute

1617 Cole Boulevard
Golden, Colorado 80401-3393

Prepared for the
U.S. Department of Energy
Contract No. DE-AC02-83CH10093

This publication was reproduced from the best available camera-ready copy submitted by the subcontractor and received no editorial review at SERI.

NOTICE

This report was prepared as an account of work sponsored by an agency of the United States government. Neither the United States government nor any agency thereof, nor any of their employees, makes any warranty, express or implied, or assumes any legal liability or responsibility for the accuracy, completeness, or usefulness of any information, apparatus, product, or process disclosed, or represents that its use would not infringe privately owned rights. Reference herein to any specific commercial product, process, or service by trade name, trademark, manufacturer, or otherwise does not necessarily constitute or imply its endorsement, recommendation, or favoring by the United States government or any agency thereof. The views and opinions of authors expressed herein do not necessarily state or reflect those of the United States government or any agency thereof.

Printed in the United States of America
Available from:
National Technical Information Service
U.S. Department of Commerce
5285 Port Royal Road
Springfield, VA 22161

Price: Microfiche A01
Printed Copy A06

Codes are used for pricing all publications. The code is determined by the number of pages in the publication. Information pertaining to the pricing codes can be found in the current issue of the following publications which are generally available in most libraries: *Energy Research Abstracts (ERA)*; *Government Reports Announcements* and Index (*GRA* and I); *Scientific and Technical Abstract Reports (STAR)*; and publication NTIS-PR-360 available from NTIS at the above address.

PREFACE

This project's objective is to improve our fundamental understanding of the generation, recombination, and transport of carriers within III-V homo- and heterostructures. The research consists of fabricating and characterizing solar cell "building blocks" such as junctions and heterojunctions as well as basic measurements of material parameters. A significant effort is also being directed at characterizing loss mechanisms in high-quality, III-V solar cells fabricated in industrial research laboratories throughout the United States. The project's goal is to use our understanding of the device physics of high-efficiency cell components to maximize cell efficiency. A related goal is the demonstration of new cell structures fabricated by molecular beam epitaxy (MBE). The development of measurement techniques and characterization methodologies is also a project objective. We expect that the insight into III-V device physics occurring during the course of this work will help to identify paths towards higher efficiency III-V cells.

This report describes our progress during the fourth year of the project. The past year's efforts centered on completing studies of heavy doping effects in p^+-GaAs and assessing the importance of similar effects in n^+-GaAs, and at continuing research on characterizing, controlling, and passivating perimeter recombination currents. We also initiated work to identify the dominant loss mechanisms in $Al_{0.2}Ga_{0.8}As$ solar cells and brought on-line a new MBE growth facility and demonstrated the high-quality of the films by fabricating, with assistance from Spire Corporation, 23.8% 1-sun solar cells.

Our work has benefited greatly from interactions with industrial researchers. We owe special thanks to Steve Tobin, Stan Vernon, and their colleagues at Spire Corporation for providing $Al_{0.2}Ga_{0.8}As$ films and cells for our basic studies and for fabricating high-efficiency cells from our MBE-grown films. The work described in this report was supported by the Solar Energy Research Institute. Cecile Lebouef and John Benner of SERI have provided the long term guidance and encouragement that has made this work possible. Our research also benefited by collaborations with two graduate student researchers not supported by SERI. H.L Chuang was supported by the Indiana Corporation for Science and and Technology and M.E. Klausmeier-Brown by a fellowship from the Eastman Kodak Company.

SUMMARY

Project Overview

Motivation

The efficiencies of both single and multiple junction III-V solar cells continue to increase rapidly, and, although much of the progress now occurring is due to improving material quality, it is becoming increasingly important to carefully examine the internal device physics of solar cells so that cell designs can be tailored to the material constraints. The need for a sound understanding of internal device physics is clearly illustrated by Stanford University's research on point contact silicon cells in which a new design approach, specifically tailored to the dominant loss mechanisms in crystalline silicon cells, led to a marked increase in cell efficiency. Although there is no assurance that the point contact design would similarly benefit III-V cells, the example does illustrate the benefits of careful cell design guided by detailed knowledge of device physics. Our research consists of basic studies directed at expanding the device physics knowledge base for III-V solar cells and of applying this evolving knowledge in order to explore new approaches for enhancing solar cell efficiency. While these basic studies are contributing to the steady progress of III-V cell efficiencies, they may at the same time lead to innovative new approaches for achieving substantial efficiency gains.

Project Objectives

Our research is *device-directed*; it begins by characterizing state-of-the-art, high-efficiency solar cells and quantifying their internal loss mechanisms. One project objective, therefore, is the development of characterization techniques and methodologies for identifying and analyzing specific loss mechanisms in modern, crystalline solar cells. Based on the cell characterization results, specific research objectives are then prioritized. During previous years, we focused on crystalline GaAs cells; this year's work marks a transition from GaAs to $Al_xGa_{1-x}As$. The ternary, $Al_xGa_{1-x}As$, was selected not because we are convinced that it is the optimum photovoltaic material but, rather, because it serves as a good model III-V semiconductor in which to explore the inter-relationships of material quality, device physics, and device design. At the $x = 0$ compositional point, the material is GaAs, which is becoming a very well-understood, well-characterized semiconductor. As the Al mole fraction increases, the material properties, device physics, and design issues, change profoundly. Basic studies on this material system should provide device characterization, analysis, and design approaches that are applicable to all crystalline III-V solar cells.

The general objectives of the project can be broadly stated as

- To examine the device physics of minority carrier injection, transport, and recombination in III-V solar cells
- To identify and quantify loss mechanisms in state-of-the-art, high-efficiency, III-V, crystalline solar cells
- To develop new techniques and approaches for characterizing solar cells and for measuring basic parameters
- To explore new approaches for enhancing III-V solar cell efficiency

For the past year, our specific project objectives have been:

- Heavy doping studies in p^+ and n^+ GaAs
- Studies of surface and perimeter recombination
- Loss analysis of MOCVD- and MBE-grown $Al_{0.2}Ga_{0.8}As$ solar cells
- Turn-on and characterization of a Varian GEN II MBE system and demonstration of photovoltaic quality GaAs.

The heavy doping work continued our group's previous work on examining the band structure modifications associated with heavy impurity doping and at examining the implications of such effects on solar cell performance. Our group's previous work has also established the importance of perimeter recombination currents — even in quite large (= 2 cm × 2 cm) cells. The surface and perimeter recombination studies consist of developing techniques for characterizing perimeter recombination, studies to relate perimeter recombination to the conditions of the GaAs surface, and exploration of techniques for passivating the surface and perimeter by chemical treatments. The loss analysis of $Al_{0.2}Ga_{0.8}As$ cells is directed at establishing the dominant loss mechanisms in this material in order to prioritize future research. Since our research makes use of MBE-grown films, it is also important to relate these studies to the more widely-used MOCVD-grown films. Finally, because an important objective of ours is to explore new approaches, it was necessary to establish an improved MBE growth facility and to establish the films it produced were of photovoltaic quality.

Relation to DOE Mission

One component of the national photovoltaic program is directed at developing concentrator photovoltaic systems based on high-efficiency, crystalline solar cells. It is generally felt that efficiencies must exceed 35% in the long term if this approach is to become economically viable. The III-V semiconductors are particularly interesting for such applications. GaAs, for example is a relatively mature photovoltaic material that seems certain to produce solar cells exceeding 30% efficiency. Various III-V heterostructure combinations make possible multiple junction solar cells with the potential for achieving conversion efficiencies well above 35%. Although the number of III-V semiconductors under investigation is quite large, our work, which focuses on the technologically important GaAs/AlGaAs system, should be broadly applicable. By centering our work on a relatively mature (in comparison with other III-V's, that is) material system, we ensure that we are dealing with basic physical effects central to III-V cell design — not with the difficult to control material quality issues that arise with immature technologies. Since the various III-V semiconductors have much in common, the basic findings of our work should provide useful guidelines for III-V crystalline research in general.

Relation to Other DOE-Funded Research

Because many of the design issues for III-V cells are similar, this research is broadly applicable to much DOE-funded III-V cell research. At the same time, however, we've developed some specific relationships with other DOE-funded programs. We've been fortunate to collaborate with researchers at Spire Corporation on GaAs, and more recently on AlGaAs, solar cells. This collaboration has included work on heteroface recombination, heavy doping effects, perimeter recombination, and on heterojunction back surface fields. The work has served to ensure that our efforts were directed at issues of general concern and not on issues specific to our MBE-grown material. It has at the same time provided useful basic information that assisted Spire's continuing success in increasing GaAs cell efficiencies and has resulted in a number of joint publications.

A more recent relationship has developed with Dr. Richard Arhenkiel and his laboratory at SERI. This work centers on using Dr. Ahrenkiel's time-of-flight (TOF) measurement to characterize minority carrier mobilities in GaAs. Because the electron mobility in GaAs is so high, the electrical response is rapid. The microwave techniques we're employing to package our solar cell test structures, should significantly extend the range of the TOF measurement. There has also been a relatively recent appreciation of the role of so-called photon recycling effects in these measurements. A detailed computer simulation of the coupled, minority carrier - photon diffusion process will enable us to quantitatively assess the effects of photon recycling on the TOF measurement for the first time.

Project History

Initial work on this project, which began in 1985, was directed at the general objectives as stated above. The first year's efforts were largely directed at establishing an MBE film growth facility and on developing procedures for electrically characterizing solar cells and test structures. Our first MBE growth facility employed a first-generation Perkin-Elmer machine, but films are now grown with a Varian GEN II system.

Beginning at the second year, our efforts have centered on conducting basic studies. The second year's efforts were directed at identifying loss mechanisms in high-quality GaAs cells supplied by Spire Corporation. This work identifyed a need for improving the heteroface recombination velocity. (Subsequent work by Spire researchers has produced high-quality interfaces with correspondingly high ($\simeq$ 100%) internal quantum efficiencies.) During the second year, we also conducted an experiment, using our own MBE-grown films, which established the importance of heavy doping effects on GaAs solar cells, and we also demonstrated that a heterojunction back-surface-field could, apparently by gettering impurities, provide benefits quite distinct from their minority carrier confining properties. Heterojunction back-surface-fields have subsequently become a standard feature in the Spire cell design. Finally, application of current DLTS for characterizing large area solar cells was also demonstrated during the second year of the project.

The third year's work centered on detailed characterization of electron injection in p^+-GaAs using MOCVD-grown films supplied by Spire Corporation. Though limited to doping densities below 10^{19} cm^{-3}, the work demonstrated for the first time that heavy doping effects have important consequences for GaAs solar cells. The role of perimeter recombination on solar cell performance was also addressed during the third year, and a new chemical treatment for passivating surfaces was devised and demonstrated.

The fourth year's work extends, and in some cases completes, work initiated in earlier years and initiates new research directed at $Al_xGa_{1-x}As$. The fourth year's activities are the subject of this report and are surveyed below.

Scientific and Technical Activities: 1988 - 1989

During the past year, our activities have focused on: 1) completing work on heavy doping effects in p^+-GaAs, 2) assessing the importance of analogous effects in n^+-GaAs, 3) continuing efforts to characterize and control perimeter recombination, 4) work to understand and further develop chemical passivation treatments, 5) conducting a baseline study of loss mechanisms in $Al_{0.2}Ga_{0.8}As$ solar cells, and 6) bringing on-line a new MBE growth facility. Work on these tasks is described in this report and in the reprints appended to it. Key results include: 1) extension of bandgap narrowing measurements in p^+-GaAs to one order of magnitude higher in doping, 2) demonstration that effective bandgap shrinkage is not an important factor in n^+-GaAs, 3) observation of an orientation-dependence to perimeter recombination, 4) demonstration that

losses in both MOCVD- and MBE-grown $Al_{0.2}Ga_{0.8}As$ appear to be dominated by similar defects, and 5) successful turn-on and operation of a new MBE growth facility and the subsequent demonstration of GaAs solar cells with 23.8% conversion efficiency under 1-sun, AM1.5 global operating conditions.

Overview of the Report

Many of last year's research activities are described in the various chapters of this report; others are described in the reprints included in the Appendix. The report begins with two chapters describing recent work on bandgap narrowing in p^+-GaAs. An experimental technique, based on using a homojunction bipolar transistor, was developed to measure the product, $n_{ie}^2 D_n$ in very heavily doped GaAs. The experimental technique is described in **Chapter 1**, and the results are presented and discussed in **Chapter 2**. (Papers based on Chapters 1 and 2 have been submitted for publication.) Although our understanding of the electronic properties of heavily doped GaAs is far from complete, it now seems sufficient for solar cell design. Our future work in this area will focus on basic physical mechanisms and on the implications for AlGaAs/GaAs bipolar transistors. This work will continue to benefit the solar cell community but will be supported by the National Science Foundation.

Gallium arsenide films now being grown in our Varian GEN II MBE are quite comparable in quality to high-quality, MOCVD-grown GaAs. In **Chapter 3**, we describe our experimental work, conducted in collaboration with Spire Corporation, to compare high-quality MOCVD- and MBE-grown films for photovoltaic applications. A paper based on the results in Chapter 3 has been written and submitted for publication.

Chapter 4 describes our first work to examine loss mechanisms in $Al_{0.2}Ga_{0.8}As$ solar cells; it compares an MOCVD-grown film with an MBE film targeted to be identical. The work is motivated by the possible use of AlGaAs for top cell applications in multi-junction cells and because AlGaAs will serve as a model semiconductor for future basic studies of III-V cells. This chapter is a written version of a poster presented at the 9th Photovoltaic Advanced Research and Development Review Meeting in Golden in May of 1989. A shorter version of Chapter 4, without some of the figures and the discussion on oval defects, has been submitted to *Solar Cells*.

Some of the variations in III-V solar cell performance that occur as cells age is a result of the aging perimeters and their associated recombination losses. Previous work by our group has demonstrated that perimeter recombination has a significant influence on the one-sun performance of GaAs cells and that it is often the dominant effect in small area diodes utilized for diagnostics. In **Chapter 5**, we describe a recent experiment in which a strong orientation dependence to perimeter recombination was noted. Perimeter recombination is especially important for relatively small area test devices commonly used for diagnostics or for solar cell development. The strong variation in results that occurs as the orientation varies, must be accounted for in order to properly interpret experiments.

The oxides that form on bare GaAs surfaces produce large surface state densities that often dominate the electrical performance of devices. Recent work by our group and others has demonstrated that sulfide chemical treatments can reduce recombination losses in solar cells, increase the gain of bipolar transistors, and modify the barrier height of metal-GaAs contacts. It is therefore, of great technical importance to determine the exact nature of the sulfide-treated GaAs surface. **Chapter 6** presents a detailed XPS study of ammonium sulfide treated GaAs surfaces and demonstrates that the treatment removes surface oxides and leaves behind less than one monolayer of sulfer which inhibits further oxidation. This chapter is a written version of a poster presented at the 16th Conference on Physics and Chemistry of Semiconductor Interfaces and has

been accepted in paper form for publication in the ournal of Vacuum Science and Technology B.

The report also contains two appendices. **Appendix 1** contains preprints of several papers that were published during 1988-1989, and **Appendix 2** is a complete list of the publications that have resulted during the course of the project.

Conclusions

When we began these basic studies three years ago, we viewed GaAs as a poorly characterized semiconductor when compared with Si. We now understand much more about the fundamental device physics of GaAs and the importance of various loss mechanisms in state-of-the-art cells. With this knowledge, it should now be possible to critically assess, with a high degree of confidence, the potential for innovative GaAs-based solar cell designs. The general features of these results should also apply to other III-V semiconductors. For example conversations with C. Gordia and A. Rohatgi indicate effective bandgap shrinkage effects similar to those we observed in p^+-GaAs appear to be degrading the performance of InP solar cells. The work described in this report marks a transition in two different respects. First, our emphasis is shifting to $Al_xGa_{1-x}As$, which should serve as a model for the material parameter and device physics issues faced by III-V cells in general. Second, with our new MBE growth facility and the high-quality films now being produced, we plan to place more emphasis on the demonstration of innovative concepts for enhancing the efficiency of III-V solar cells.

TABLE OF CONTENTS

CHAPTER 1: HEAVY DOPING EFFECTS IN p^+ GaAs: Experimental Technique 1

CHAPTER 2: HEAVY DOPING EFFECTS IN p^+ GaAs: Results 13

CHAPTER 3: HIGH-EFFICIENCY MBE-GROWN GaAs SOLAR CELLS 22

CHAPTER 4: PHOTOVOLTAIC CHARACTERIZATION OF $Al_{0.2}Ga_{0.8}As$ CELLS 35

CHAPTER 5: ORIENTATION-DEPENDENT EDGE EFFECTS IN GaAs DIODES 52

CHAPTER 6: CHEMICAL PASSIVATION OF GaAs SURFACES 61

APPENDIX 1: REPRINTS OF 1988-1989 PUBLICATIONS 81

APPENDIX 2: BIBLIOGRAPHY OF SERI-SUPPORTED PUBLICATIONS 108

CHAPTER 1

HEAVY DOPING EFFECTS IN p^+GaAs: Experimental Technique

1.1 INTRODUCTION

Changes in the energy band structure associated with heavy impurity doping profoundly influence both the gain of Si bipolar transistors and the efficiency of Si solar cells [1]. Optical properties of GaAs are also strongly affected by heavy doping [2], but the effects on the electrical operation of devices have only recently been addressed. In a previous paper we presented an analysis of electron injection currents in p^+-n GaAs diodes, and found heavy doping effects in p^+-GaAs much like to those observed in p^+-Si [3]. Those diode-based measurements were the first attempt to explore the implications of heavy doping for the electrical performance of GaAs devices, but the need to separate the electron and hole injection components of the diode current limited the technique to p-type doping $\leq 10^{19}$ cm^{-3}. In this chapter we report new results concerning heavy doping effects in p^+-GaAs based on measurements of the collector current versus base-emitter voltage ($I_C - V_{BE}$) characteristics of n-p^+-n GaAs homojunction transistors. Such transistor-based measurements yield a natural separation of electron and hole currents, so electron injection currents can be characterized in p^+-GaAs doped much greater than 10^{19} cm^{-3}.

In heavily doped Si and GaAs, carrier-carrier and carrier-dopant interactions reduce the bandgap, and distort the densities-of-states by introducing band tails [4,5]. Detailed calculations [5] have shown that this perturbation of the band structure causes the $n_o p_o$ product in heavily doped p-type GaAs to be greater than its value in lightly doped material. For p-type dopant concentrations in the range 10^{18} to 10^{19} cm^{-3}, diode-based measurements confirm that $n_o p_o > n_{io}^2$, and that the $n_o p_o$ product increases with doping [3]. For electrical devices with heavily doped p-layers (e.g. bipolar transistors) the most important effect of energy band structure distortion is this strong enhancement of the $n_o p_o$ product. In heavily doped p-type GaAs,

$$n_{ie}^2 \equiv n_o p_o > n_{io}^2 . \tag{1.1}$$

where n_{ie} is the effective intrinsic carrier concentration and n_{io} is the value of the $n_o p_o$ product in lightly doped material.

We have previously reported measurements of electron injection currents in p^+-n GaAs diodes. Those diodes were designed with the unpassivated p-layer thickness W_p much less than the electron diffusion length, so that the electron component of current (J_n) was much greater than the hole component [6]. Under such conditions, the current component associated with electron injection into the p-layer is given by

$$J_n = q\,\frac{(n_{ie}^2 D_n)}{N_A W_p}(e^{qV/k_BT} - 1). \tag{1.2}$$

Using a generalization of (1.2), it was possible to extract the quantity $(n_{ie}^2 D_n)$ without knowledge of the surface recombination velocity by varying the thickness of the p-layer, W_p, by etching. (Unfortunately, it is not possible to separate n_{ie}^2 from the minority carrier diffusion coefficient, D_n, using steady-state current measurements.) Figure 1.1 shows a comparison of the measured $(n_{ie}^2 D_n)$ values with the curve expected assuming that heavy doping does not perturb the band structure. The solid curve was constructed assuming parabolic bands, and the reduction of the $n_o p_o$ product at high dopant densities due to majority carrier degeneracy was accounted for [7]; minority carrier mobilities predicted by Walukiewicz et al. for uncompensated material were assumed [8], with mobility related to diffusion coefficient by $k_B T \mu_n = q D_n$. The difference in the measured $(n_{ie}^2 D_n)$ values and those computed assuming unperturbed energy bands is an order of magnitude at 10^{19} cm^{-3}.

In order to reduce the sheet resistance in the base layer of AlGaAs/GaAs N-p^+-n HBTs, recent work has emphasized very heavy base doping, $\geq 10^{20}$ cm^{-3} [9]. A diode-based technique [6] is inadequate for measuring $(n_{ie}^2 D_n)$ at such high p-type doping levels because the electron and hole current components become similar in magnitude. In contrast, transistor-based current measurements allow a natural separation of hole and electron components.

1.2 EXPERIMENT

The collector current versus base-emitter voltage (I_C–V_{BE}) characteristic of a bipolar transistor is described by an equation similar to (1.2), which may be expressed for moderate values of V_{BE} as [10]

$$\ln I_C = \ln\left[\frac{qA_E(n_{ie}^2 D_n)}{N_A W_B}\right] + \frac{qV_{BE}}{k_B T}, \tag{1.3}$$

where A_E is the emitter area and W_B is the base thickness. Note that both (1.2) and (1.3) assume a flat p-type dopant profile. The quantity $(n_{ie}^2 D_n)$ is determined from the intercept of the linear portion of a plot of $\ln I_C$ versus V_{BE}; the device temperature can also be found very accurately from the slope of the line [1]. To ensure the validity of (1.3), we require that the base thickness be negligible compared to a minority carrier diffusion length:

$$L_n^2 = D_n \tau_n >> W_B^2\,, \tag{1.4}$$

where L_n is the electron diffusion length and τ_n is the electron lifetime.

Homojunction transistors, consisting only of GaAs layers, were chosen for this experiment in lieu of the more common AlGaAs/GaAs HBT configuration. Improper grading of the aluminum

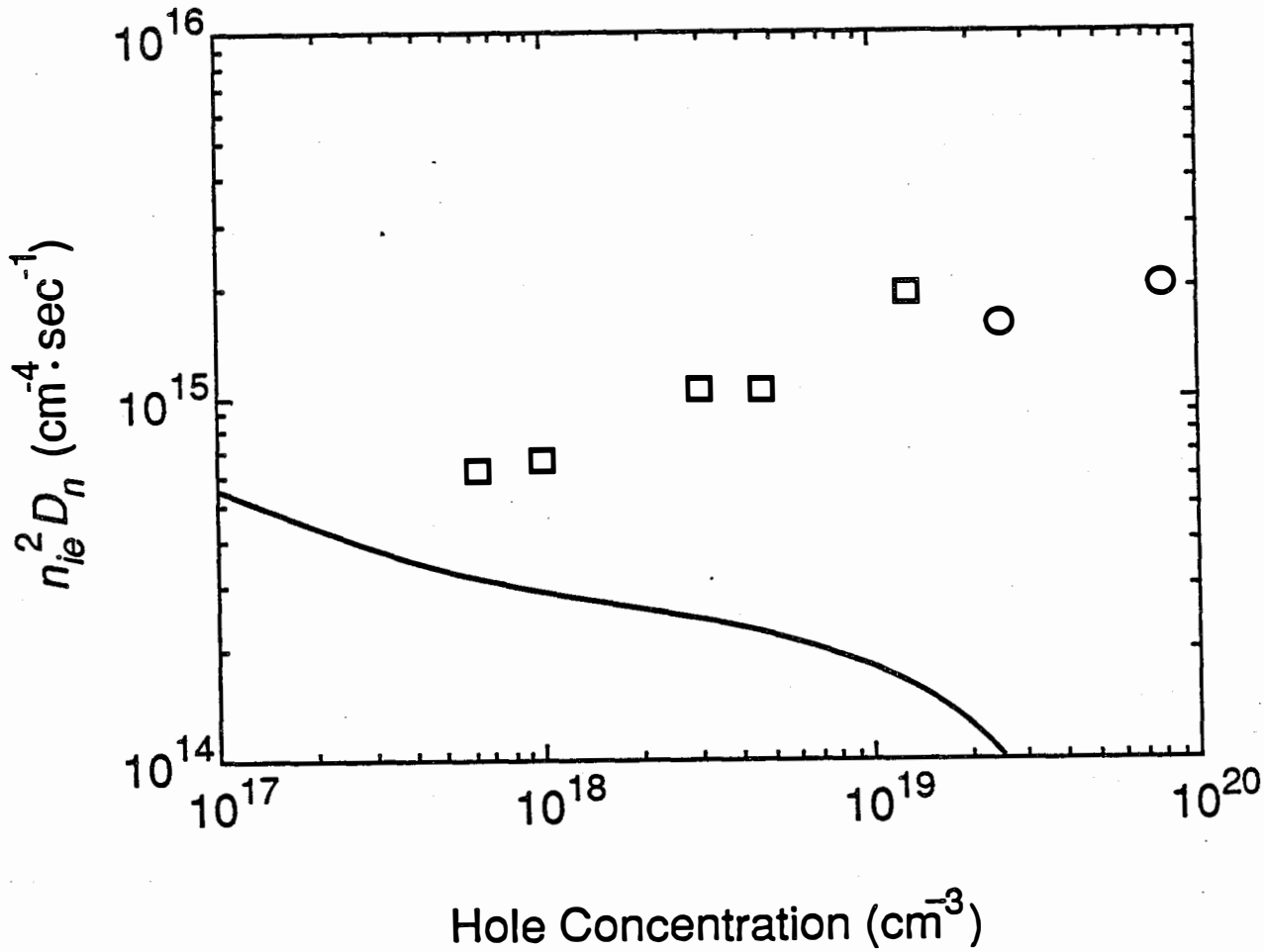

Fig. 1.1 The quantity ($n_{ie}^2 D_n$) versus carrier concentration in p-type GaAs at T = 300 K. The squares represent values measured using Zn-doped, MOCVD-grown diodes; the measurements employing Be-doped, MBE-grown homojunction bipolar transistor are represented by the circles.

composition in the emitter of an HBT, or misalignment of the compositional and doping junctions could result in a conduction band energy barrier at the emitter-base junction, which would invalidate (1.3). However, the ($I_C - V_{BE}$) characteristics of homojunction bipolar transistors should always be well-described by (1.3).

The epitaxial films required for this study were grown in a Varian GEN-II molecular beam epitaxy (MBE) system on n^+-GaAs substrates. The substrates were mounted in In, and were rotated at 5 rpm during the growth. The growth rate was 1 μm/hr at a substrate temperature of 600°C (the oxide desorption temperature was 580°C.) The As_4 to Ga beam equivalent pressure was 20, as determined by an ion gauge placed in the substrate growth position. Film thickness was monitored by counting oscillations in the reflection high-energy electron diffraction (RHEED) pattern at the beginning of film growth. The n-type dopant was Si, and the p-type dopant was Be. The slope of a plot of carrier concentration in the p-type material versus Be oven temperature was found to be consistent with the vapor pressure curve of Be in the concentration range 2×10^{18} to 8×10^{19} cm^{-3}, implying the absence of significant precipitation of Be even at the highest doping level [11, 12].

Standard optical lithography and wet-etching techniques were employed in device fabrication. The emitter contacts were Ge:Au:Ni/Ti/Au, alloyed at 320°C for 60 seconds; the base contacts were non-alloyed Ti/Au. Indium was used to mount the substrates in the MBE system during growth, and proved to be an effective means of contacting the collector layer (through the substrate). The mask set used included transistors of widely varying dimension, test patterns for measuring sheet resistance of the emitter and base layers, and structures for determining hole mobility and concentration in the base by Hall effect.

The dopant concentrations were probed by secondary ion mass spectroscopy (SIMS) at Charles Evans and Associates using 8 keV O_2^+ ion bombardment and positive sputtered ion mass spectrometry. A semi-insulating GaAs wafer, implanted at 150 keV with a 1×10^{15} cm^{-2} dose of Be, served as a calibration standard for the SIMS analysis of Be concentration. Concentration of Si was also monitored in the SIMS analysis. Carrier concentration in the emitter layer was checked by electrochemical capacitance-voltage profiling (ECV) at Solecon Laboratories.

1.3 RESULTS and DISCUSSION

Results for two similar transistor films, with targeted base layer Be concentrations of 8×10^{19} cm^{-3} and 3×10^{19} cm^{-3}, will be presented here. The targeted film parameters are listed in Table 1.1. We first discuss results for the film with the more heavily doped base (8×10^{19} cm^{-3}). The resistivity of the base layer material was found to be 1.4×10^{-3} Ω–cm, as measured both by using the Hall bar pattern, and by a transmission line technique. The hole mobility and concentration were found by Hall effect measurements to be 76 cm^2–V^{-1}–sec^{-1} and 6×10^{19} cm^{-3},

Table 1.1 Layer composition of the MBE-grown, homojunction bipolar transistor films.

Layer Composition	Function	Thickness (nm)	Dopant Concentration (cm^{-3})
n^+-GaAs	Contact Layer	100	$\geq 3\times10^{18}$
n-GaAs	Emitter	100	5×10^{17}
p^+–GaAs	**Base**	**100**	**3×10^{19}** **8×10^{19}**
n-GaAs	Collector	$\cong$ 300	2×10^{17}
n^+-GaAs	Sub-Collector	1000	$\geq 10^{18}$
n^+-GaAs	Substrate	···	$\geq 10^{18}$

respectively, assuming a Hall r-factor of unity (several authors have pointed out that the Hall r-factor may be much different than unity in p-type GaAs [13, 14].) Figure 1.2(a) shows the result of SIMS profiling of the film. The accuracy of the SIMS analysis of Be concentration was estimated to be ±20%, with a detection limit of ≈ 5×10^{15} cm^{-3}. The spatial coordinate was calibrated using the Si profile; spatial resolution was limited by beam mixing to ≈ 15 nm. The Be profile is quite sharp, and broadly peaked at about 8×10^{19} cm^{-3}. However, some diffusion of Be is evident on the substrate side of the base.

For the case of a non-uniform base doping profile, (1.3) may expressed as [15]

$$\ln I_C = \ln\left[qA_e\left(\int \frac{N_A(x)}{n_{ie}^2(x)D_n(x)}dx\right)^{-1}\right] + \frac{qV_{BE}}{k_BT}, \tag{1.5}$$

where integration is over the quasi-neutral base. If we let $\overline{(n_{ie}^2 D_n)}$ represent the average value of $(n_{ie}^2 D_n)$ in the base, then (1.5) becomes

$$\ln I_C = \ln\left[\frac{qA_E\,\overline{(n_{ie}^2 D_n)}}{Q_B}\right] + \frac{qV_{BE}}{k_BT}, \tag{1.6}$$

where Q_B is the number of holes in the base per unit area. It is difficult to determine the precise quasi-neutral base width from the SIMS profile shown in Fig. 1.2(a) because of beam mixing during SIMS analysis, which limits the spatial resolution to ≈ 15 nm, and because of actual Be diffusion during film growth. To estimate the quasi-neutral base width, W_B, we first integrated the Be concentration, as measured by SIMS, from 100 nm to 400 nm distance from the film's surface (the nominal position of the base layer was 200 to 300 nm.) The result of this integration as a function of position is shown in Fig. 1.3. The curve is normalized such that its maximum value represents 100% of the integrated Be concentration. A straight line was then fit to the values of the curve shown in Fig. 1.3 which lie between 10 and 90%. The intersection of that line with the values zero and unity define the position of the quasi-neutral base, which was found to extend from 194 nm to 302 nm, indicating a value of W_B = 108 nm (which is very close to the targeted value of 100 nm; note that the quasi-neutral base width is only negligibly narrowed by depletion). By again integrating the Be concentration, this time from 194 nm to 302 nm, we found $Q_B = 8.5\times10^{14}$ cm^{-2}, which is very near the targeted value of 8.0×10^{14} cm^{-2}. This method of calculating the base width was chosen because it assures that nearly all the charge will be represented in the quantity Q_B.

The average doping in the base was defined to be $\overline{N_A} \equiv Q_B/W_B$. Its value was found to be 7.9×10^{19} cm^{-3}, nearly equal to the targeted doping. A numerical average of the values of Be concentration defined by the 10 to 90% points of the curve in Fig. 1.3 also yielded an estimate of 7.9×10^{19} cm^{-3} for the average base doping.

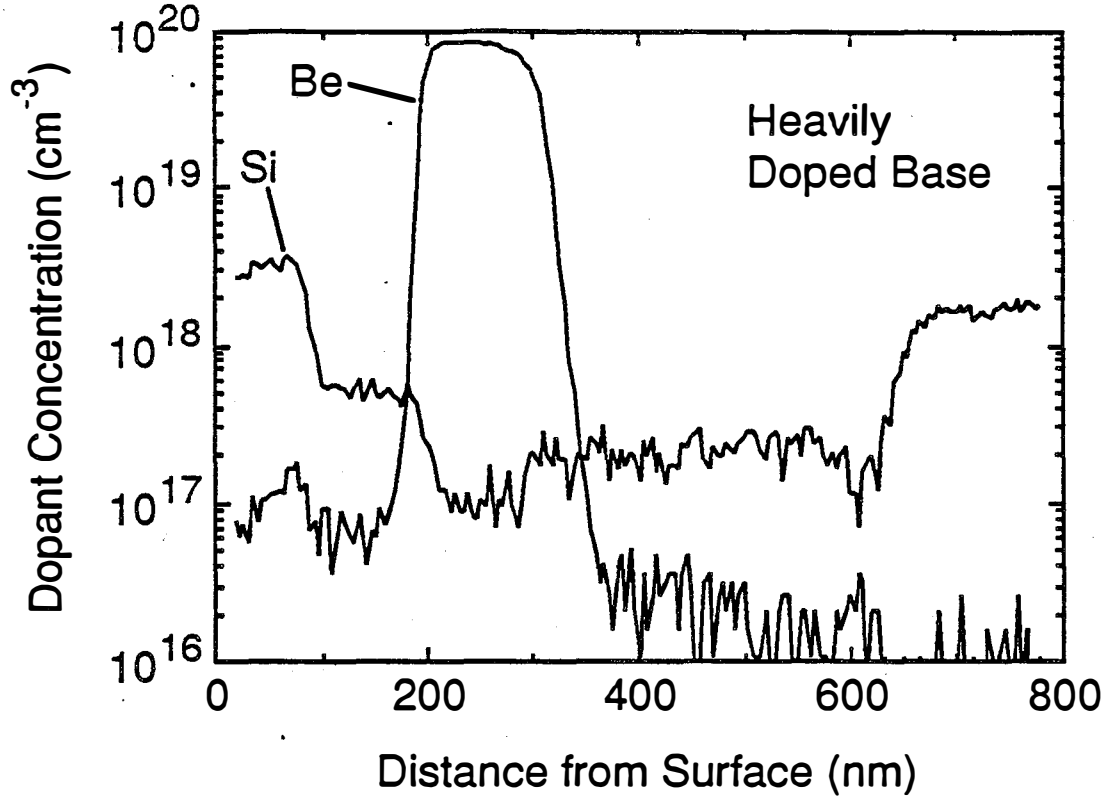

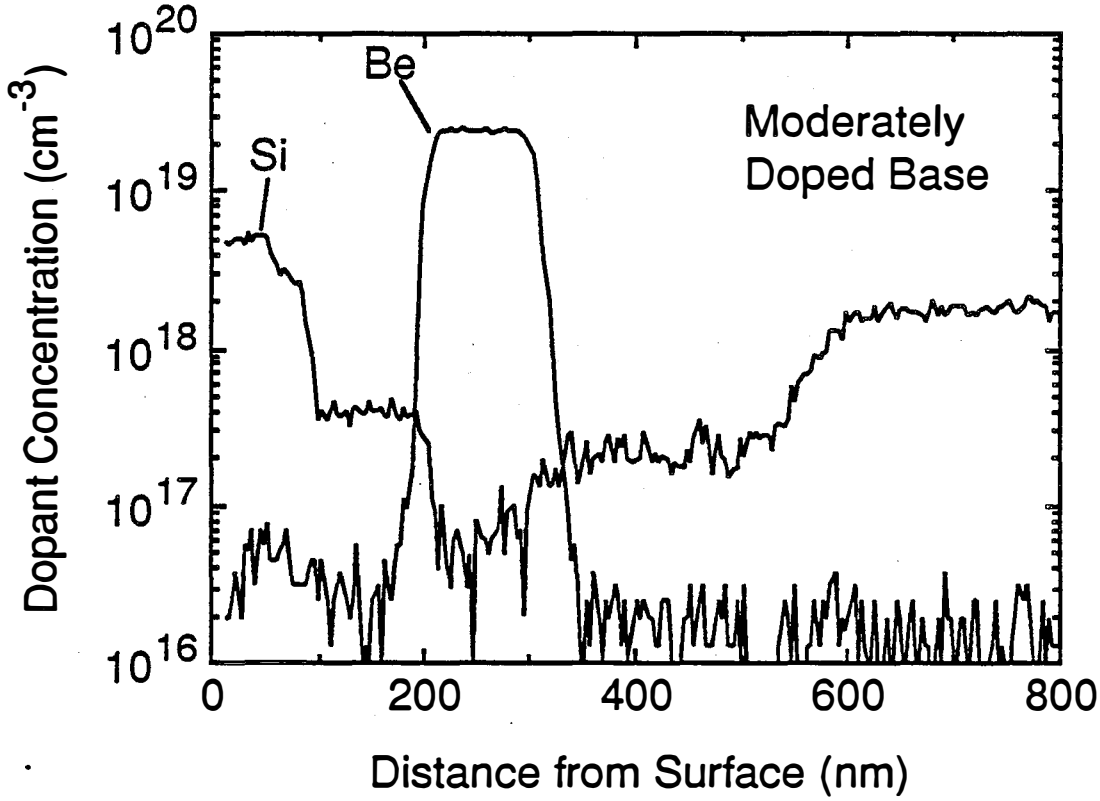

Fig. 1.2 Profile of dopant concentration in the homojunction bipolar transistor films as a function of distance from the surface, as measured by secondary ion mass spectroscopy (SIMS): (a) heavily doped base layer; (b) moderately doped base layer.

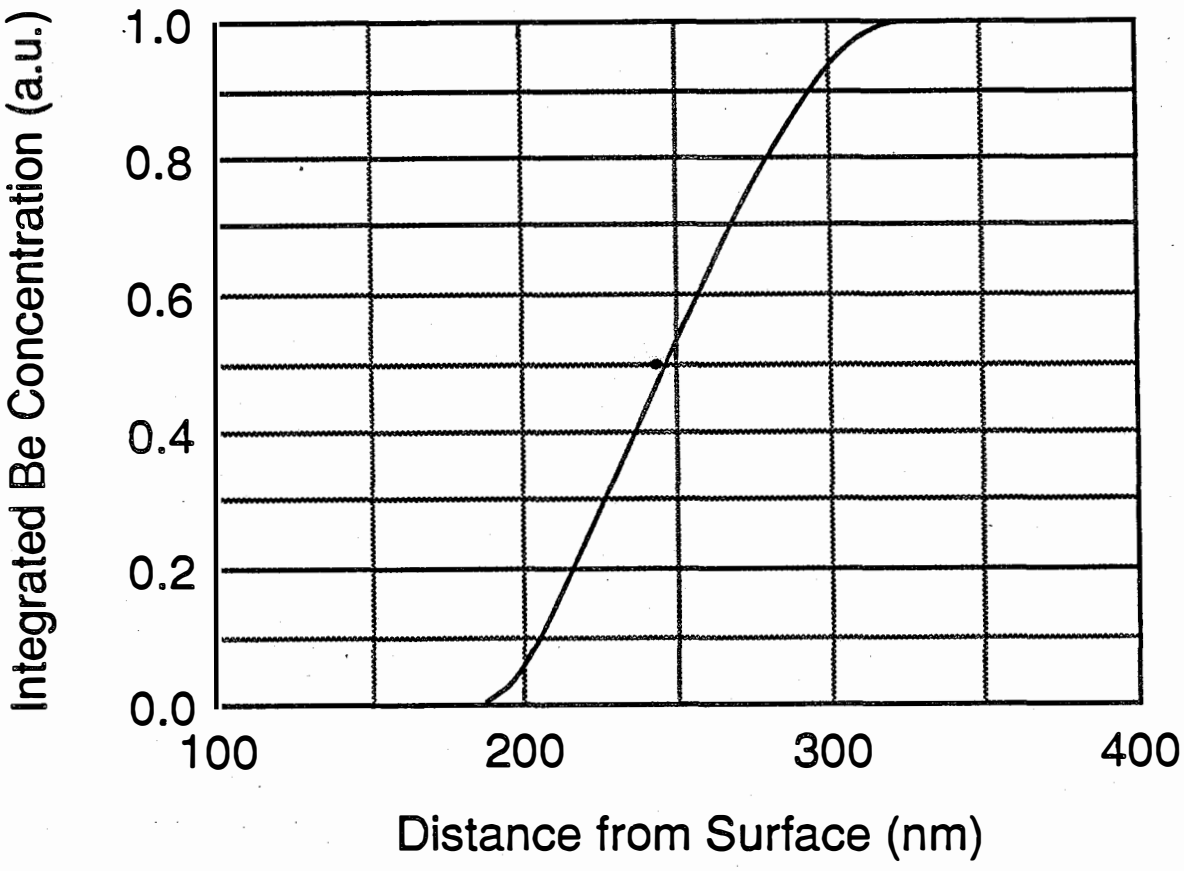

Fig. 1.3 Integral of the Be concentration from 100 to 400 nm distance from the surface of the transistor film with the heavily doped base layer, as measured by SIMS analysis; the curve is normalized such that its maximum value represents 100% of the integrated Be concentration.

The validity of assumption (1.4) may be tested by extrapolating the available data for minority electron diffusion coefficient [16] and lifetime [17]. At a hole concentration of 7.9×10^{19} cm^{-3}, reasonable estimates are $D_n = 20\ cm^2\cdot sec^{-1}$ and τ_n = 0.1 nsec, which yields $L_n \cong 400$ nm. Lievin et al. reported $L_n \approx 250$ nm at a hole concentration of about 10^{20} cm^{-3} [12]. For a base thickness W_B = 108 nm, (1.4) should be well-satisfied. We find that a diffusion length less than 125 nm would be required to reduce the measured collector current by 10% relative to the ideal expression given by (1.3).

I_C-V_{BE} data were compiled for 21 transistors with heavily doped base layers, with emitter dimensions varying from 24 μm × 24 μm to 160 μm × 560 μm. No dependence of collector current density on emitter size was observed. (However, it was necessary to use the fabricated, rather than as-drawn, emitter dimensions in calculating $(n_{ie}^2 D_n)$ from the I_C-V_{BE} characteristic, because of a slight spreading of ≅ 0.5 μm in each direction of the photoresist used to define the emitter mesa.) Data for a 160 μm × 160 μm transistor are displayed in Fig. 1.4. The data comprising the curve labelled "inverted" were measured by reversing the role of the emitter and collector layers. Both curves roll off at higher voltages due to series resistance effects. Note the reciprocal behavior displayed by the linear portion of the curves.

The slope and intercept of the linear part of the I_C-V_{BE} data shown in Fig. 1.4 were determined by least squares fitting. Using (1.6), with $Q_B = 8.5\times10^{14}$ cm^{-2}, we found $(n_{ie}^2 D_n) = 2.09\times10^{15}$ $cm^{-4}\cdot sec^{-1}$ and T = 299.4 K. Room temperature, as measured by a thermocouple in the probe station chuck, was also 299.4 K. In order to compare values of $(n_{ie}^2 D_n)$ measured at slightly different temperatures, we can scale the results to T = 300 K [18], using the known temperature dependence of n_{io} [19]. Nine I_C-V_{BE} data sets which were well-described by (1.3) over several orders of magnitude of current were selected for fitting; an average value of $(n_{ie}^2 D_n) = 2.08\times10^{15}$ $cm^{-4}\cdot sec^{-1}$ (σ = 1.9%) at T = 300 K was extracted. This value is displayed along with the previously-measured diode data [3] in Fig. 1.1 as an open circle.

Figure 1.2(b) shows the SIMS profile of the second film, with the more moderately doped base layer. The Be profile is ideal, within the resolution of the SIMS technique, having very steep sides and a flat peak $\overline{N_A} = 2.4\times10^{19}$ cm^{-3}. The base width and base charge were W_B = 103 nm and $Q_B = 2.4\times10^{14}$ cm^{-2}, respectively, resulting in an average base doping of $N_A = 2.4\times10^{19}$ cm^{-3}. Because of the lack of Be diffusion in this film, the base charge could also have been calculated from the product of the average doping and the targeted base width, so the value of $(n_{ie}^2 D_n)$ is not an average quantity in this case. The resistivity of the base layer material was 2.9×10^{-3} Ω–cm, and the hole mobility and concentration from Hall effect measurements were 88 $cm^2-V^{-1}-sec^{-1}$ and 2.4×10^{19} cm^{-3}, respectively. I_C-V_{BE} data were measured for 17 transistors at temperatures ranging from 297.7 to 298.0 K. Fitting the data to (1.3) and scaling the results to T = 300 K yielded $(n_{ie}^2 D_n) = 1.51\times10^{15}$ $cm^{-4}\cdot sec^{-1}$ (σ = 3.9%).

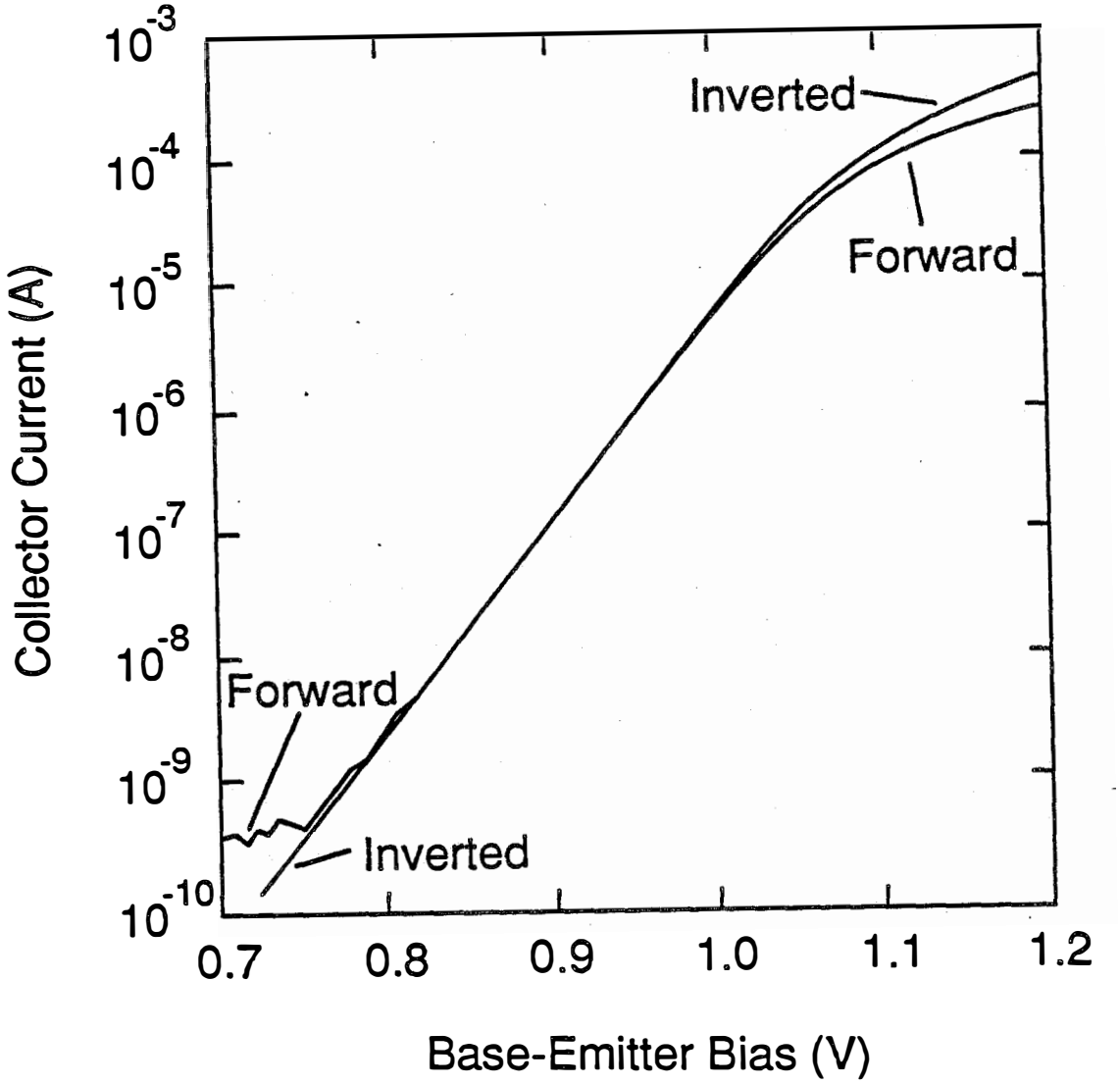

Fig. 1.4 Collector current as a function of base-emitter voltage for a homojunction bipolar transistor with emitter dimensions 160 μm × 160 μm, measured for both normal and inverted operation at a temperature of 299.4 K.

The values of $(n_{ie}^2 D_n)$ measured using the two transistor films discussed here are much larger than those that would be expected assuming a band structure unperturbed by heavy doping. (Note that the solid curve shown in Fig. 1.1, which was calculated assuming an unperturbed band structure as described in the introductory section of this paper, continues to fall off sharply above 3×10^{19} cm^{-3} due to majority carrier degeneracy.) We attribute the large measured values of the collector current to perturbations of the band structure associated with heavy doping, which increase n_{ie}^2. This result is in qualitative agreement with the theoretical work of Bennett and Lowney, who used a detailed many-body approach to calculate the $n_o p_o$ product in p^+-GaAs as a function of acceptor concentration [5]. However, a direct comparison of their results with the experimental data presented in this paper is difficult, because the minority carrier diffusion coefficient D_n has not (to our knowledge) been measured for hole concentrations above 4×10^{18} cm^{-3}.

1.4 CONCLUSIONS

We have demonstrated a transistor-based technique for measuring electron injection currents in p^+-GaAs doped greater than 10^{19} cm^{-3}. Use of a homojunction bipolar transistor allows a straight-forward interpretation of the measured currents relative to the use of heterojunction bipolar transistors (HBTs) because (1) it facilitates separation of electron and hole current components, and (2) because it assures ideal emitter-base junction behavior. We interpret the large injection currents measured as evidence for significant effective bandgap shrinkage effects. As was found to be the case for Si, these effects must be taken into account for accurate analysis and design of GaAs-based bipolar transistors and solar cells [1,10,18].

Future experimental work should include additional measurements of $(n_{ie}^2 D_n)$ at hole concentrations in the range 10^{18} to 10^{20} cm^{-3}, as well as measurements of the minority carrier mobility for acceptor concentrations from mid-10^{18} to 10^{20} cm^{-3}. Such heavy p-type doping is now commonly employed in the GaAs base of HBTs, where the base transit time is influenced by the minority electron mobility. In addition, knowledge of the minority carrier mobility at high acceptor concentrations would allow the $n_o p_o$ product to be deduced from $(n_{ie}^2 D_n)$ data, and could also shed light on fundamental scattering processes in heavily doped GaAs.

CHAPTER 1 REFERENCES

[1] J. W. Slottboom and H. C. de Graaff, *Solid-State Electron. 19,* 857 (1976).

[2] H. C. Casey, Jr. and F. Stern, *J. Appl. Phys. 47,* 631 (1976).

[3] M. E. Klausmeier-Brown, M. S. Lundstrom, M. R. Melloch and S. P. Tobin, Appl. *Phys. Lett. 52,* 2255 (1988).

[4] E. O. Kane, *Solid-State Electron. 28,* 3 (1985).

[5] H. S. Bennett and J. R. Lowney, *J. Appl. Phys. 62,* 521 (1987).

[6] M. E. Klausmeier-Brown, C. S. Kyono, P. D. DeMoulin, S. P. Tobin, M. S. Lundstrom and M. R. Melloch, *IEEE Trans. Electron Devices ED-35,* 1159 (1988).

[7] F. A. Lindholm and J. G. Fossum, *Electron Device Lett. EDL-2,* 230 (1981).

[8] W. Walukiewicz, J. Lagowski, L. Jastrzebski and H. C. Gatos, *J. Appl. Phys. 50,* 5040 (1979).

[9] M.-C. Chang, P. M. Asbeck, K. C. Wang, G. J. Sullivan, N.-H. Sheng, J. A. Higgins and D. L. Miller, *Electron Device Lett. EDL-8,* 303 (1987).

[10] M. E. Klausmeier-Brown, M. S. Lundstrom, and M. R. Melloch, to appear in *IEEE Trans. Electron Devices* (1989).

[11] R. A. Hamm, M. B. Panish, R. N. Nottenburg, Y. K. Chen and D. A. Humphrey, *Appl. Phys. Lett. 54,* 2586 (1989).

[12] J. L. Lievin, C. Dubon-Chevallier, F. Alexandre, G. Leroux, J. Dangla and D. Ankri, *IEEE. Electron Device Lett. EDL-7,* 129 (1986).

[13] J. D. Wiley, in *Semiconductors and Semimetals, Vol. 10,* ed. by R. K. Willardson and A. C. Beer (Academic Press, New York, 1975) p. 91.

[14] D. C. Look, *Electrical Characterization of GaAs Materials and Devices* (John Wiley & Sons, New York, 1989) p. 59.

[15] A. H. Marshak and C. M. Van Vliet, *Proc. IEEE 72,* 148 (1984).

[16] H. Ito and T. Ishibashi, *J. Appl. Phys. 65,* 5197 (1989).

[17] R. K. Ahrenkiel, in *Current Topics in Photovoltaics, Vol. 3,* ed. by T. J. Coutts and J. D. Meakin (Academic Press Ltd., London, 1988) p. 51.

[18] J. A. del Alamo and R. M. Swanson, *Solid-State Electron. 30,* 1127 (1987).

[19] J. S. Blakemore, *J. Appl. Phys. 53,* R123 (1982).

CHAPTER 2

HEAVY DOPING EFFECTS IN p^+ GaAs: Results

2.1 INTRODUCTION

Measurements of the collector current versus base-emitter voltage characteristics of n-p-n Si bipolar transistors showed a strong enhancement of the electron current injected into p^+-Si [1]. Those enhanced electron injection currents have been attributed to doping-induced perturbations of the band structure which increase the $n_o p_o$ product [2]. Such heavy doping effects must be treated for accurate design and modeling of Si bipolar transistors and solar cells [1, 3]. While heavy p-type doping has been known to affect optical transitions in GaAs [4], its effect on the electrical performance of GaAs devices has only recently been explored. In a previous paper we characterized electron injection currents in p^+-n GaAs diodes with p-layers doped from mid-10^{17} to 10^{19} cm^{-3} [5]. Those results showed heavy doping effects in p^+-GaAs analogous to those observed in p^+-Si, but the technique used was limited to dopings $\leq 10^{19}$ cm^{-3}. In Chapter 1 we presented a new technique for measuring heavy doping effects in p-GaAs based on characterization of the collector saturation current of n-p^+-n GaAs homojunction bipolar transistors. This new transistor based technique has allowed us to extend the doping range where we have measured the effects of acceptor doping of GaAs to 8×10^{19} cm^{-3}. The results show significant heavy doping effects up to 8×10^{19} cm^{-3} and are consistent with the diode measurements below 10^{19} cm^{-3}. These heavy doping effects must be treated to accurately model GaAs bipolar devices.

Consider an n-p-n homojunction bipolar transistor (BJT) having a spatially uniform base doping profile. When the emitter-base junction is forward-biased and the base-collector junction short-circuited or reverse-biased, the collector current density versus base-emitter voltage characteristic is described by

$$J_c = \frac{q(n_o D_n)}{W_B} \exp\left[\frac{qV_{BE}}{kT} - 1\right] \tag{2.1}$$

where n_o is the equilibrium electron concentration in the p-type base, D_n is the diffusion coefficient of the minority-carrier electrons, and W_B is the width of the quasi-neutral portion of the base. A quantity called the effective intrinsic carrier concentration n_{ie} may be introduced to relate n_o to the ionized dopant density N_A, such that $n_o \equiv \frac{n_{ie}^2}{N_A}$. Measurements in heavily doped Si have shown that n_{ie} considerably exceeds n_{io}, the intrinsic carrier concentration in lightly doped Si. For the purpose of device modeling , the measured relationship between n_{ie} and n_{io} may be described by defining a non-physical effective bandgap shrinkage parameter [3, 6].

Homojunction bipolar transistors were chosen for this work instead of the more common heterojunction bipolar transistors (HBTs); misalignment of the doping and compositional junctions due to dopant diffusion, or improper grading of the emitter aluminum composition in an HBT could result in a conduction band energy barrier at the emitter-base junction which would invalidate (2.1). The technique used in this work to quantify electron injection currents as a function of p-layer hole concentration was pioneered by Slotboom and de Graaff [1], and was described in detail in Chapter 1 for GaAs BJTs and also in reference [7]. Such transistor measurements facilitate the separation of hole and electron current components. In this chapter the results are reported in terms of the quantity most directly obtained from the measurement of collector current versus base-emitter voltage, the product (n_oD_n).

2.2 EXPERIMENTAL RESULTS

The targeted layer thicknesses and dopings of the films used in these experiments are described in Table 2.1. The films were all grown in a Varian GEN-II molecular beam epitaxy (MBE) system on n^+-GaAs substrates at a substrate temperature of 600°C (the oxide desorption temperature was 580°C). The growth rate was 1 5m/hr; film thickness was monitored by counting oscillations in the reflection high-energy diffraction (RHEED) pattern during non-critical portions of the growth. The p- and n-type dopants were Be and Si, respectively. Standard optical lithography and wet etching procedures were employed in device fabrication. Seven films were studied, with targeted base layer Be concentrations of 2×10^{18} to 8×10^{19} cm^{-3}. The slope of a plot of carrier concentration in the p-type material as a function of Be oven temperature was consistent with the vapor pressure curve of Be in this doping range, implying the absence of significant precipitation of Be even at the highest doing level. Further details of film growth and device fabrication have been described elsewhere [7].

Dopant and carrier concentrations in the p-type base layer of each film were characterized in several ways. Secondary ion mass spectroscopy (SIMS) was used to probe the Be profile. Use of a Be-implanted calibration standard resulted in an absolute accuracy of ±20 %. Si concentration was also monitored during the SIMS analysis, and the Si profile was used to calibrate the spatial coordinate; beam mixing limited spatial resolution to 150 Å. The base layer hole concentrations were also probed by Hall effect. The average Be concentration found in the base layer of each film by SIMS is listed in the first column of Table 2.2; also displayed in Table 2.2 are the base layer hole concentration and mobility found by Hall effect measurements (assuming a Hall r-factor of unity). Although the hole concentration values derived from Hall effect measurements are as much as 30% lower than the Be concentration values given by SIMS, we believe that the p-type material is essentially uncompensated. Several authors have pointed out that the Hall r-factor may be quite different than unity in p-type GaAs, leading to uncertainty concerning the reliability of hole concentration values derived from Hall effect measurements [8, 9]. Since the incorporation of Be in the films was ideal [7], we equate the base layer hole concentration p_o with the average base layer Be concentration in each film.

TABLE 2.1 Targeted layer thicknesses and dopings of the MBE-grown homojunction bipolar transistor films used in this study.

Layer Composition	Function	Thickness (Å)	Dopant Concentration (cm^{-3})
n^+-GaAs	Contact Layer	1000 to 2000	$\geq 2\times10^{18}$
n-GaAs	Emitter	1000	5×10^{17}
p^+-GaAs	**Base**	**1000 to 3000**	**2×10^{18} to 8×10^{19}**
n-GaAs	Collector	2000 to 3000	2×10^{17}
n^+-GaAs	Sub-Collector	10,000	$\geq 10^{18}$
n^+-GaAs	Substrate	...	$\geq 10^{18}$

TABLE 2.2 Summary of the measurements made using homojunction bipolar transistors.

Be Concentration from SIMS (cm^{-3})	Targeted Base Width (Å)	Hole Concentration from Hall Effect (cm^{-3})	Hole Mobility from Hall effect ($cm^2\ V^{-1}\ s^{-1}$)	Measurement Temperature (K)	($n_o D_n$) at 300 K ($10^{-5}\ cm^{-1}\ s^{-1}$)
2.0×10^{18}	3000	1.4×10^{18}	178	297.4	51.5
6.5×10^{18}	2000	4.6×10^{18}	134	299.2	23.1
1.5×10^{19}	1000	1.0×10^{19}	104	298.1	10.5
2.4×10^{19}	1000	2.4×10^{19}	88	297.9	6.30
3.2×10^{19}	1000	2.6×10^{19}	86	298.7	4.94
5.3×10^{19}	1000	4.1×10^{19}	82	298.3	3.60
7.9×10^{19}	1000	6.0×10^{19}	76	299.4	2.63

The SIMS profiles of Be in the all but two of the films were ideal, within the resolution of the analysis, exhibiting very steep sides and flat peaks. The Be profile was slightly non-uniform in each of the two most heavily doped films, displaying broad flat peaks over most of the base width, but showing evidence of some diffusion of Be on the substrate side of the base [7]. The base width and average base doping for those two films was estimated by a careful spatial integration of the Be profile, and the reported value of $(n_o D_n)$ necessarily represents an average quantity as described in Ref. [7].

The collector current density was measured as a function of emitter-base voltage, with the base and collector shorted, for a number of transistors on each film. The $J_c - V_{BE}$ data were well-described by (2.1) in all cases, except at low biases where leakage currents were important, and at high biases where series resistance was important. The quantity $(n_o D_n)$ was determined from the intercept of the linear portion of a plot of $\ln J_c$ versus V_{BE}; the device temperature could also be found from the slope of the plot. The temperature measured by a thermocouple agreed with the temperature found from fitting the $\ln J_c$ versus V_{BE} plot to within 0.2 K for all devices.

Equation (2.1) is valid only so long as recombination in the base is not significant. This constraint is most severe for the film with the most heavily doped base layer (7.9×10^{19} cm^{-3}). For this film we estimate that an electron diffusion length less than 1250 Å would be required to reduce the measured collector current by 10%, whereas Lievin et al. reported a diffusion length of approximately 2500 Å at a hole concentration of about 10^{20} cm^{-3} [10], so it seems likely that (2.1) is valid even in this case.

Results of the extraction of $(n_o D_n)$ from the measured $J_c - V_{BE}$ data are listed in the last column of Table 2.2. The actual measurement temperature is also listed in Table 2.2. Following del Alamo [3], we have scaled all $(n_o D_n)$ products to T = 300 K using the known temperature dependence of n_{io} [11]. The maximum error introduced by this temperature scaling should not exceed 2%. Fig. 2.1 is a plot of $(n_o D_n)$ as a function of hole concentration in p-type GaAs at T = 300 K. Both the transistor data listed in Table 2.2 and the previously reported diode data [5, 12] are shown in Fig. 2.1. (Recall that $(n_o D_n)$ is proportional to the electron current injected into the base of a bipolar transistor, so its value has a direct relationship to the gain of an HBT [6].) Two other curves are shown in Fig. 2.1 for comparison with the measured data. The lower curve, labeled "No Bandgap Shrinkage", was computed without considering any heavy doping effects except degeneracy of the hole gas [5], with $n_{io} = 2.25\times10^6$ cm^{-3} [11]; D_n was estimated from a fit to the measured minority-carrier mobility values [6]. The curve is dashed above 4×10^{18} cm^{-3} because that is the highest hole concentration at which the minority electron mobility has been measured [13]. The difference between this curve and the measured data is more than an order of magnitude above 10^{19} cm^{-3}, and underlines the importance of considering these effects. The second curve in Fig. 2.1, labeled "Theory", makes use of the theoretical work of Bennett and Lowney, who used a detailed many-body approach to calculate the ratio n_{ie}/n_{io} as a function of hole concentration in p^+-GaAs [14]. Again, $n_{io} = 2.25\times10^6$ cm^{-3}, and D_n was estimated from

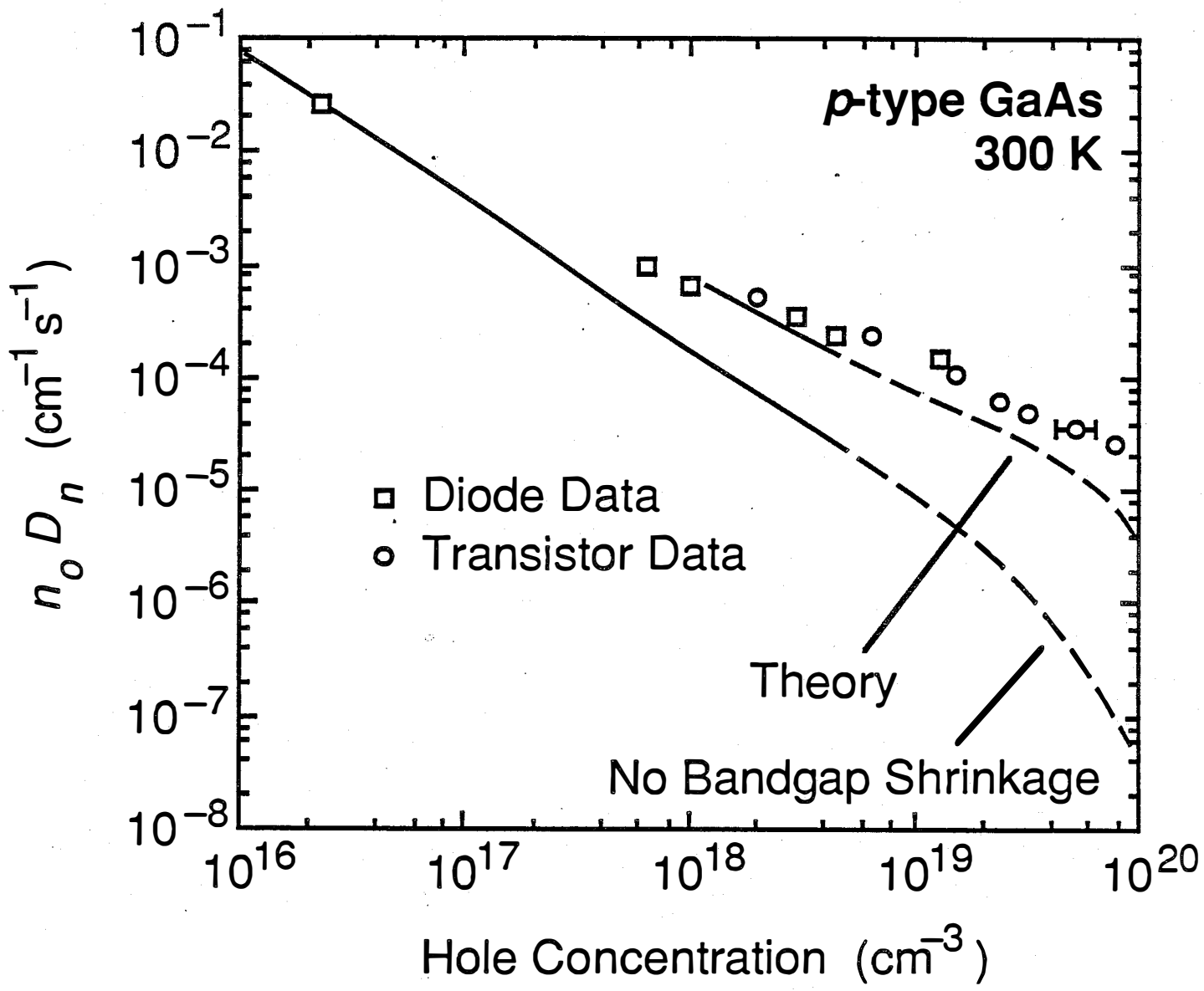

FIG. 2.1 The quantity (n_oD_n) in p-type GaAs at T = 300 K. The squares represent diode data [5, 12], and the circles represent the transistor data from Table 2.2. The error bar represents an uncertainty of ±20% in the magnitude of the Be concentration from SIMS analysis of the transistor films. The curve labelled "Theory" was constructed from calculations of n_{ie}/n_{io} [14] combined with a fit to measured minority carrier mobility data [6]. The curve labelled "No Bandgap Shrinkage" was constructed assuming no heavy doping effects except hole gas degeneracy [5].

measured values as just described. The theoretical curve agrees within a factor of two with the measured results over most of the measured range of hole concentrations.

One might expect that effective bandgap shrinkage in p^+-GaAs would be qualitatively similar to the well-characterized effects in p^+-Si. Fig. 2.2 is a plot of $(n_o D_n)$ as a function of hole concentration in p-type Si at T = 300 K. The experimental curve was constructed using fits for minority electron mobility (i.e. D_n) and effective bandgap shrinkage as functions of hole concentration, as given by Swirhun et al. [15]. The curve labeled "No Bandgap Shrinkage" was constructed in the same way as the analogous curve in Fig. 2.1, using the minority-carrier mobility fit of Swirhun et al. Both curves in Fig. 2.2 were constructed using $n_{io} = 1.18\times10^{10}$ cm^{-3}. A comparison of Fig. 2.1 and Fig. 2.2 reveals that the behavior of $(n_o D_n)$ as a function of hole concentration in p^+-GaAs and p^+-Si displays a similar trend. (The large difference in the vertical scale factor is accounted for by the large difference in n_{io} for GaAs and Si.) While caution is necessary in extrapolating the p^+-GaAs minority-carrier mobility data, it appears that the effective bandgap shrinkage is somewhat stronger in p^+-Si for dopant concentrations above 10^{19} cm^{-3}.

For the purpose of device modeling, a non-physical effective bandgap shrinkage parameter is often introduced to describe the measured relationship between n_{ie} and n_{io}, where $n_{ie}^2 \equiv n_o N_A$. A commonly used definition is [3, 6]:

$$\Delta_G^o \equiv k_B\, T \ln(n_{ie}^2/n_{io}^2)$$

We do not quote apparent bandgap shrinkage values in this letter because extraction from the measured $(n_o D_n)$ values depends on knowledge of the minority-carrier mobility (or D_n). A previously presented expression for Δ_G^o as a function of hole concentration which was based on measurements of $(n_o D_n)$ at lower dopant concentrations [6] appears to overestimate the effective bandgap shrinkage for dopant concentrations > 10^{19} cm^{-3}.

2.3 SUMMARY

In summary, measurements of electron current injected into the base of n-p^+-n GaAs homojunction transistors were presented. The large magnitude of the measured currents was attributed to heavy doping effects in p^+-GaAs. These effects are analogous to the so-called bandgap shrinkage effects observed in p^+-Si. As was found to be the case for Si, heavy doping effects must be treated to correctly model GaAs-based bipolar transistors and solar cells [6, 16]. However, further work is necessary to measure the minority electron mobility for hole concentration greater than 10^{19} cm^{-3}, and to examine the effects of heavy doping in n-type GaAs.

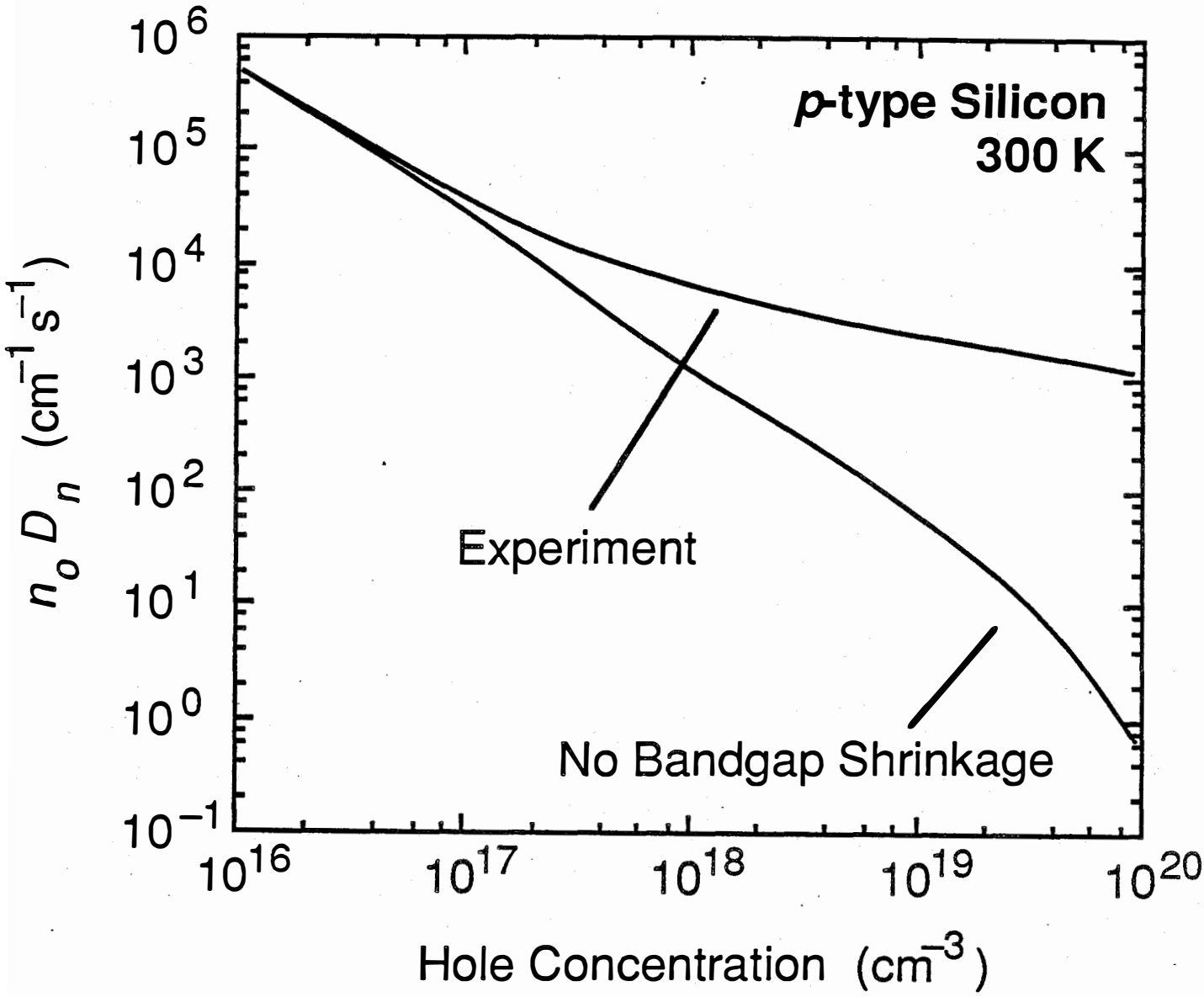

FIG. 2.2 The quantity (n_oD_n) in p-type Si at T = 300 K. The curve labelled "Experiment" was constructed using fits for minority electron mobility (i.e. D_n) and effective bandgap shrinkage as functions of hole concentration, as given by Swirhun et al. [15]. The curve labelled "No Bandgap Shrinkage" was constructed assuming no heavy doping effects except hole gas degeneracy.

CHAPTER 2 REFERENCES

[1] J. W. Slotboom and H. C. de Graaff, *Solid-State Electron. 19*, 857 (1976).

[2] J. R. Lowney and H. S. Bennett, *J. Appl. Phys. 53*, 433 (1981).

[3] J. A. del Alamo and R. M. Swanson, *Solid-State Electron. 30*, 1127 (1987).

[4] H. C. Casey, Jr. and F. Stern, *J. Appl. Phys. 47*, 631 (1976).

[5] M. E. Klausmeier-Brown, M. S. Lundstrom, M. R. Melloch and S. P. Tobin, *Appl. Phys. Lett. 52,* 2255 (1988).

[6] M. E. Klausmeier-Brown, M. S. Lundstrom and M. R. Melloch, *IEEE Trans. Electron Devices* (in press).

[7] M. E. Klausmeier-Brown, M. R. Melloch and M. S. Lundstrom, *J. Electron. Mater.* (in press).

[8] J. D. Wiley, in *Semiconductors and Semimetals*, edited by R. K. Willardson and A. C. Beer (Academic, New York, 1975) p. 91, Vol. 10.

[9] D. C. Look, *Electrical Characterization of GaAs Materials and Devices* (Wiley, New York, 1989) p. 59.

[10] J. L. Lievin, C. Dubon-Chevallier, F. Alexandre, G. Leroux, J. Dangla and D. Ankri, *IEEE Electron Device Lett. EDL-7*, 129 (1986).

[11] J. S. Blakemore, *J. Appl. Phys. 53*, R123 (1982).

[12] H. L. Chuang, P. D. DeMoulin, M. E. Klausmeier-Brown, M. R. Melloch, and M. S. Lundstrom, *J. Appl. Phys. 64*, 6361 (1988).

[13] M. I. Nathan, W. P. Dumke, K. Wrenner, S. Tiwari, S. L. Wright and K. A. Jenkins, *Appl. Phys. Lett. 52*, 654 (1988).

[14] H. S. Bennett and J. R. Lowney, *J. Appl. Phys. 62*, 521 (1987).

[15] S. E. Swirhun, D. E. Kane, and R. M. Swanson, *IEDM Tech. Dig.*, 298 (1988).

[16] M. E. Klausmeier-Brown, P. D. DeMoulin, M. S. Lundstrom, and M. R. Melloch, *Conf. Rec. 20th IEEE Photovoltaic Specialists Conference,* 503 (1988).

CHAPTER 3

HIGH-EFFICIENCY MBE-GROWN GaAs SOLAR CELLS

3.1 INTRODUCTION

Molecular beam epitaxy (MBE) has proven to be an important film growth technique for most advanced device research due to the relative ease with which complex compositional and doping profiles can be grown. However, solar cells fabricated from MBE-grown material have been inferior in performance to those fabricated from metal organic chemical vapor deposited (MOCVD) material. Solar cells are large area minority carrier devices and typically range in area from 0.25 cm^2 to 4 $cm.^2$ Table 3.1 is a summary of solar cell results for MOCVD [1-4] and MBE [5-8] films clearly illustrating that previous to this work solar cells fabricated from MOCVD material were superior to solar cells fabricated from MBE material. The previously best reported MBE-cell had a 1-sun AM1.5 efficiency of 15.7% without an antireflection coating [8] while MOCVD-cells have achieved efficiencies of 24.8% [4].

We have recently fabricated solar cells on an MBE-grown film whose material quality and cell performance are comparable to MOCVD-grown solar cells. Details of the MBE system preparation and MBE film growth procedure along with a detailed evaluation of the solar cells will be presented.

3.2 PREPARATION OF THE MBE SYSTEM

The MBE system used was a modular Varian GEN II. The furnaces were originally outgassed one at a time in a 35 cm-long, 6 cm-diameter nipple which was attached to a port on the entry chamber of the MBE. The nipple was mounted vertically via a 90° elbow. The nipple was water cooled with a copper tube which was wrapped around and brazed to the nipple. (The furnace sizes used for each source are listed in Table 3.2 along with the maximum temperatures used for outgassing.) The furnaces without pyrolytic born nitride (PBN) crucibles were outgassed for approximately 3 hrs at the maximum temperatures listed in Table 3.2. The furnaces were than ramped from room temperature to there maximum operating temperatures several times to have maximum current flowing through the heater windings and hence maximum heating and outgassing. A PBN crucible was then loaded into the furnace and outgassed for 1-2 hours at the temperature listed in Table 3.2. The furnace was then loaded into the growth chamber.

When all the furnaces were loaded in the growth chamber, a thermal cleaning of the growth chamber was conducted. With dry nitrogen flowing through the radial vane and cryoshrouds,

Table 3.1 Summary of MOCVD- and MBE-grown solar cell performance.

Growth Technique	Spectrum	Eff (%)	V_{oc} (V)	J_{sc} (mA/cm^7)	FF (%)	Area (cm^2)	Group	Ref
MOCVD	AM1.5	24.5	1.033	27.28	86.8	1.0	Spire	1
MOCVD	AM1.5	24.0	1.046	27.12	84.5	4.0	Varian	2
MOCVD	AM1.5	23.7	1.019	27.35	84.9	1.0	Kopin	3
MOCVD	AM1.5	24.8	1.029	27.89	86.43	0.25	Spire	4
MBE	AM1.5	23.8	1.018	27.56	84.65	0.25	Purdue	This Work
MBE	AM1	16.0	0.92	23.0	76.0	0.095	Lincoln Labs	5
MBE	AM1	17.5	0.867	29.2	69.3	0.25	Rockwell	6
MBE	AM1.5	17.1	0.94	23.9	76.3	-	NTT	7
MBE	AM1.5	15.8*	0.939	22.07	76.5	0.05	CNRS	8

*Cells did not have an anti-reflection coating.

Table 3.2 Source furnace outgas temperatures

Source	Varian oven size	Maximum Outgas temperature without PBN crucible	Maximum Outgas temperature with PBN crucible
As_4	120 cc	800°C	1050°C
Ga	60 cc	1000°C	1100°C
Al	60 cc	1000°C	1100°C
Si	5 cc	1500°C	1600°C
Be	5 cc	1500°C	1600°C

the furnaces were heated to 600°C along with the substrate heater. The purpose of the dry nitrogen was to avoid any excessively hot spots. The substrate heater was pointed for 45 min at the top, bottom, and load positions to heat the chamber walls. After the growth chamber walls were thermally cleaned, with liquid nitrogen now flowing through the radial vane and cryoshrouds, the furnaces were outgassed at the maximum temperatures listed in Table 3.2 for 3 hours.

The vendors and purities of the source material used are listed in Table 3.3. Since the Be and Si furnaces were placed in downward looking ports, the dopant sources had to be melted in the crucibles so they would adhere to the walls of the crucible. This melting was performed in the outgas nipple which was mounted vertically on the entry chamber and hence results in a symmetrical distribution of the dopant in the crucible. One gram of Be and 1/3 cc of Si chips were used in the dopant furnaces. The Ga crucible was filled with 75 gm of material. Seven Al pellets of 3 mm x 4-8 mm diameter were placed in the 60 cc crucible. This small amount of Al in the 60 cc crucible allows refreezing of the Al everyday without cracking of the PBN crucible. After loading the source material, the MBE system was baked for 72 hrs at 180°C. All furnaces were set at 200°C during the bake-out except for the As_4 furnace which was not heated. As a final note on the MBE system, all furnaces are set at 200°C except for the As_4 furnace which is set to 100°C and liquid nitrogen is not circulated through the radial vane or cryoshroud when the system is not in use.

3.3 MBE FILM GROWTH

The film was grown on a two-inch n^+ GaAs liquid-encapsulated-Czochralski wafer. It was the 33rd film grown in the MBE system after the initial loading of source material. (It should be noted that the 25th film grown in this system was a modulation doped heterojunction which had a mobility of $2x10^6 cm^2/Vs$ at 4.2 K indicating extremely high material quality [9].) The wafer was degreased, etched in a 60°C solution of 5:1:1 H_2SO_4:H_2O_2:H_2O for one minute, and placed in a non-indium wafer mount. The sample was then loaded on a carrying trolley and placed into the entry chamber of the MBE. The sample and trolley was outgassed at 200°C for two hours in the entry chamber. The trolley was then moved into the buffer chamber of the MBE. The sample was outgassed at 300°C for one hour on a heater station in the buffer chamber immediately before being loaded in the growth chamber. Liquid nitrogen was circulated through the radial vane and cryoshrouds starting two hours before initiating growth.

The MBE layers were grown at a substrate temperature of 600°C (580°C is the oxide desorption temperature) and the wafers were rotated at five revolutions per minute during most of the film growth. The film growth rates were determined from monitoring the intensity of the specular spot of the reflection high energy electron diffraction pattern [10].

The cross-section of the film is shown in Fig. 3.1. All layers were grown at a rate of 1.0 μm/hr except for part of the superlattice back surface field (BSF) layer. At a GaAs growth rate of 1

Table 3.3 Source Material

Source	Vendor	Form	Purity
As	Furakawa	120 cc slug	7N
Ga	Alcan Electronic Materials	100 gm bottle	8N
Al	Morton Thiokal Incorporated	3mm thick X 4-8mm diameter pellets	6N
Be	Atomergic Chemetals Corp.	0.33 gm chunks	5N
Si	Wacker-Chemitronic GMBH	crystalline wafer	carrier concentration $< 10^{14}$ cm^{-3}

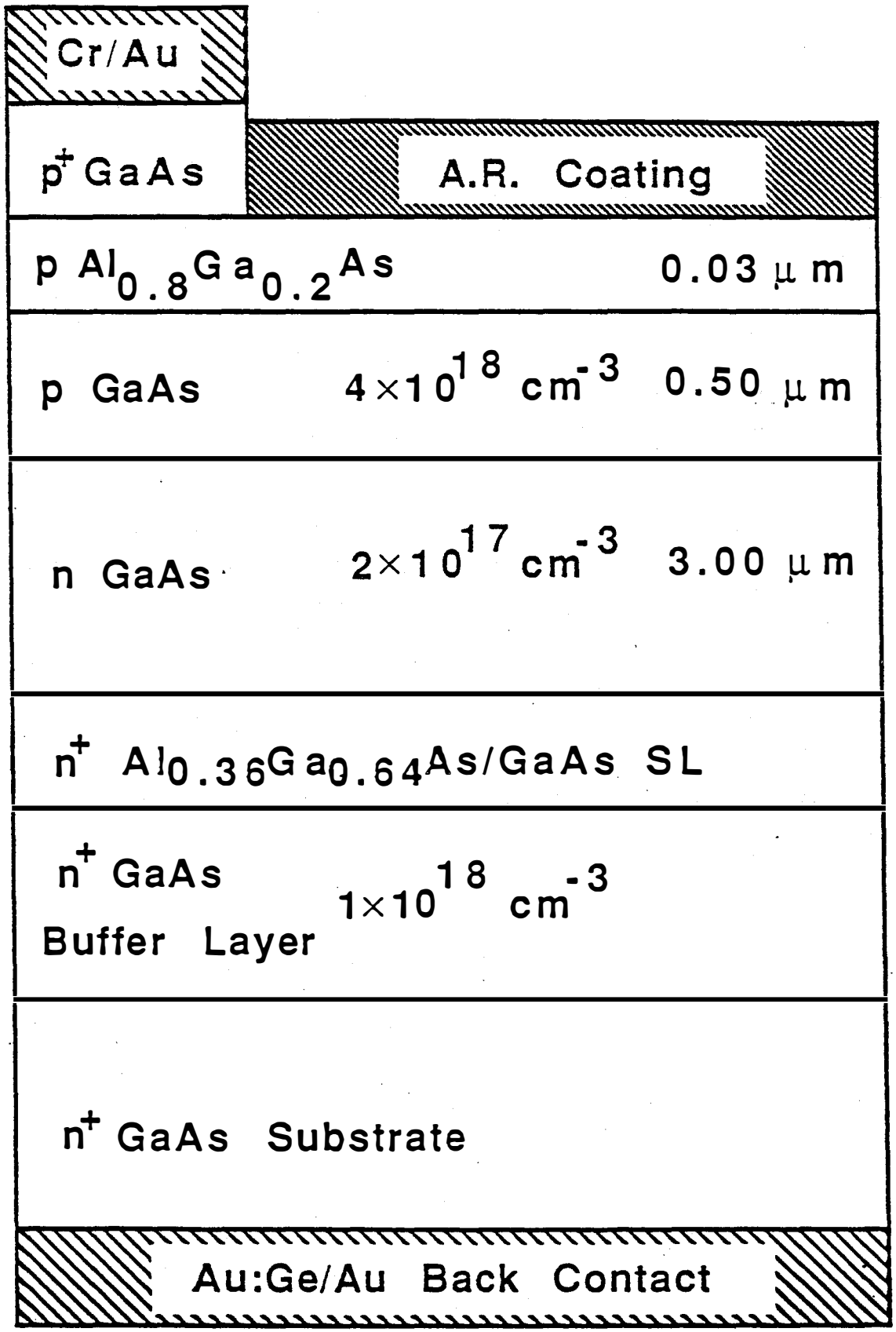

Fig. 3.1 Cross-section of the GaAs solar cell.

μm/hr, the As_4 to Ga beam equivalent pressure was 20 as determined by an ion gauge placed in the substrate growth position. The superlattice BSF layer consisted of a 20 period superlattice of 28Å $Al_{0.36}Ga_{0.64}As$ barriers and 27Å wells. (The $Al_{0.36}Ga_{0.64}As$ barriers were grown at a rate of 1.0 μm/hr and the GaAs wells at 0.64 μm/hr.) The superlattice BSF layer acts as a barrier to minority carrier holes in the n-GaAs region which increases the probability of their collection across the pn junction. A superlattice was used for this purpose rather than just a thick AlGaAs region since, in MBE, a GaAs region grown on a superlattice exhibits a better electrical interface than when a GaAs region is grown on a thick AlGaAs region [11,12].

After film growth the wafer was cleaved in half and solar cells were fabricated on one half. Test devices were fabricated and film characterizations (electrochemical profiling) were performed on the other half. The post-growth solar cell processing sequence was performed at Spire Corporation and has been described previously [13] and is briefly as follows. First, the wafer front was coated with SiO_2. Next a thin AuGe back ohmic contact layer was evaporated and alloyed, followed by an evaporated Au back metallization. Image-reversal photolithography was used to form a pattern for front grid metallization[14]. After etching SiO_2 in the grid openings, Cr and Au were evaporated for front contacts. The photoresist was dissolved to lift off excess metal, then the contacts were sintered. Photolithography was used to define a pattern for the mesa etch (0.5cm by 0.5 cm junctions), then a phosphoric acid-based etchant was used to form the mesa. All remaining SiO_2 was removed just prior to a selective cap removal etch (ammonium hydroxide-hydrogen-peroxide system). The etch removed the GaAs cap layer everywhere except under the grid lines and exposed the AlGaAs window layer. Finally, a double-layer antireflection coating of ZnS and MgF_2 was thermally evaporated.

3.4 EXPERIMENTAL RESULTS

The half of the wafer which was processed into solar cells contained 15 solar cells of dimension 0.5 cm by 0.5 cm. The solar cells were measured under 1-sun AM1.5 conditions at Spire Corporation and the Solar Energy Research Institute. A yield of 100% was obtained with the best cell demonstrating an efficiency of 23.8%. Excellent uniformity was also obtained with an average efficiency of 23.1% and a standard deviation of 0.4%. The measured solar cell parameters for our most efficient MBE-grown cell are listed as the first MBE entry in Table 3.1.

As can be seen from the Table 3.1 comparison of MOCVD- and MBE-grown solar cells, ours is the first MBE-grown solar cell of comparable performance to MOCVD-grown solar cells. In comparing our MBE-grown solar cell to the best reported MOCVD-grown cell [4], the major difference in the cells is the fill factor (FF). FF relates the maximum power (P_m) obtainable from the cell to the product of the open-circuit voltage (V_{oc}) and short-circuit current (I_{sc}) of the cell, $FF=P_m/I_{sc}V_{oc}$. The more nearly square the diode's current-voltage (IV) characteristic, the higher the FF. The lower FF for our MBE-grown cells is due to non-ideal leakage currents at low current levels. These leakage currents will be discussed below.

The current of a mesa-isolated GaAs pn junction is comprised of components due to recombination in the bulk space-charge region, recombination within the space-charge region exposed at the perimeter of the mesa, and recombination in the bulk neutral regions. Therefore, the current-voltage characteristic of a GaAs pn junction is expected to have the form,

$$I=J_{O2B}A(e^{qV/2kT}-1)+J_{O2P}P(e^{qV/2kT}-1)+J_{O1}A(e^{qV/kT}-1) \quad (3.1)$$

where J_{O2B} is the bulk saturation current component (A/cm^2), J_{O2P} is the perimeter component (A/cm), J_{O1} is the diffusion saturation current component (A/cm^2), A is the area of the diode and P is the perimeter. A non-ideal leakage current manifests itself as a region of the lnI vs V plot whose slope is less than q/2kT. Such a leakage current will result in a decrease in the FF of a solar cell.

To investigate leakage currents in our films, a series of mesa-isolated diodes were fabricated on the other half of our two-inch wafer and also on a second wafer whose film structure was similar to that shown in Fig. 3.1. These mesa-isolated diodes ranged in area from 2.5×10^{-5} cm^2 to 0.25 cm.^{2} Shown in Fig. 3.2 is th IV characteristic for one of the 0.25 cm^2 diodes which exhibits a non-ideal leakage current. All 15 of the solar cells and all 5 of the 0.25 cm^2 diodes exhibit this non-ideal leakage current. (Note a solar cell has a grid metallization on the top surface while a diode is completely metalized.) Also shown in Fig. 3.2 is the IV characteristic for two different 0.01 cm^2 diodes. The IV characteristic of one of these 0.01 cm^2 diodes is ideal without any leakage current while the other 0.01 cm^2 diode has a leakage current. The correlation between leakage current and diode area is more fully displayed in Table 3.4 and indicates that the source of the leakage current is isolated defects. The oval defect density in our two films was 500 cm^{-2} and also displayed in Table 3.4 is the average number of oval defects for that given area diode. Because the top surface of the diode was metallized, the actual number of oval defects a diode had could not be determined. However the correlation between the oval defect density and the leakage currents suggest that the oval defects are a likely source of leakage currents.

The q/2kT current of a mesa-isolated GaAs diode is comprised of components due to recombination in the bulk space-charge region and within the space-charge region exposed at the perimeter of the mesa. From equation (1) we see that we can write the q/2kT saturation current as,

$$I_{O2}=J_{O2B}A+J_{O2P}P \quad (3.2)$$

By plotting I_{O2}/A versus perimeter-to-area (P/A) ratio, the bulk and perimeter components can be extracted from the slope and intercepts of the plot. The series of mesa-isolated diodes described previously had P/A ratios varying form 40 to 800 cm.$^{-1}$ From the measured IV characteristics of these test diodes, the q/2kT current was extracted by curve fitting to (1) and plotted as shown in Fig. 3.3. From the slope of Fig. 3.3 one obtains $J_{O2P}=1.58\times10^{-13}$ A/m. Because the intercept is small an accurate value for J_{O2B} cannot be obtained but we can say that $J_{O2B}<2.5\times10^{-11}$ A/cm.^{2} So even for the large 0.25 cm^2 solar cells the q/2kT current is due to perimeter recombination as has been observed before for high quality MOCVD GaAs diodes

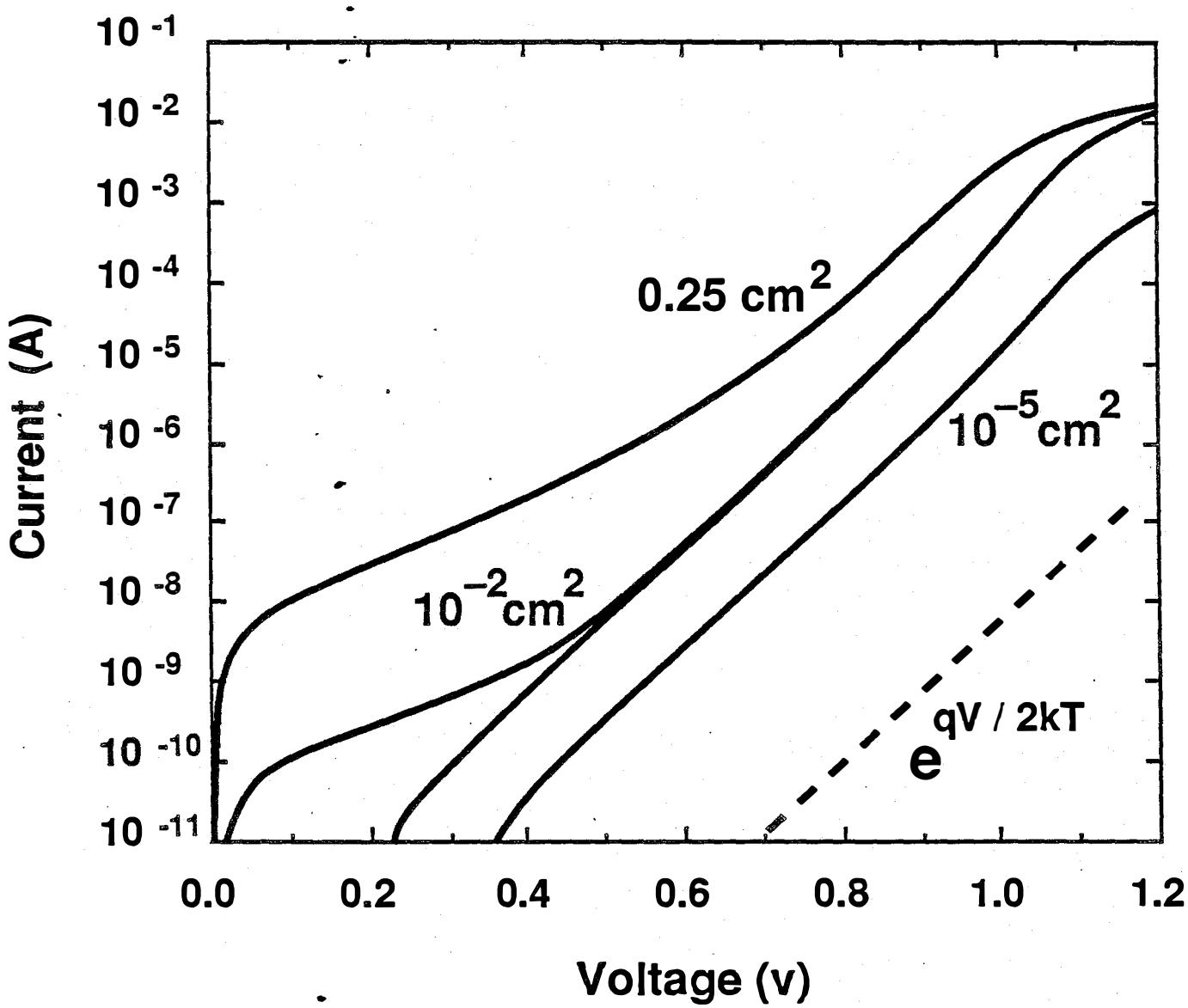

Fig. 3.2 Comparison of current-voltage characteristics for different area GaAs diodes.

Table 3.4 Correlation between diode area and leakage currents.

diode area (cm^2)	number of diodes tested	number of diodes exhibiting leakage currents	average number of oval defects
0.25	20	20	125
0.01	24	12	5
2.5×10^{-3}	24	6	1.25
1×10^{-4}	24	2	0.05

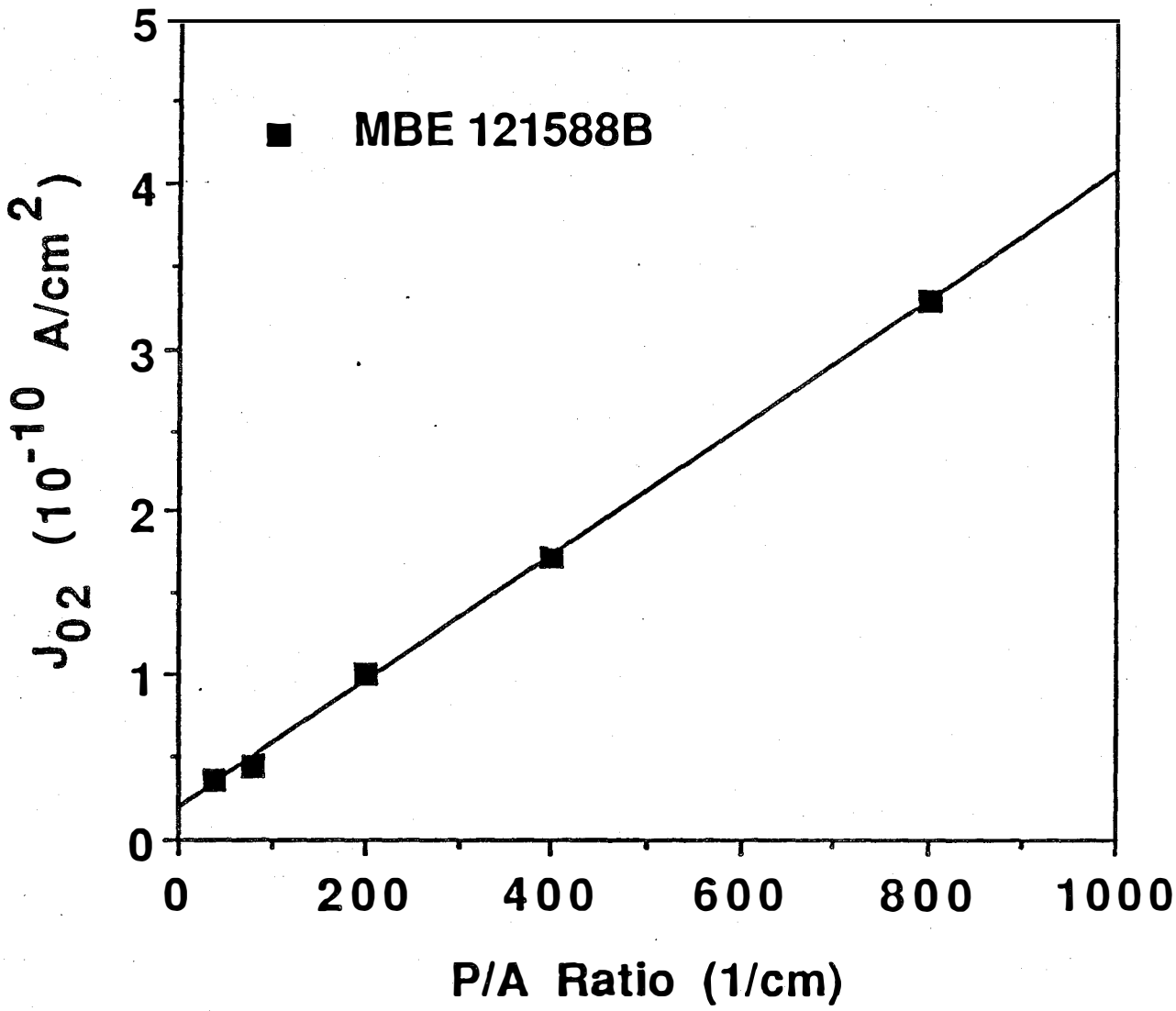

Fig. 3.3 Plot of extracted J_{o2} versus perimeter-to-area ratio for MBE-grown GaAs diodes.

[15]. The fact that the bulk q/2kT component is so small for our MBE-grown diodes indicates high space-charge-recombination lifetimes.

3.5 SUMMARY

We have obtained 1-sun AM1.5 efficiencies of 23.8% for 0.25 cm^2 GaAs solar cells fabricated on MBE-grown material. This is the first solar cell fabricated on MBE-material which is of comparable performance to solar cells fabricated on MOCVD-grown material. The major efficiency limiting mechanism of our MBE solar cells are leakage currents at low current levels which reduce the fill factors (FF) of the cells. These leakage currents are due to isolated defects and appear to correlate with the oval defects in the film. The oval defect density of the film was 500 cm^{-2} which can be reduced significantly in the future [16-17] and should result in even higher MBE-grown solar cell efficiencies.

CHAPTER 3 REFERENCES

[1] S.P. Tobin and S.M. Vernon, *Technical Digest of the 4th International Photovoltaic Science and Engineering Conference*, Sydney, Australia, February 14-17, 1989.

[2] K. Burkess, M. Ladle, and H.C. Hamaker, *Conference Record of the 20th IEEE Photovoltaic Specialists Conference*, Las Vegas, Nevada, September 1988.

[3] R.P. Gale, R.W. McClelland, B.D. King, and J.V. Gormley, *Conference Record of the 20th IEEE Photovoltaic Specialists Conference,* Las Vegas, Nevada, September 1988.

[4] S.P. Tobin, S.M. Vernon, C. Bajgar, S.J. Wojtczuk, M.R. Melloch, A. Keshavarzi, T.B. Stellwag, S. Venkatensan, M.S. Lundstrom, and K.A. Emery, to appear in *IEEE Transactions on Electron Devices*, February 1990.

[5] John C.C. Fan, A.R. Calawa, Ralph L. Chapman, and George W. Turner, *Appl. Phys. Lett.* **35**, 804(1979).

[6] D.L. Miller and J.S. Harris, Jr., *Appl. Phys. Lett.*, **33**, 1104(1981).

[7] Chikara Amano, Masafumi Yamaguchi and Atsushi Shibukawa, *Technical Digest of the International PVSEC-1*, Kobe Japan, 845(1984).

[8] A. Saletes, J.P. Contour, M. Leroux, J. Massies, N. Defrànould, and G. Pelous, *Solar Cells*, **17**, 373(1986).

[9] M.R. Melloch, D.C. Miller, and B. Das, *Appl. Phys. Lett.*, **54**, 943(1989).

[10] J.H. Neave, B.A. Joyce, P.J. Dobson, and N. Norton, *Appl. Phys. A*, **31**, 1(1983).

[11] T.J. Drummond, J. Klem, D. Arnold, R. Fischer, R.E. Thorne, W.G. Lyons, and H. Morkoc, *Appl. Phys. Lett.*, **42**, 615(1983).

[12] K.L. Tan, M.S. Lundstrom, and M.R. Melloch, *Appl. Phys. Lett.*, **48**, 428(1986).

[13] S.P. Tobin, S.M. Vernon, C. Bajgar, L.M. Geoffroy, C.J. Keavney, M.M. Sanfacon, and V.E. Haven, *Solar Cells*, **24**, 103(1988).

[14] S. P. Tobin, M.B. Spitzer, C. Bajgar, L. Geoffroy, and C.J. Keavney, *Conference Record of the 19th IEEE Photovoltaics Specialists Conference*, pp. 70-75, 1987.

[15] P.D. DeMoulin, S.P. Tobin, M.S. Lundstrom, M.S. Carpenter, and M.R. Melloch, *IEEE Elec. Dev. Lett.*, **EDL-9**, 368(1988).

[16] S-L. Weng, C. Webb, Y.G. Chai, and S.G. Bandy, *Appl. Phys. Lett.*, **47**, 391(1985).

[17] A. Salokatve, J. Varrio, J. Lammasniemi, H. Asonen, and M. Pessa, *Appl. Phys. Lett.*, **51**, 1340(1987).

CHAPTER 4

PHOTOVOLTAIC CHARACTERIZAT ›N OF $Al_{0.2}Ga_{0.8}As$ SOLAR CELLS

4.1 INTRODUCTION

The ternary semiconductor $Al_xGa_{1-x}As$ is being widely-stuc ›d as a material for the top cell in tandem cell applications [1-5]. To optimize $Al_xGa_{1-x}As$ ce efficiency, a detailed understanding of recombination losses and their relation to materia quality and cell design is required. In this chapter we compare the material properties of vo $Al_{0.2}Ga_{0.8}As$ films, one grown by molecular beam epitaxy (MBE), the other by metalorgar : chemical vapor deposition (MOCVD). The objective is to quantify recombination losses, rei :e them to material parameters, project cell performance achievable with present-day material and, finally, to prioritize the research problems that need to be addressed in order to maximize A $_xGa_{1-x}As$ cell performance.

4.2 FILM GROWTH AND DEVICE PROCI ›SING

The MBE AlGaAs layers were grown on a two inch n^+ liq d encapsulated Czochralski (LEC) substrate in a Varian GEN II MBE system at Purdue Uni rsity. The source materials consisted of elemental Ga, As, Al, Si, and Be. AlGaAs layers we : grown at an elevated temperature of $\simeq 675°C$ to reduce the nonradiative mid-gap trap, ME [6], while the GaAs buffer and cap layers where grown at 600°C (the oxide desorption temper ure was 580°C). Reflection high energy electron diffraction patterns were used to determine e growth rates and monitor the growth conditions. The measured growth rates were one micr neter per hour for both the AlGaAs and the GaAs layers. To retain high bandgap and dopi ; uniformity, the wafer was rotated at five revolutions per minute.

The MOCVD film was grown on an n^+ horizontal Bridg an substrate in a SPI-MO CVD™ 450 epitaxial reactor at the Spire Corporation. The re tor is a vertical-geometry, barrel-type operating at atmospheric pressure. Trimethylgallium, t nethylaluminum, and arsine were the source gases, with silane and dimethylzinc diluted in hy ogen used for n- and p-type dopants. The active layers were grown at 800°C with a 20:1 grou V-III flow ratio. The temperature was lowered to 700°C during the growth of the cap layer t assure a high p^+ doping for low-resistance, non-alloyed p-type contacts.

Because the objective of this work was the diagnostic evaluation of material quality and identification of recombination losses, no attempt to fabricate high-efficiency cells was undertaken. Rather, a variety of test structures was fabricated. By processing the MBE- and MOCVD-grown films together, the effects of processing variations were minimized. Two different processing runs with two different mask sets were completed. The first run produced diodes with areas ranging from 2.5×10^{-5} cm^2 to 0.01 cm^2 and perimeter to area ratios from 40 to 600 cm^{-1}. Solar cells for internal quantum efficiency measurements were produced in the second fabrication run. Both diodes and solar cells were processed using standard photolithography, lift-off, and mesa etching techniques. For the solar cells, a selective etch was used to remove the GaAs cap, and SiO_2 was deposited to passivate the exposed window surface and act an a non-optimized antireflection coating. (Later, it was found that the etch attacked the high Al content window, so all cells suffered from a high front surface recombination velocity.)

4.3 DEVICE CHARACTERIZATION

A variety of measurements was undertaken in order to characterize the AlGaAs material and to quantify recombination losses. Although the MBE and MOCVD films were targeted to be identical, differences invariably occurred in the Al content and layer dopings. The doping profile of the MBE-grown film was measured by electrochemical and junction C-V profiling, and the results are displayed in Fig. 4.1a. Electrochemical profiling was unsuccessful for the MOCVD-grown film, but the measured slope of the reverse-biased $1/C^2$ vs. voltage characteristic was consistent with the targeted dopings displayed in Fig. 4.1b.

Room temperature photoluminescence (PL) was used to determine the Al content of the films. The PL intensity was measured using a 514.5 nm Ar^+ laser with a power density of 1.0 W/cm^2. To avoid intensity shifts due to different doping levels and dopant types, the cells were etched to expose the AlGaAs base. The results shown in Fig. 4.2, therefore, represent the n-type AlGaAs. The Al content was determined from the peak in the PL intensity using the room temperature band gap versus mole fraction formulae as given by Casey and Panish [8]. A mole fraction of 0.18 was deduced for the MOCVD-grown material and 0.22 for the MBE-grown film. Previous work on PL wafer mapping showed that a mole fraction variation of about 0.02 across a wafer is typical for these MOCVD-grown films [5]. It was also noted that the intensity of the PL emission was more than a factor of two lower for the MBE-grown film, which suggests that its minority carrier lifetime was somewhat lower than that of the MOCVD-grown film.

The forward-biased dark current-density versus voltage characteristics were measured using a HP 4145 semiconductor parameter analyzer. Fig. 4.3 displays the measured characteristics for small (1.0×10^{-4} cm^2) and large (0.25 cm^2) area diodes. The smaller cells display a linear slope of q/2kT which indicates that their dark current in this range is dominated by recombination in space-charge regions. The larger MOCVD cells behave much like the small MOCVD cells, but

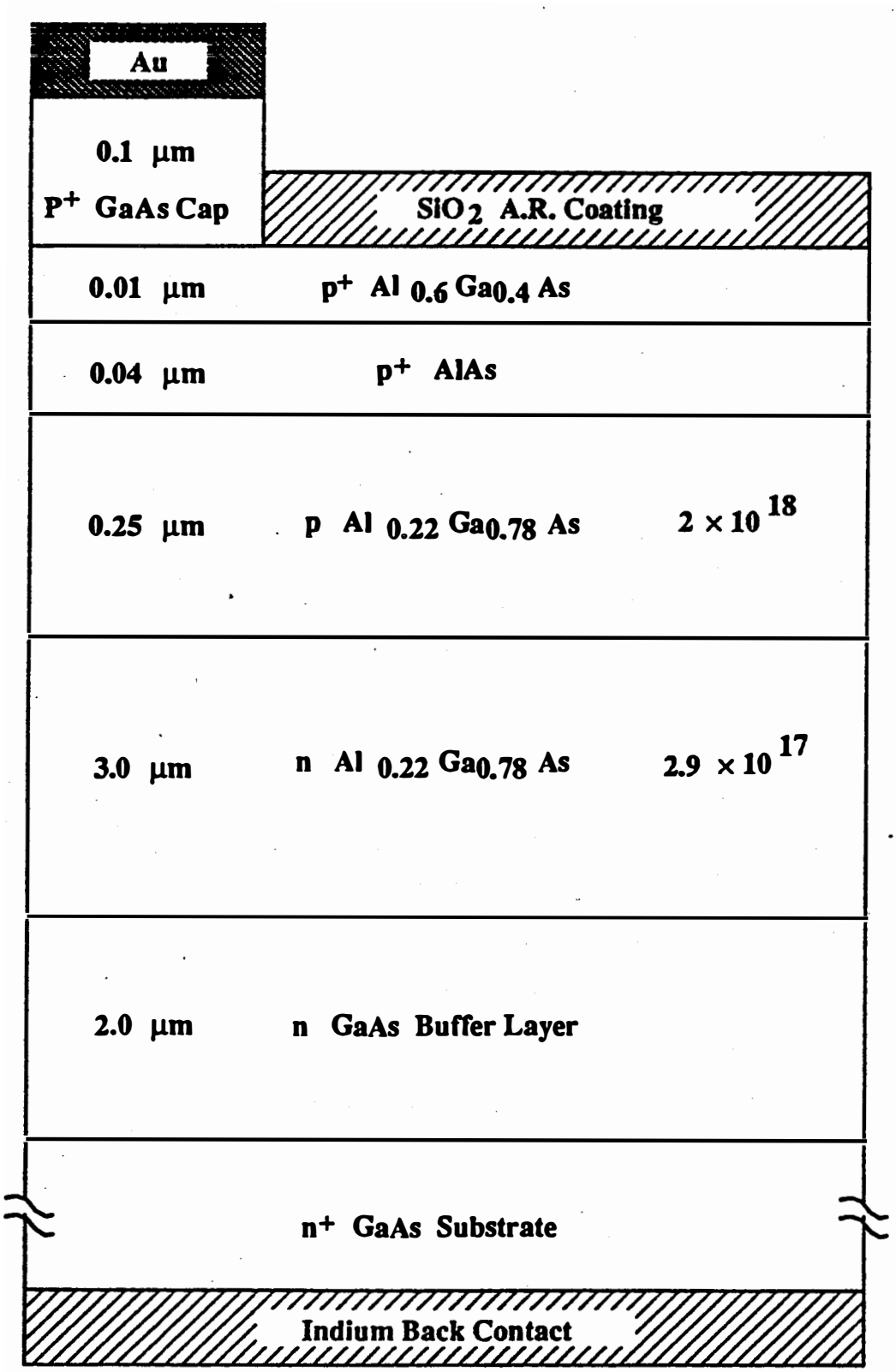

Fig. 4.1a Device structure for diodes fabricated on MBE-grown films.

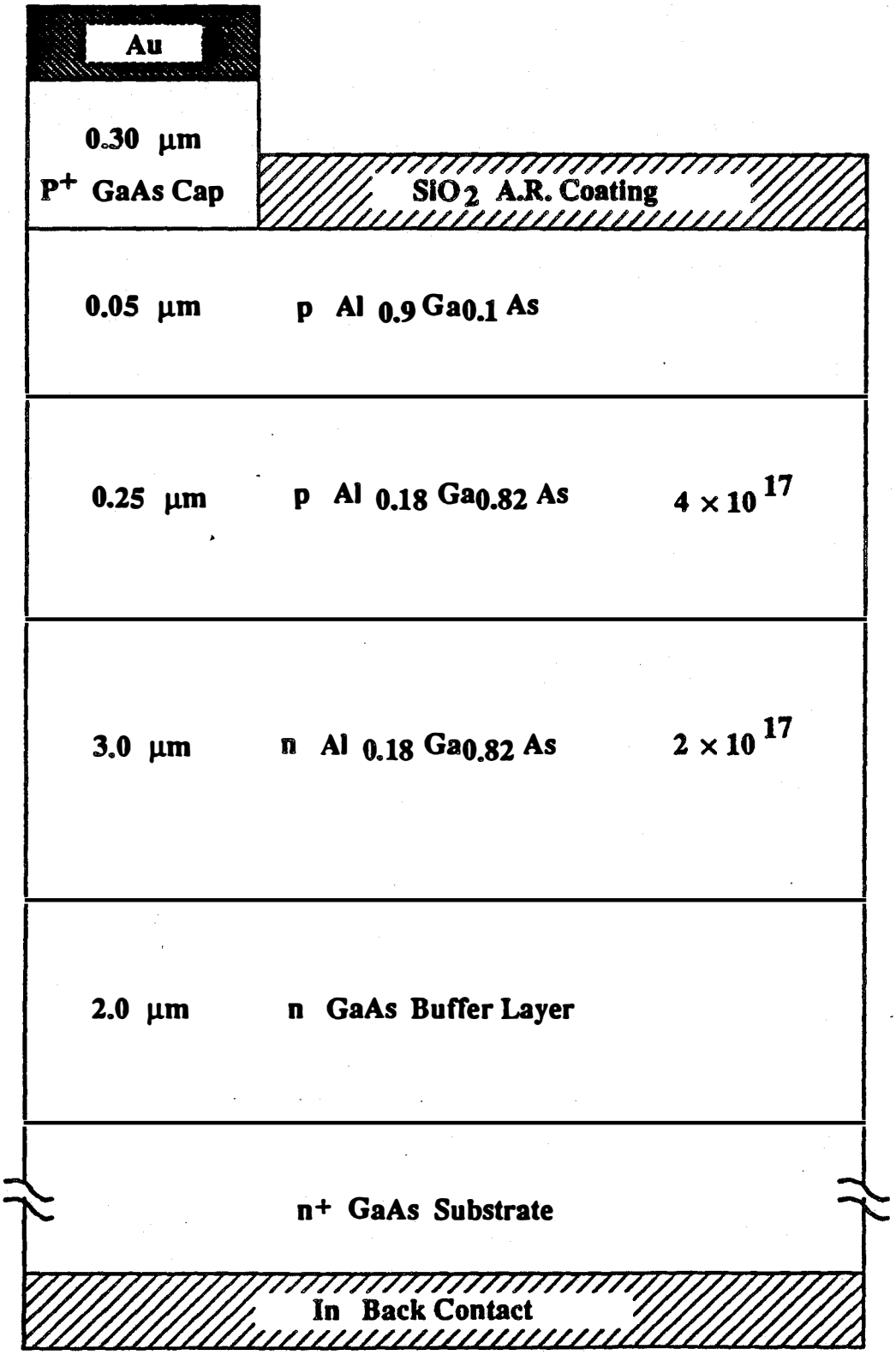

Fig. 4.1b Device structure for diodes fabricated in MOCVD-grown films.

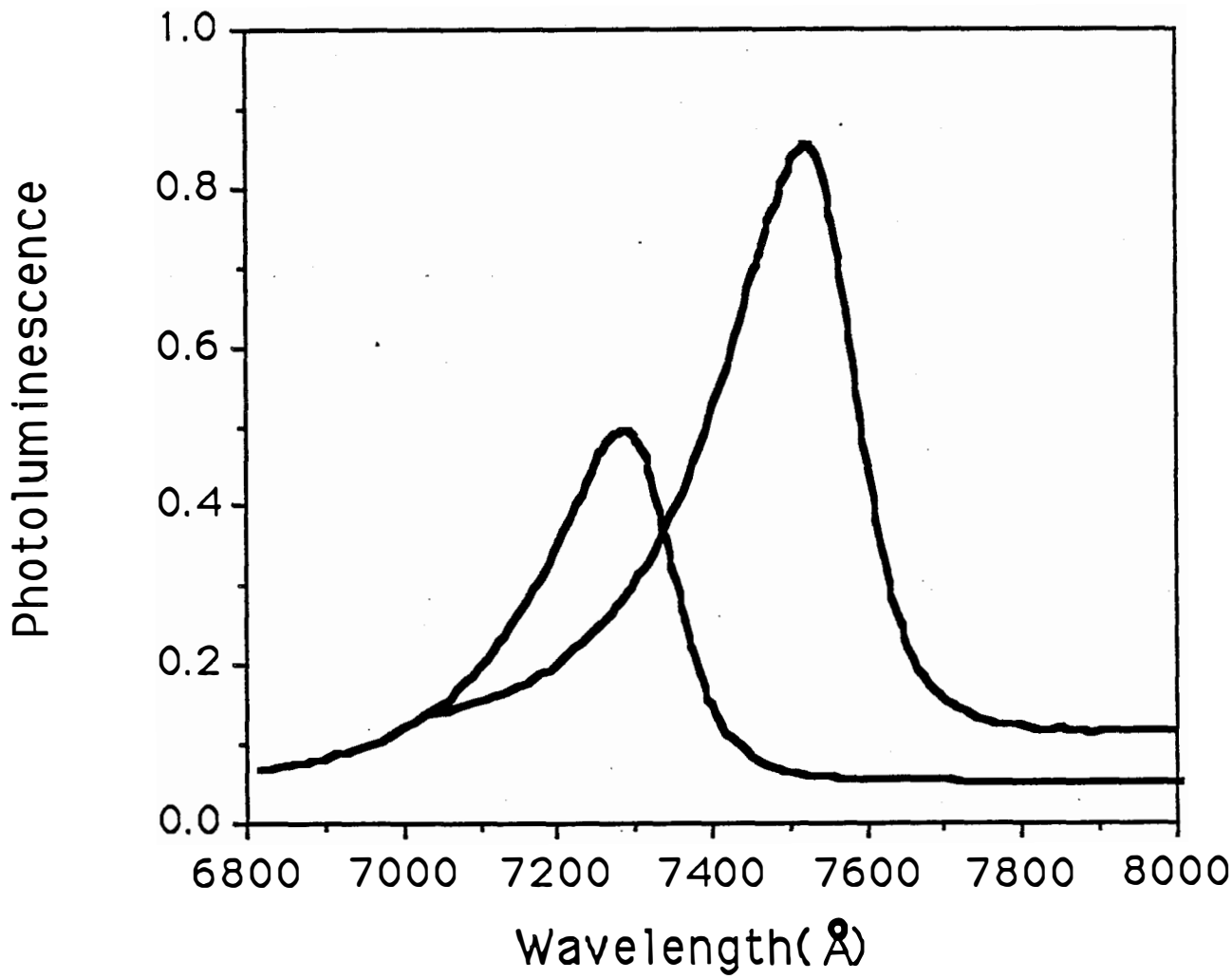

Fig. 4.2 Comparison of room temperature photoluminescence spectra of MBE-grown and MOCVD-grown n-type $Al_{0.2}Ga_{0.8}As$ films. The peak PL emission intensity is more than a factor of 2 lower for MBE-grown film.

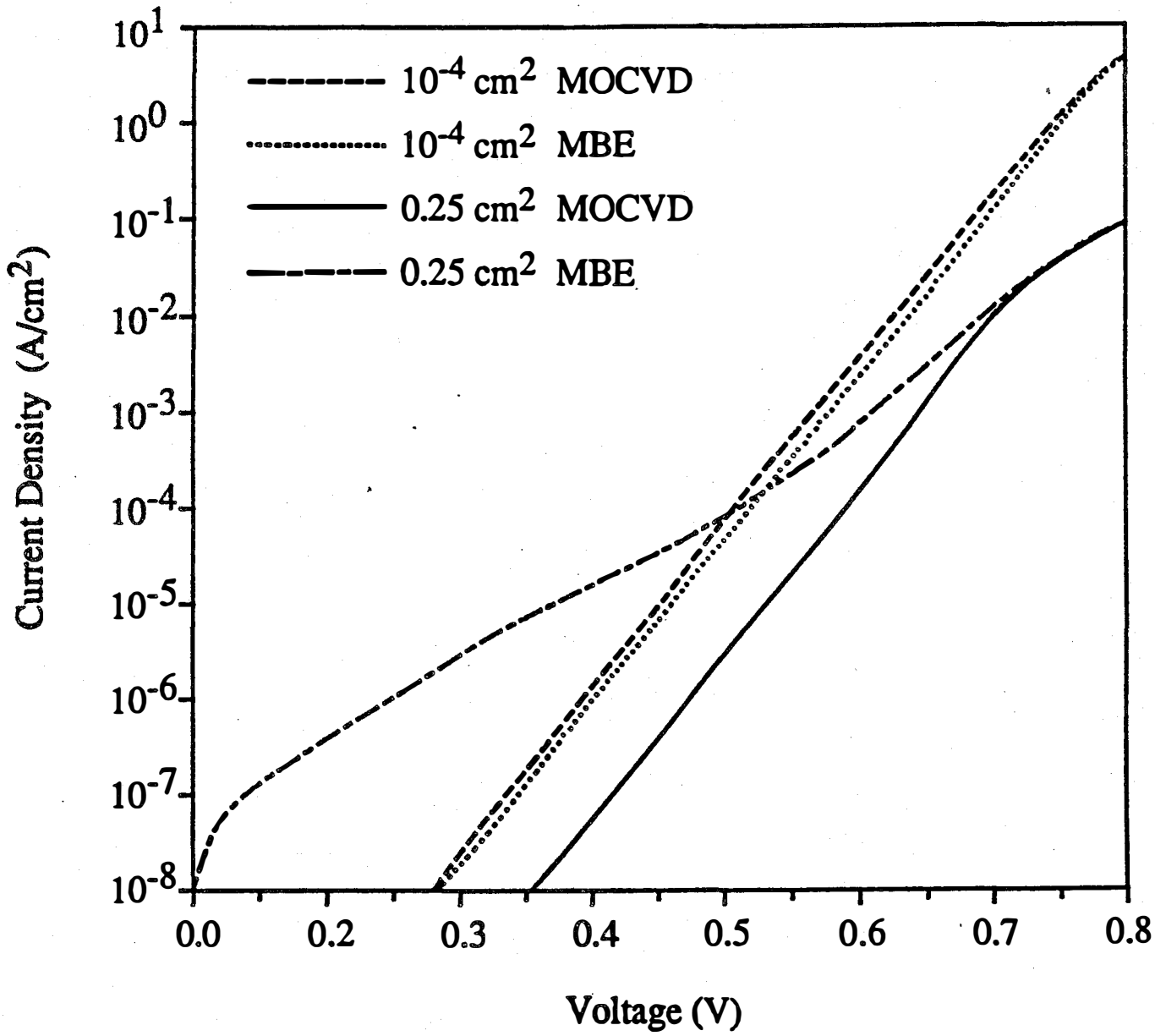

Fig. 4.3 Dark I-V characteristic at 25°C for small and large area diodes. Small diodes have an area of 1.0×10^{-4} cm^2; the large ones have an area of 0.25 cm^2. For the MOCVD diodes, the results displayed are the lowest measured currents of 15 diodes, and for the MBE film they are the lowest currents from 13 diodes. (The highest currents were about 25% greater on the MOCVD diodes and about 30% higher on the MBE diodes.) Note the higher current density of smaller diodes due to perimeter recombination current.

a sizeable shunt leakage is observed in large area, MBE cells. The shunt leakage is thought to be related to bulk defects because it was observed with increasing frequency as the diode area increased.

A careful study of the MBE films reveals the existence of oval defects with density of 300 to 400 per cm^2. Such defects are not present on the MOCVD-grown films. Their size ranges from 1 to 20 μm. Oval defects can have their origins in particulates and other contaminants on the surface of the starting substrate prior to the growth and/or defects introduced during the growth by the MBE system [15]. The presence of oval defects has been shown to increase p-n junction leakage currents [11, 16]. Common sources of leakage current include edges (junction perimeter), metal spiking through the p/n junction, and defects, which can produce defect-assisted tunneling or shunt conduction paths. Both MBE and MOCVD films had the same structure and were processed simultaneously, so edge leakage and metal spiking, which are sensitive to device fabrication, are unlikely to be the source of the leakage. This suggests that the $n > 2$ shunt leakage current is caused by oval defects or some other inherent defects in MBE-grown AlGaAs. Similar effects have also been observed in MBE-grown GaAs solar cells, but the leakage is typically small at the operating voltage [11]. (Although the leakage did reduce the fill factor somewhat, 1-sun AM1.5 conversion efficiencies of 23.8% for 0.5 cm by 0.5 cm GaAs solar cells were still achieved [11].) To maximize cell efficiency for MBE-grown films, however, the cause of the leakage current will need to be identified and its magnitude reduced because the shunt $n > 2$ leakage current will limit the fill factor and will cause a small open circuit voltage loss.

The time at which oval defects are formed during film growth can also be crucial in determining the magnitude of the leakage current [16]. Poor quality and leakage may be observed for solar cells and diodes where a defect is formed before p/n junction formation, whereas, oval defects formed near the surface do not seriously affect diode properties. The logorithmic plot of the dark current versus voltage measured at 26.5°C of various 0.01 cm^2 solar cells containing different number of oval defects is shown in Fig. 4.4. There are four dark I-V curves representing cells containing zero, one, two, and three particulate type oval defects from bottom to top. This figure demonstrates that there is no one-to-one correlation between the number of oval defects present on a device and the magnitude of the observed leakage current. But the data do suggest that the leakage increases as the number of oval defects increases. Electrically inactive oval defects and their time of formation may be the cause of this phenomena. The dark I-V of a relatively low leakage 0.01 cm^2 solar cell without any oval defects is shown in the bottom curve of Fig. 4.4. The small magnitude of the shunt leakage in this cell as compared to the much larger leakage current of the cells containing oval defects suggests that although other defects are present in AlGaAs material, they don't seem to contribute significantly to the observed leakage in the MBE films. It is still necessary to investigate the electrically active defects present in our films using an infra-red microscope or electron induced beam current in an SEM. Such measurements should enable us to relate the the magnitude of the shunt leakage to the number of electrically active oval defects.

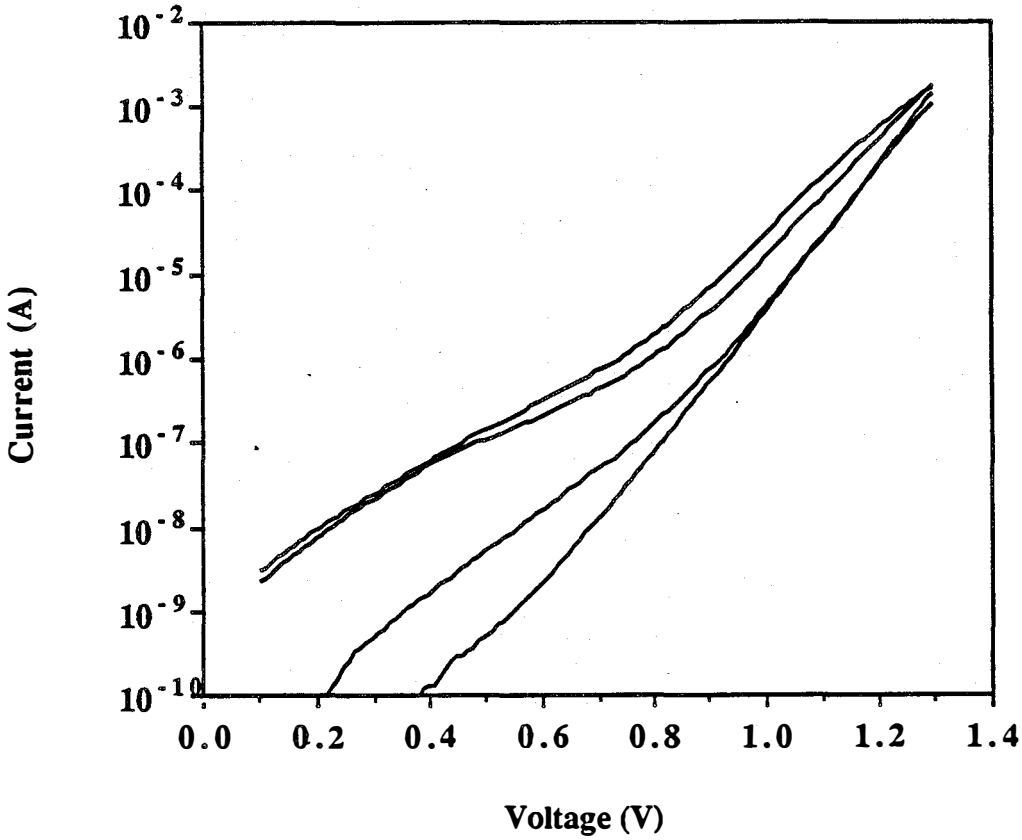

Fig. 4.4 Dark I-V characteristic at 26.5°C of 0.01 cm^2 MBE-grown $Al_{0.2}Ga_{0.8}As$ solar cells used for oval defects study. The oval defects counted are mainly the type due to particulate contaminants prior to the growth having density of 300 to 400 per cm^2. The leakage current increases as the number of oval defects increases. Four plots represent dark I-V of 0.01 cm^2 cells containing zero, one, two, and three oval defects in order from bottom to top. The region of interest is at low voltage bias and the magnitude of shunt leakage does not vary linearly with the number of oval defects. Current axis is logarithmic and the only conclusion is that the leakage current will increase as the frequency of defects increases. Note that the cell without any oval defects is still a little bit leaky.

At Purdue, the oval defects are mainly attributed to the substrate cleanliness and preparation. The wafers are cleaned in a different building than the one containing the MBE system. Although as much care as possible is taken to maintain a clean substrate, particulates have a good chance of being present on the starting substrate. Oval defect densities should be greatly reduced in the near future when class 100 cleanroom conditions are employed for preparing the substrates.

It is also interesting to note that the small area diodes display a higher current density (defined simply as the measured current divided by the diode area) than do the larger diodes as displayed in Fig. 4.3. This result suggests that the n = 2 current component is comprised of components from both the bulk and perimeter space-charge regions. The n = 2 saturation current density can be written as

$$J_{o2} = J_{o2p} \frac{P}{A} + J_{o2b} \tag{4.1}$$

where J_{o2b} (units= A/cm^2) is the bulk component and J_{o2p} (A/cm) is the perimeter component. The saturation current density, J_{o2}, was extracted from the measured J-V characteristic by least squares curve fitting. When the extracted J_{o2} is plotted versus P/A as displayed in Fig. 4.5, both the perimeter and bulk current components can be determined. When the results of Fig. 4.5 are scaled to a 0.5 cm × 0.5 cm cell, we find that bulk and perimeter recombination contribute about equally to the n = 2 current component. By contrast, similar sized GaAs cells were observed to be dominated by perimeter recombination [12]. These observations suggest that the bulk lifetimes in AlGaAs films are somewhat lower than they are in high-quality GaAs.

Recombination losses under illuminated conditions were probed by performing internal quantum efficiency (QE) measurements on both MBE and MOCVD cells. Because emitters are typically thinner than a minority carrier diffusion length, it is generally impossible to extract the front surface recombination velocity and emitter diffusion lengths independently from such measurements. Moreover, due to the processing problems encountered during cap removal, very high front surface recombination velocities resulted. The base layers, however, were thicker than a diffusion length, so it was possible to extract the base diffusion length with confidence. For the MOCVD-grown film, a base diffusion length of $L_p = 1.5$ μm was obtained, and for the MBE-grown film we found $L_p = 0.8$ μm. Assuming similar diffusion coefficients for the two films, these results suggest that the minority carrier hole lifetime in the n-AlGaAs films grown by MOCVD is roughly 3-4 times higher than the lifetime in the MBE-grown film. The internal QE measurements are consistent with the PL measurements which showed a factor of 2.4 larger signal for the MOCVD-grown film.

To relate the photoluminescence and internal quantum efficiency measurements to material quality, deep level transient spectroscopy (DLTS) measurements were made on 2.22×10^{-3} cm^2

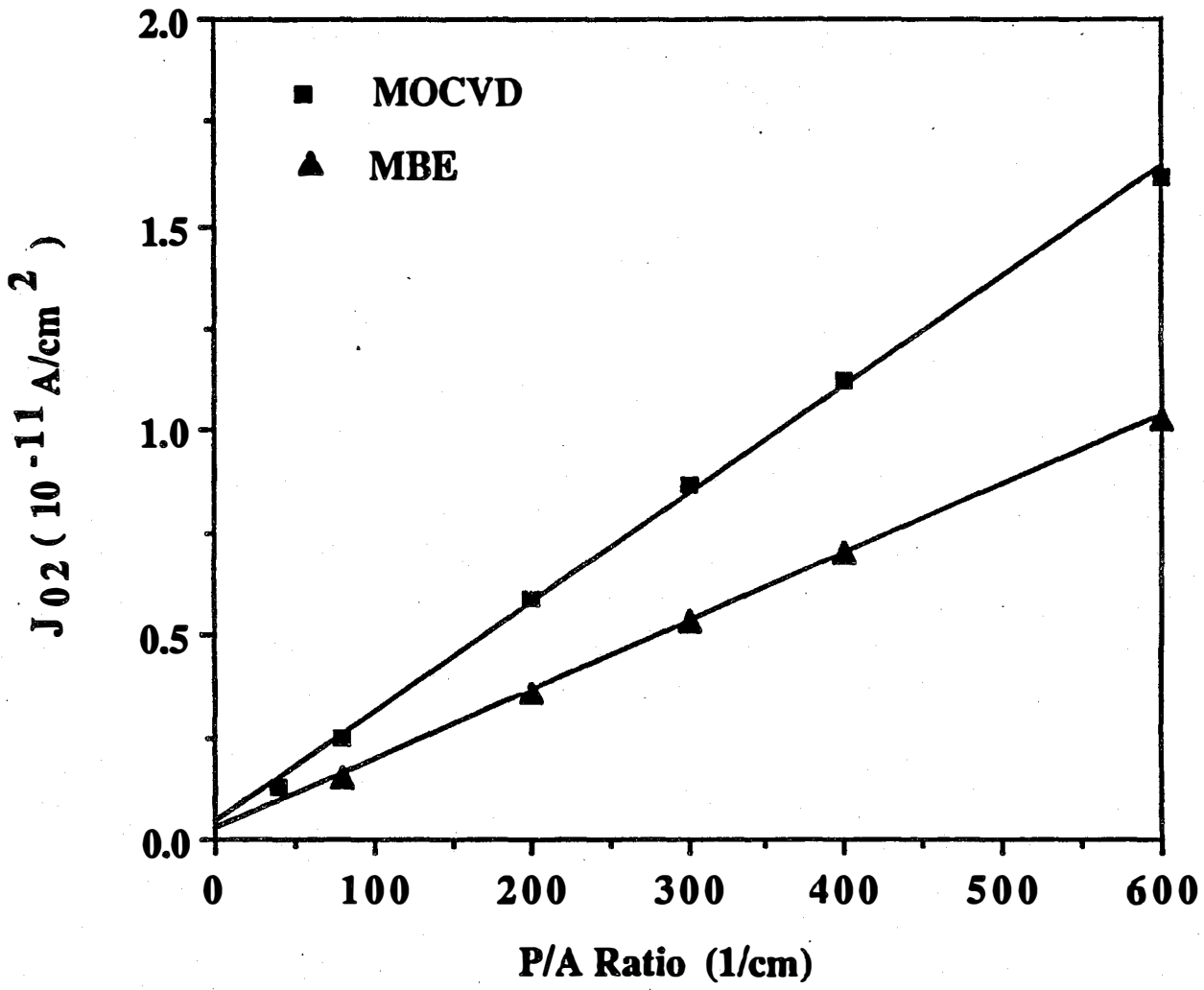

Fig. 4.5 Plot of J_{o2} versus perimeter to area ratio, P/A. The slope and intercept are perimeter and bulk components respectively of n=2 current. These measurements are from the same die used for the J-V measurements displayed in Fig. 4.3.

diodes from each film. Deep levels were observed in both films as show in Fig. 4.6. The trap parameters are summarized in Tables 4.1 and 4.2. The trap at 0.45 ± 0.01 eV below the conduction band edge, observed in both the MOCVD- and the MBE-grown films is identified as the donor-vacancy complex (DX) [6]. The concentration of DX centers in the MBE film is approximately eight times the concentration in the MOCVD material, which is consistent with its higher Al content.

A trap associated with a DLTS peak at approximately 370°K was also detected in both the MBE and the MOCVD films. This trap is characterized by an activation energy of 0.66 eV; its capture cross-section, σ_n, and concentration, N_T, are detailed in Tables 4.1 and 4.2. Previous investigations of AlGaAs films (grown by both MBE and MOCVD techniques) have detected the presence of a similar trap [6,9]. Comprehensive studies of electron traps in MBE AlGaAs [6] have shown that the trap (identified as ME6 in the MBE literature) is highly sensitive to the growth conditions. Its presence in MBE films has been attributed to arsenic oxide originating from the arsenic source [6]. The origin of the trap in MOCVD films has not been conclusively identified, although investigators have suggested that it may be tied to an Al-O or an O-vacancy complex [9]. For MBE films, the concentration of ME6 increases with Al content and decreases as the substrate temperature increases. For our MBE-grown films, the concentration of ME6 was about 2.7 times higher than in the MOCVD-grown films.

Finally, the trap at $E_C - 0.79$ eV was observed only in the MOCVD material. This trap has been associated with native defects in the AlGaAs films and is commonly identified as EL2 [10]. Both EL2 and ME6 traps have been shown to function as non-radiative recombination centers [6,12]. As noted previously, the ME6 concentration in the MBE-grown film was greater than the combined ME6 and EL2 concentration in the MOCVD-grown film, while the PL emission intensity was more than a factor of two lower in the MBE film. The base diffusion length extracted from the internal QE measurements was likewise shorter in the MBE solar cell than in the MOCVD solar cell. Both the PL and internal QE measurements are, therefore, consistent with the higher trap concentrations observed in the MBE-grown films.

4.4 DISCUSSION

In order to assess the quality of these films for high-efficiency solar cell applications, it is of interest to project achievable efficiencies using the measured and estimated material parameters. For these projections, we assumed that the minority carrier electron lifetime in the p^+-emitter (which was not measured) was equal to the hole lifetimes observed in the n-base. Because high-quality AlGaAs/GaAs window layers with interface recombination velocities of less than 10^4 cm/sec are now regularly achieved [13], a front surface recombination velocity of 10^4 cm/sec was assumed. The n = 2 dark current was then evaluated assuming 0.5 cm × 0.5 cm cells along with the measured bulk and perimeter saturation current densities. Using well-known

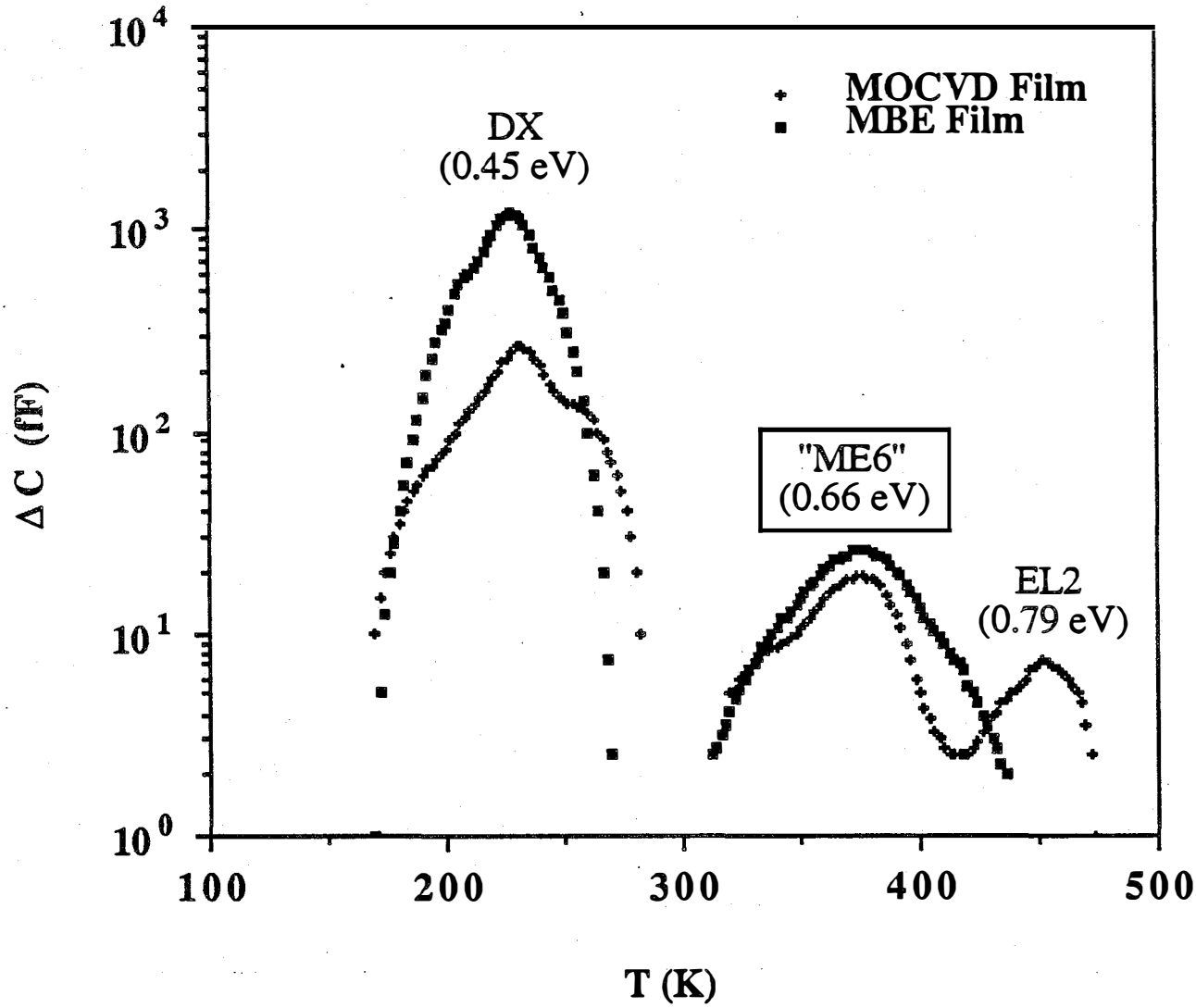

Fig. 4.6 Comparison of DLTS spectra of MBE-grown and MOCVD-grown n-type $Al_{0.2}Ga_{0.8}As$. All scans were performed at the window rate of 200 sec^{-1}.

Table 4.1

Summary of DLTS measurements on the MBE-grown film

Trap Parameters for MBE Film			
Trap	$\sigma_n(cm^2)$	$N_T(cm^{-3})$	$E_C - E_T(eV)$
DX	4.7×10^{-13}	2.9×10^{15}	0.45 ± 0.01
ME6	8.9×10^{-15}	7.2×10^{13}	0.66

Table 4.2

Summary of DLTS measurements on the MOCVD-grown film

Trap Parameters for MOCVD Film			
Trap	$\sigma_n(cm^2)$	$N_T(cm^{-3})$	$E_C - E_T(eV)$
DX	1.8×10^{-13}	3.7×10^{14}	0.45 ± 0.01
ME6	9.1×10^{-15}	2.7×10^{13}	0.66
EL2	5.3×10^{-15}	6.0×10^{12}	0.79

solutions to the minority carrier diffusion equation, the n = 1 current component was projected from the cell structure, measured hole lifetime, and from the assumed electron lifetime and front surface recombination velocity. The internal QE versus wavelength was similarly projected using well-known expressions along with the measured and assumed material properties. The short-circuit current was obtained by multiplying the resulting internal QE versus wavelength by the incident flux of a standard AM1.5 global spectrum normalized to 100 mW/cm^2. Shadowing and reflection losses were not modeled. Finally, the light and dark currents were superimposed and the projected solar cell parameters computed.

Projections of solar cell performance are summarized in Tables 4.3 and 4.4. Projections for the MBE cell are somewhat lower than for the MOCVD cell primarily as a result of the lower bulk lifetimes observed in the MBE-grown films. (The shunt leakage observed in the large area MBE cells was not modeled for these projections.) These projections should be realistic estimates of

the efficiencies achievable for $Al_{0.2}Ga_{0.8}As$ cells with present-day material quality. Films from the same MOCVD growth run were, in fact, previously fabricated into cells with optimized grid patterns and AR coatings [5]. Those cells displayed 1-sun conversion efficiencies of ≃ 17%. The primary reason for the lower than expected conversion efficiency is thought to be due to high recombination velocity at the hetero-interface. Techniques now used for producing high-quality windows for GaAs cells [13], should be directly applicable to AlGaAs and should permit the achievement of the efficiencies projected in Table 4.4.

Table 4.3
Projected saturation current densities for MBE- and MOCVD-grown films

Saturation Current Densities			
Film	J_{o2p}(A/cm)	J_{o2b}(A/cm^2)	J_{o1}(A/cm^2)
MBE	1.7×10^{-14}	2.14×10^{-13}	4.1×10^{-24}
MOCVD	2.7×10^{-14}	4.2×10^{-13}	1.6×10^{-23}

Table 4.4
Projected solar cell performance for MBE- and MOCVD-grown films

Projected Solar Cell Output Parameters (1-sun, AM1.5)				
Film	V_{oc}(V)	J_{sc}(mA/cm$^{2)}$	FF	Eff.(%)
MBE	1.25	18.7	0.85	19.8
MOCVD	1.18	20.5	0.86	21.0

In order to improve solar cell performance, it is also necessary to identify the source(s) of the recombination losses under both short-circuit and open-circuit conditions. Table 4.5 shows how recombination in the bulk and perimeter space-charge regions contribute to the n = 2 losses and how recombination in the quasi-neutral emitter and base layers contribute to losses associated with the n = 1 current. As deduced from Table 4.5, recombination in the bulk and perimeter space-charge regions is a sizeable loss component for $Al_{0.2}Ga_{0.8}As$ cells under 1-sun conditions. For concentrator applications, V_{oc} would be limited by recombination in the quasi-neutral base.

Table 4.5

Distribution of recombination losses under open-circuit conditions

Dark Current Losses at $V=V_{oc}$ (1-sun, AM1.5)				
Film	J_{o2p}(%)	J_{o2b}(%)	J_{o1e}(%)	J_{o1b}(%)
MBE	27.0	42.7	1.9	28.3
MOCVD	10.6	20.9	1.4	67.1

The losses at J_{sc} represent the collection efficiency of each region of the device and these can be found using Hovel's equations [7] and the AM1.5 spectrum. Table 4.6 shows the recombination losses at short circuit in each region for both cells. Nearly 85% of the collection losses of each cell occur in the base, while little recombination occurs in the emitters. Although the thin emitter aids collection in that region, it also means more carriers are generated in the base region where the short diffusion length prevents efficient collection.

Table 4.6

Distribution of recombination losses under short-circuit conditions

Recombination Losses at $J=J_{sc}$ (1 sun, AM1.5)			
Film	Window	Emitter	Base
MBE	12%	2%	86%
MOCVD	14%	2%	84%

4.5 CONCLUSIONS AND FUTURE DIRECTIONS

We have measured, analyzed, and characterized $Al_{0.2}Ga_{0.8}As$ solar cells fabricated on films grown by MBE and MOCVD. DLTS measurements show that both MBE- and MOCVD-grown films possess DX centers and a trap labeled as ME6. In addition, the EL2 defect was observed in the MOCVD-grown film. The concentrations of ME6 in the two films, the PL intensities, and the long wavelength internal quantum efficiencies all display the same trend. The performance

of both MBE and MOCVD cells is adversely affected by low bulk lifetimes which increase the bulk component of J_{o2} and lower the internal quantum efficiency.

Further improvements in $Al_{0.2}Ga_{0.8}As$ cell efficiency will require improvements in both material quality and cell design. The concentration of ME6, a known recombination center, can be reduced by proper growth conditions [14]. The source of leakage in large area, MBE diodes must also be identified and suppressed. Finally, device design can also enhance cell performance. The use of n on p cells rather than the p on n cells considered here may prove beneficial for enhancing base diffusion lengths, and the application of doping or compositional variations may prove useful for improving collection efficiency.

Acknowledgement- The authors thank David Mathine for performing the photoluminescence measurements.

CHAPTER 4 REFERENCES

[1] G. F. Virshup, C. W. Ford, and J. G. Werthen, *Appl. Phys. Lett.*, 47 (1985) p. 1319.

[2] R. P. Gale, J. C. C. Fan, G. W. Turner, R. L. Chapman, and J. V. Pantano, *Appl. Phys. Lett.*, 44 (1984), p. 632.

[3] C. Amano, A. Shibukawa, and M. Yamaguchi, *J. Appl. Phys.*, 58 (1985), p. 2780.

[4] R. Zerdoum, L. Mayet, M. Gavand, and A. Laugier, *7th Eur. Com. Conf. on Photovoltaic Solar Energy,* Sevilla, 1986, Reidel, London, 1987, p. 938.

[5] S. M. Vernon, S. P. Tobin, and R. G. Wolfson, Final Subcontract Report, April 1984 - April 1986, (July 1987), Spire Corporation, SERI, U.S. Department of Energy, P. 2-15.

[6] K. Yamanaka, S. Naritsuka, K. Kanamoto, M. Mihara, and M. Ishii, *J. Appl. Phys.*, 61(11), (1987), pp. 5062-5068.

[7] H.J. Hovel and J.M. Woodall, *Proc. 10th IEEE Photovoltaic Spec. Conf.*, Palo Alto, CA, New York, (1973), p. 327.

[8] H. C. Casey, Jr. and M. B. Panish, *Heterostructure Lasers,* Academic Press, New York, 197, p. 193.

[9] P.K. Bhattacharya and S. Subramian, *J. Appl. Phys.*, 55(10), (1984), pp. 3664-3668.

[10] T. Matsumoto and P.K. Bhattacharya, *Appl. Phys. Lett.*, 41(7), (1982), pp. 662-664.

[11] S.P. Tobin, S.M. Vernon, C. Bajgar, S.J. Wojczuk, M.R. Melloch, A. Keshavarzi, T.B. Stellwag, S. Venkatesan, M.S. Lundstrom, and K.A. Emery, submitted for publication, (1989).

[12] P.D. DeMoulin, S.P. Tobin, M.S. Lundstrom, M.S. Carpenter, and M.R. Melloch, *IEEE Electron Dev. Lett.*, (9), (1988), pp. 368-370.

[13] S.P. Tobin, S.M. Vernon, C. Bajgar, L.M. Geoffroy, C.J. Keavney, M.M. Sanfacon, and V.E. Haven, *Solar Cells,* (24), (1988), pp. 103-115.

[14] K. Yamanaka, S. Naritsuka, M. Mannoh, T. Yuasa, Y. Nomura, M. Mihara, and M. Ishii, *J. Vac. Sci. Technolo. B,* (2), (1988), p. 229.

[15] A. Salokatve, J. Varrio, J. Lammasniemi, H. Asonen, and M. Pessa, *Appl. Phys. Lett.*, 51 (1987) p. 1340.

[16] N. Susa and H. Okamoto *Japanese J. Appl. Phys.*, 23 (1984), p. 317.

CHAPTER 5

ORIENTATION-DEPENDENT EDGE EFFECTS IN GaAs DIODES

5.1 INTRODUCTION

The performance of GaAs-based devices which contain pn junctions such as solar cells, heterojunction bipolar transistors (HBTs), and injection lasers can be significantly influenced by the mesa-etched edges which define the device geometry. The current of a mesa-isolated GaAs pn junction is comprised of components due to recombination in the bulk space-charge region, recombination within the space-charge region exposed at the perimeter of the mesa, and recombination in the bulk neutral regions. Therefore, the current-voltage characteristic of a GaAs pn junction is expected to have the form,

$$I = J_{O2B} A(e^{qV/2kT}-1) + J_{O2P} P(e^{qV/2kT}-1) + J_{O1} A(e^{qV/kT}-1) \qquad (5.1)$$

where J_{O2B} is the bulk saturation current component (A/cm^2), J_{O2P} is the perimeter component (A/cm), J_{O1} is the diffusion saturation current component (A/cm^2), A is the area of the diode and P is the perimeter. Henry et al. [1-4] found that the 2kT current was completely due to recombination at the exposssed perimeter of the mesa for double-heterostructure AlGaAs pn junctions with composition and doping levels similar to those used in injection lasers. Henry et al.'s [2,3] largest device was 125 μm x 500μm, however DeMoulin et al. [5] have shown that even in high efficiency GaAs solar cells as large as 2cm x 2cm the 2kT current is due to edge recombination. The influence of edge recombination on HBT performance was dramatically demonstrated by Sandroff et al. [6]; by passivating the periphery of an HBT with $Na_2\dot{S}9H_2O$, Sandroff et al.[6] were able to get a 60-fold increase in the current gain of their devices. We have recently discovered an interesting aspect of the edge recombination current seen in GaAs pn junctions; there is a strong orientation-dependence to the edge recombination current. The results suggest that with proper device design, perimeter recombination losses might be substantially reduced. In this chapter we describe preliminary experiments which demonstrate this orientation-dependence.

5.2 DEVICE FABRICATION

The structure of Fig. 5.1 was grown in a Varian GEN II molecular beam epitaxy (MBE) system. This MBE system has recently produced record efficiency MBE-grown GaAs pn heteroface solar cells with a structure similar to Fig. 5.1 [7]. A two-inch liquid-encapsulated-Czochralski <1 0 0>-oriented substrate was used. The layers were grown at a substrate temperature of 600° C. Two gallium furnaces were used with each producing a flux corresponding to a growth rate of 0.5 μm/hr. The As_4 to total Ga beam equivalent pressures was 27 as measured with an ion-gauge in the substrate growth position. The superlattice (SL) layer consisted of 20 periods of 28

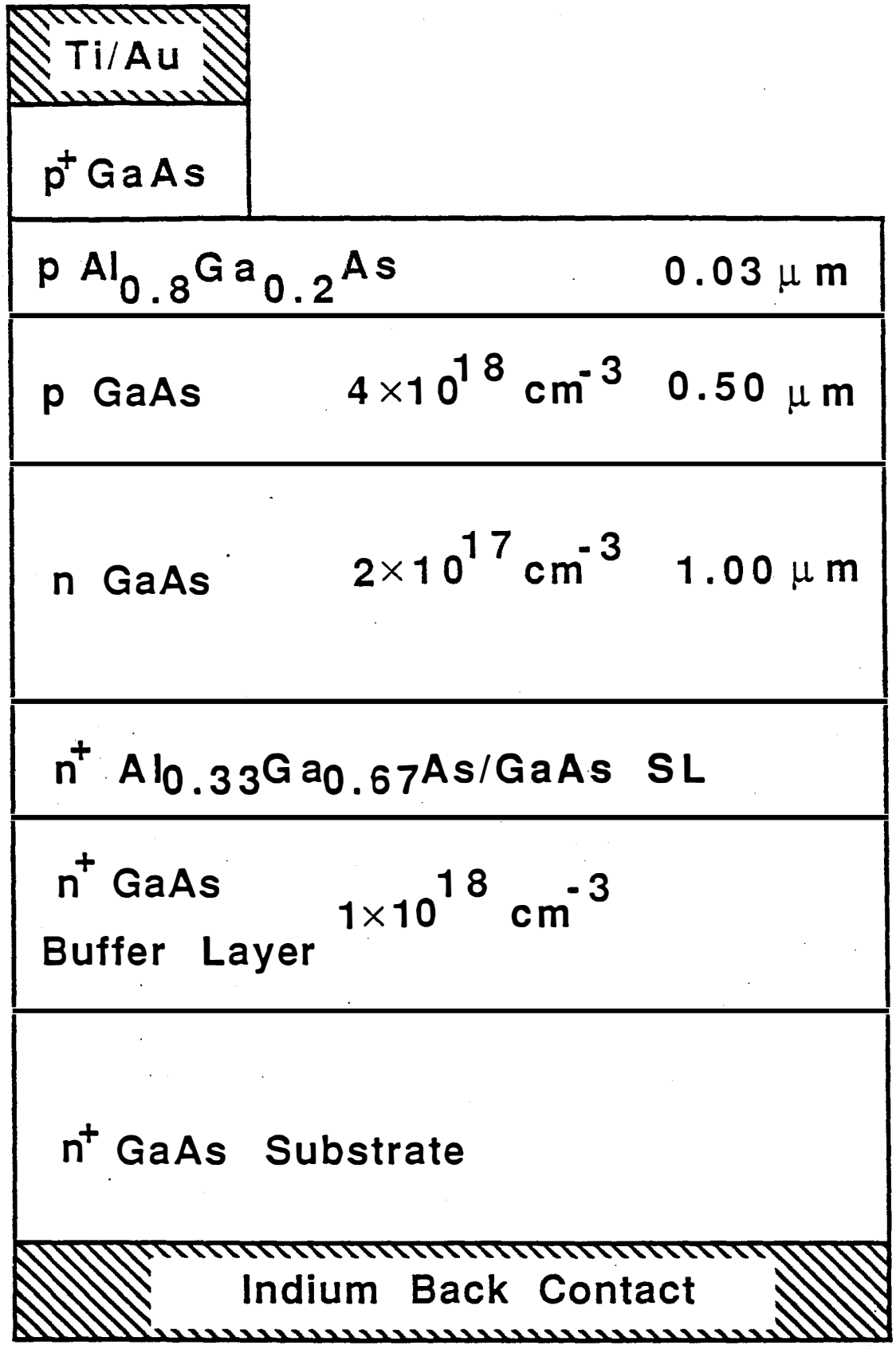

Fig. 5.1 Cross-section of MBE-grown diodes.

Å $Al_{0.33}Ga_{0.67}As$ barriers and 31 Å GaAs wells. (The SL was incorporated in the film structure to reduce any diffusion of impurities from the substrate into the growing film [8].)

A non-bonded wafer mount was used during the MBE growth, so following film growth a back ohmic contact was formed by alloying indium at 350°C for 1 min. Front metallization lift-off patterns were then defined, Ti/Au was Ebeam evaporated to form non-alloyed ohmic contacts, and the photoresist was disolved in acetone to remove excess metal. The mesas were then defined using conventional photolithography and etched in a 25° C methanol:H_2O_2:H_2O:H_3PO_4 3:1:1:1 solution for 1 min 15 sec. The etch rate was approximately two microns per minute, making this a suitable etch for mesa isolation.

The finished devices consisted of rectangular diodes with perimeter to area ratios varying from 60 to 480. In order to study the effects of orientation on the 2kT perimeter recombination current, this set of mesa-isolated diodes was rotated every forty-five degrees on the mask set with subsets rotated at fifteen degree increments.

5.3 EXPERIMENTAL RESULTS

The dark current versus voltage characteristics were measured as a function of orientation. We will define zero degrees as the orientation where the sides of length a of the rectangular diodes are along the $<0\,1\,\bar{1}>$-direction. Shown in Fig. 5.2 is the 2kT saturation current plotted versus angle of orientation for 70 μm x 500 μm rectangular diodes. This figure shows that the 2kT current is strongly dependent on the device orientation. Since the current due to the bulk space-charge region is independent of orientation, angle of rotation therefore affects the recombination at the perimeter. By properly orienting a device, this surface recombination current can be minimized.

Equation 5.1 assumed a constant J_{O2P} independent of orientation. For a rectangular diode of side lengths a and b, a more accurate description of the current voltage characteristic of a mesa-isolated GaAs pn junction is therefore,

$$I = J_{O2B}A(e^{qv/2kT}-1) + J_{O2Pa}2a(e^{qv/2kT}-1) + J_{O2Pb}2b(e^{qv/2kT}-1) + J_{O1}A(e^{qv/2kT}-1) \quad (5.2)$$

where J_{O2Pa} is the perimeter component along the sides of length a and J_{O2Pb} is the perimeter component along the sides of length b in A/cm.

From equation 5.2 we can write the q/2kT saturation current as

$$I_{O2} = J_{O2B}ab + J_{O2Pa}2a + J_{O2Pb}2b \quad (5.3)$$

where the area A was replaced by the product of the sides of the rectangular diode, ab. By plotting I_{O2}/ab versus P/A ratio for a series of diodes where a is held constant but b is allowed to vary, the perimeter component along the side of length a, J_{O2Pa}, can be determined from the

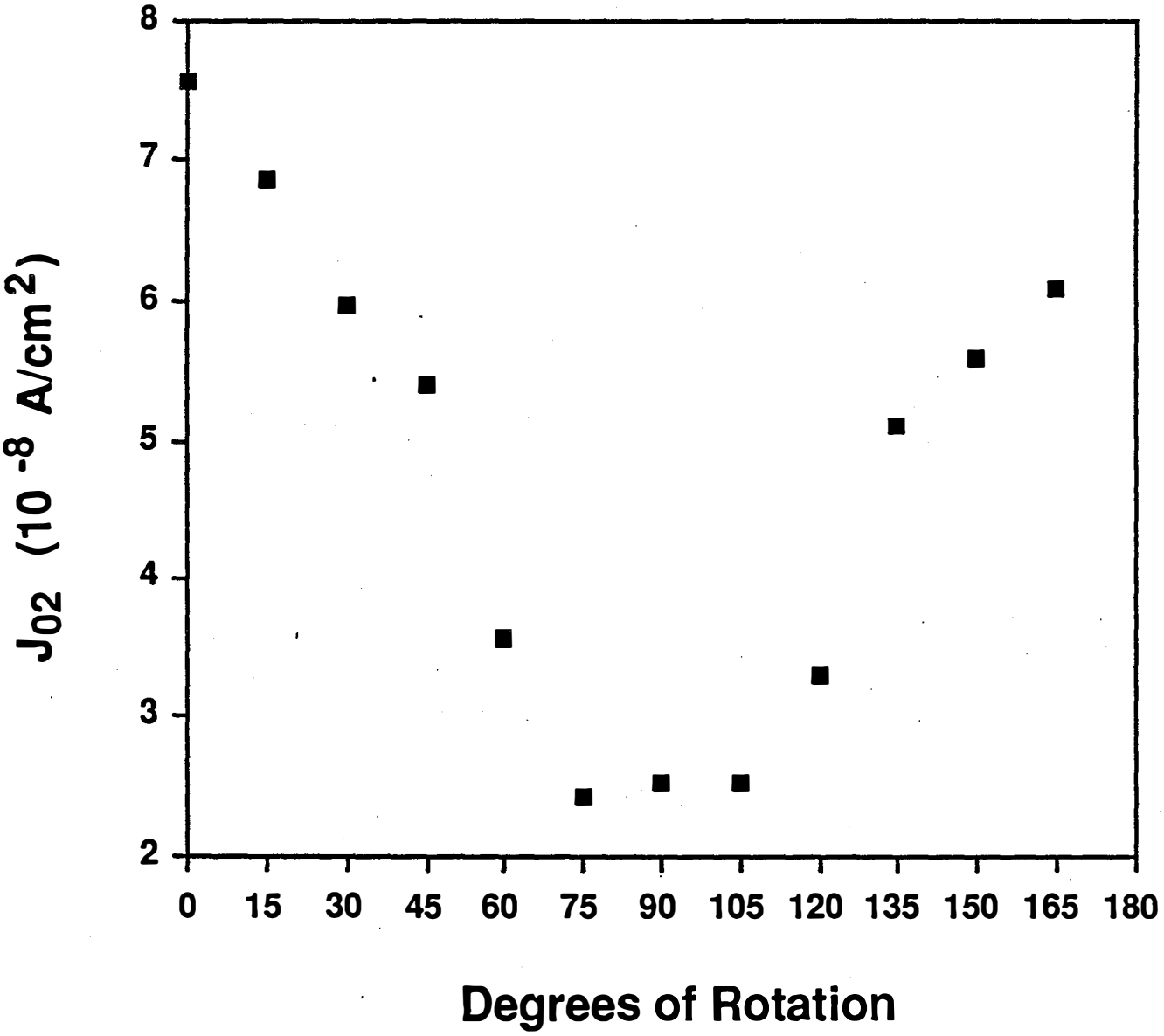

Fig. 5.2 Extracted J_{O2} as a function of diode orientation.

slope of the plot. In Figs. 5.3 and 5.4, plots of I_{O2}/ab versus P/A are shown for sets of diodes at 0, 45, 90, and 135 degrees. The plots for 45 and 135 degrees show that J_{O2Pa} is the same for edges along the <0 1 0>- or <0 0 1>-directions whereas the plot for 0 and 90 degrees exhibit a factor of four larger J_{O2Pa} for edges along the $<0\,1\,\bar{1}>$-direction as opposed to edges along the <0 1 1>-direction. Shown in Fig. 5.5a and 5.5b are scanning electron micrographs of the mesa edges along the $<0\,1\,\bar{1}>$- and <0 1 1>-directions respectively. The orientation dependent profiles seen in Fig. 5.5a and 5.5b are similar to those previously observed for GaAs mesas [9].

Following Henry et al. [4], the perimeter recombination current, J_{O2Pa} can be written as,

$$J_{O2Pa}=qn_iS_{SCR}L_s \tag{5.4}$$

where n_i is the intrinsic carrier concentration, S_{SCR} is the surface recombination velocity, and L_s is an effective surface diffusion length. We find that the $S_{SCR}L_s$ product ranges from 1.51 cm^2/s at 0 degrees to 0.3 cm^2/s at 90 degrees. This result suggests that the surface recombination velocity varies with orientation by a factor of 5. Though the J_{O2Pa} currents at 75 and 105 degrees are slightly less than at 90 degrees, the SL product for these orientations cannot be extracted due to the limited number of devices on the mask at these orientations.

5.4 SUMMARY

We have experimentally shown that the recombination current at the exposed edges of a GaAs pn junction has a strong orientation-dependence. There is also an orientation dependence to the profile of the etched mesa which is a function of the etch used [9]. Future work will involve an investigation of the effects of other mesa-isolation etches on the orientation dependence of edge recombination.

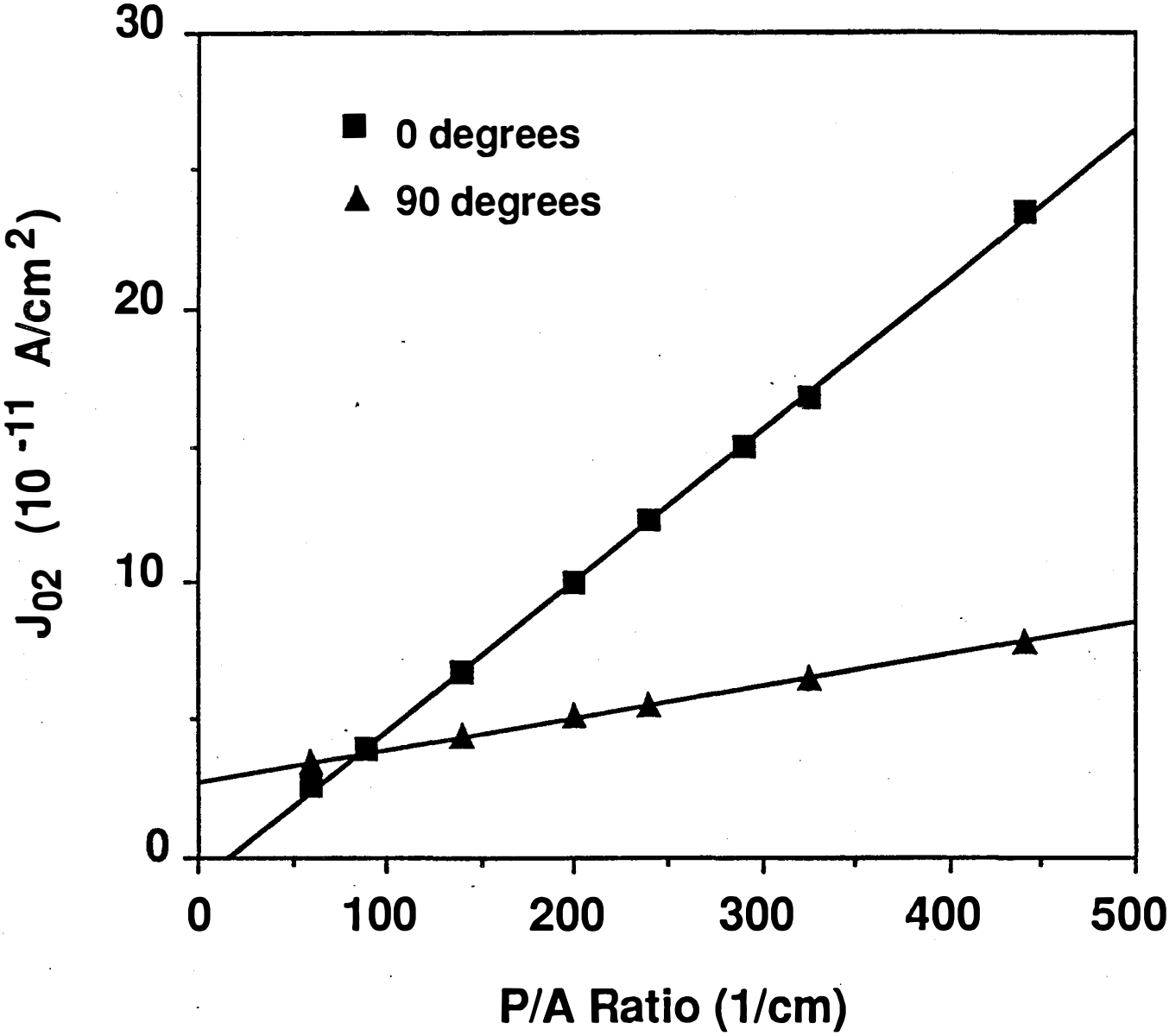

Fig. 5.3 Plot of extracted I_{02}/ab versus perimeter-to-area ratio for a series of diodes where the side of length a is held constant while the side of length b is varied. 0 degrees signifies diodes where side a is along the $\langle 0\,1\,\bar{1}\rangle$-direction while 90 degrees signifies diodes where side a is along the $\langle 0\,1\,1\rangle$-direction.

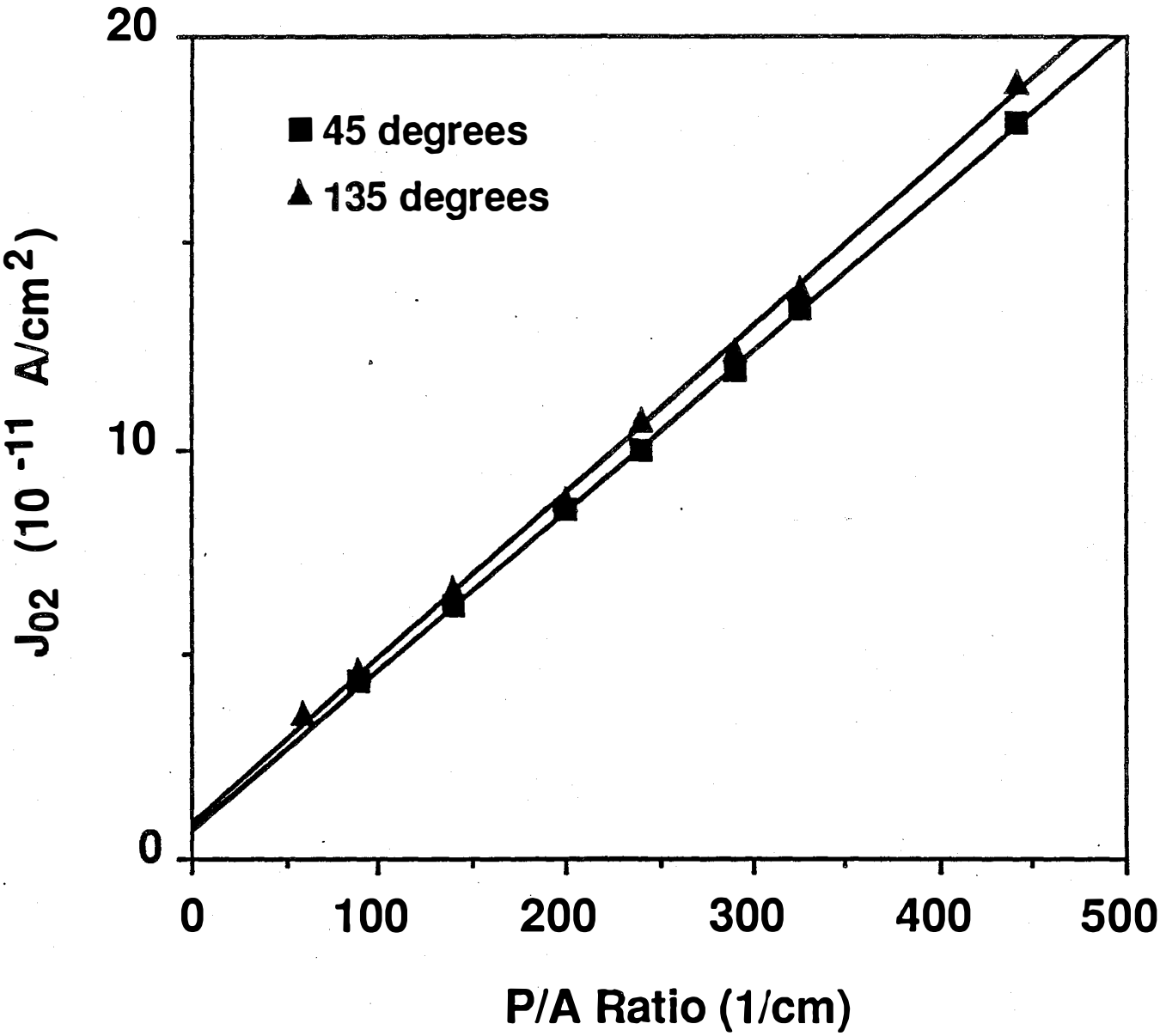

Fig. 5.4 Plot of extracted I_{02}/ab versus perimeter-to-area ratio for a series of diodes where the since of length a is held constant while the side of length b is varied. 45 degrees signifies diodes where side a is along the <0 1 0>-direction while 135 degrees signifies diodes where side a is along the <0 0 1>-direction.

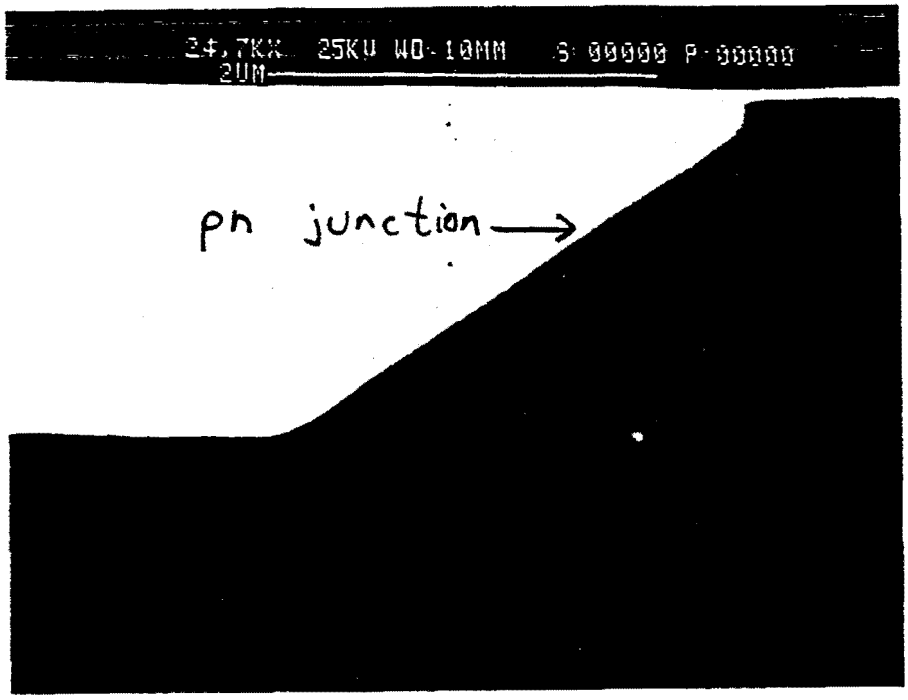

(a) <01$\bar{1}$>

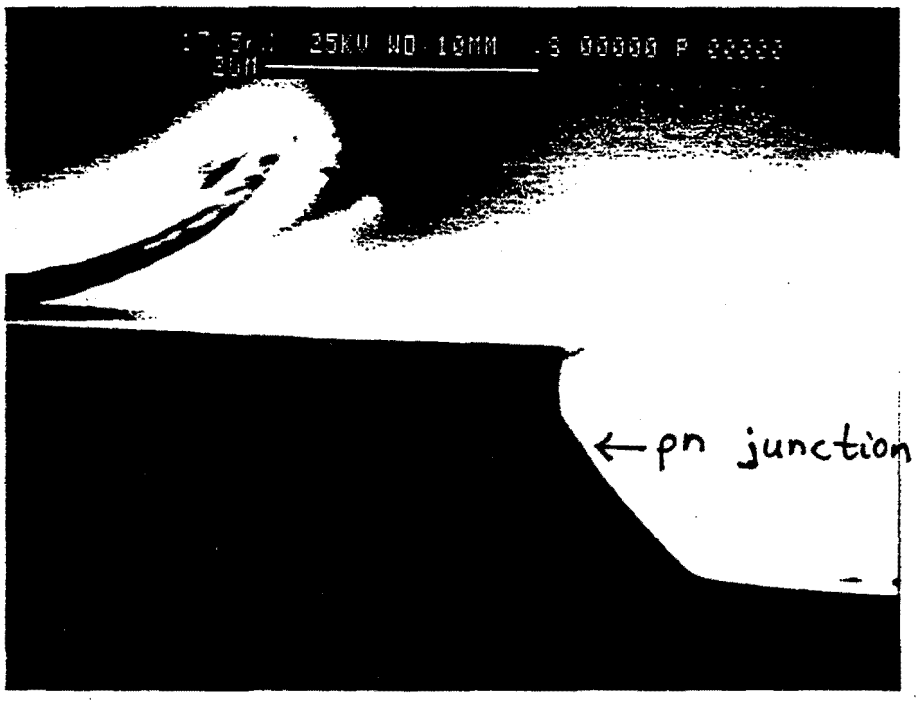

(b) <011>

Fig. 5.5 Scanning electron micrographs of the mesa edges along the (a) <0 1 $\bar{1}$>- and (b) <0 1 1>-directions.

CHAPTER 5 REFERENCES

[1] C.H. Henry and R.A. Logan, J. Appl. Phys. 48, 3962(1977).

[2] C.H. Henry, R.A. Logan, and F.R. Merritt, Appl. Phys. Lett. 31, 454(1977).

[3] C.H. Henry, R.A. Logan, and F.R. Merritt, J. Appl. Phys. 49, 3530(1978).

[4] C.H. Henry and R.A. Logan, J. Vac. Sci. Technol. 15, 1471(1978).

[5] Paul D. DeMoulin, Stephen P. Tobin, Mark S. Lundstrom, M.S. Carpenter, and Michael R. Melloch, IEEE Elec. Dev. Lett. 9, 368(1988).

[6] C.J. Sandroff, R.N. Nottenburg, J.-C. Bischoff, and R. Bhat, Appl. Phys. Lett. 51, 33(1987).

[7] M.R. Melloch, S.P. Tobin, T.B. Stellwag, C. Bajgar, A. Keshavarzi, M.S. Lundstrom, and K. Emery, presented at the Tenth Molecular Beam Epitaxy Workshop, Raleigh, NC, September 13-15,1989, and submitted to the J. Vac. Sci. and Tech. B.

[8] K.L. Tan, M.S. Lundström, and M.R. Melloch, Appl. Phys. Lett. 48, 428(1986).

[9] S. Iida and K Ito, J. Electrochem. Soc. 119, 768(1971).

CHAPTER 6

CHEMICAL PASSIVATION OF GaAs SURFACES

6.1 INTRODUCTION

The oxides which form on GaAs result in a large density of surface states which can dominate the electrical behavior of devices. Even a brief exposure of a clean GaAs surface to oxygen can result in a pinning of the Fermi level at the surface. Recent sulfide chemical treatments of the GaAs surface have resulted in dramatic improvements in device performance [1-8]. Heterojunction bipolar transistor gains have been shown to increase 60-fold by treating the edges of the emitter base junction with $Na_2S \cdot 9H_2O$ [1,2]. Reduction in edge recombination currents have been observed by $Na_2S \cdot 9H_2O$ or ammonium sulfide treatment of GaAs pn homojunction solar cells [3]. A wider range of Schottky barrier heights has been observed in metal-GaAs Schottky barriers where the GaAs was treated with ammonium sulfide prior to thermal evaporation of the metal [4-6]. It has also been shown that the surface recombination velocity of sulfide treated GaAs approaches that of the nearly ideal AlGaAs/GaAs heterojunction [7,8]. It is therefore of great technical importance to determine the exact nature of the sulfide-treated GaAs surface. In last year's annual report we presented preliminary X-ray Photoelectron Spectroscopy (XPS) studies indicating that the ammonium sulfide treatment removes the oxides on the surface of GaAs, leaving behind a monolayer or less of sulfur which inhibits oxidation of the surface [9]. Sandroff et al. [19] have made similar observations. In this chapter we will present a more complete XPS study of the ammonium sulfide treated GaAs surface. The XPS measurements are being performed by Dr. B.A. Cowans and Dr. W.N. Delgass in the School of Chemical Engineering at Purdue University. Also, reflection high energy electron diffraction (RHEED) data on the ammonium sulfide treated GaAs surface will be presented. Finally, the effect of the ammonium sulfide treatment on the formation of gold and aluminum Schottky barriers on GaAs will be presented.

6.2 X-RAY PHOTOELECTRON SPECTROSCOPY

We previously examined the effects of oxidation on ammonium sulfide treated GaAs surfaces using XPS [10]. We found that the ammonium sulfide treatment produces a slightly Ga rich surface which is covered by less than one monolayer of sulfide. This surface condition is sufficient to severly restrict initial oxidation of the GaAs surface. The chemical state of the sulfur in the layer does not change with exposure to air although we do observe growth of a layer of oxidized gallium and arsenic over the sulfur. We have now used XPS to examine the effects of sulfide concentration on GaAs (100) surfaces using either saturated or unsaturated ammonium sulfide solutions. Ion sputtered and ammonium hydroxide etched GaAs surfaces were examined for comparison.

Samples were cut from undoped or Si-doped MaCom (100) GaAs wafers to roughly 16 mm x 20 mm and etched in 1:100 H_2SO_4:H_2O for 30 seconds followed by a 30 second deionized water rinse. Samples were then immediately etched with 1:1 NH_4OH:H_2O (pH >10) for 30 seconds or with saturated (pH >10) or unsaturated (pH >8) ammonium sulfide solutions for 20 minutes. Following either procedure, samples were rinsed with deionized water, dried and mounted under a stream of UHP argon, and loaded into the spectrometer. Prior to removing samples from a sulfide etch, the solution was diluted with an excess of deionized water. In a separate experiment, a "clean" surface was prepared in the spectrometer vacuum chamber by sputtering an acid etched wafer with 3kV Ar^+ ions for 5 minutes at a current density of approximately 230 $\mu A/cm.^2$ This procedure removes all carbon and oxygen impurities from the surface. Operating conditions of the Perkin-Elmer PHI 5300 spectrometer were described previously [10].

Photoelectron spectra of the As and Ga $2p_{3/2}$ core levels are shown in Fig. 6.1. The spectra shown are for (A) sputter cleaned, (B) unsaturated ammonium sulfide etched, (C) saturated ammonium sulfide etched, and (D) ammonium hydroxide etched surfaces taken at an electron take-off angle of 15 degrees from the surface plane. The presence of As(sulfide) is clearly observed for spectra (B) and (C) from the asymmetry of the line to higher binding energy. At an electron take off angle of 45 degrees, chosen to minimize effects of electron channeling [11], the relative As(sulfide)/As(GaAs) ratios are 0.169 for the saturated sulfide etch and 0.164 for the unsaturated etch. The binding energy shifts for Ga are less than those for As, but the presence of Ga(sulfide) on the sulfide treated samples is observed from the shift of the Ga $2p_{3/2}$ level to slightly higher binding energy. Clearly, there are no oxidized arsenic or gallium species on the surface following either sulfide procedure. A large As oxide peak at 1325.7 eV is observed for the hydroxide etched surface, indicating that the preceding acid etch may have been insufficient to remove the native oxide [11].

The As $2p_{3/2}$ (Al anode) and the S 2s (Mg anode) core levels following a saturated sulfide etch are shown at high and low electron take-off angle in Fig. 6.2. Although the S 2p core levels cannot be easily separated from the Ga 3s level, the S 2s core level is clearly visible at 226.0 eV. We also observe a S Auger signal at 2114.4 eV, which is similar to that reported by Sandroff et al. [9]. An increase in the As(sulfide) and the S 2s relative intensities at low angle indicates that the sulfided species form the uppermost atomic layer.

The arsenic to gallium and the sulfur to total metal intensity ratios for both sulfide etching procedures are listed in Table 6.1. The As 3d/Ga 3d ratios clearly show that an ammonium sulfide etch results in an As-depleted surface. Furthermore, the ratio at 45 degrees is significantly less following a saturated ammonium sulfide etch than following an unsaturated etch, suggesting that the saturated solution enhances As depletion of the surface. Since the relative As(sulfide)/As(GaAs) ratios are identical for the $2p_{3/2}$ electrons, which have smaller mean-free paths, we must assume that not all of the As depletion occurs in the upper most surface layer. These results may be important to the differences in surface reconstruction observed by RHEED

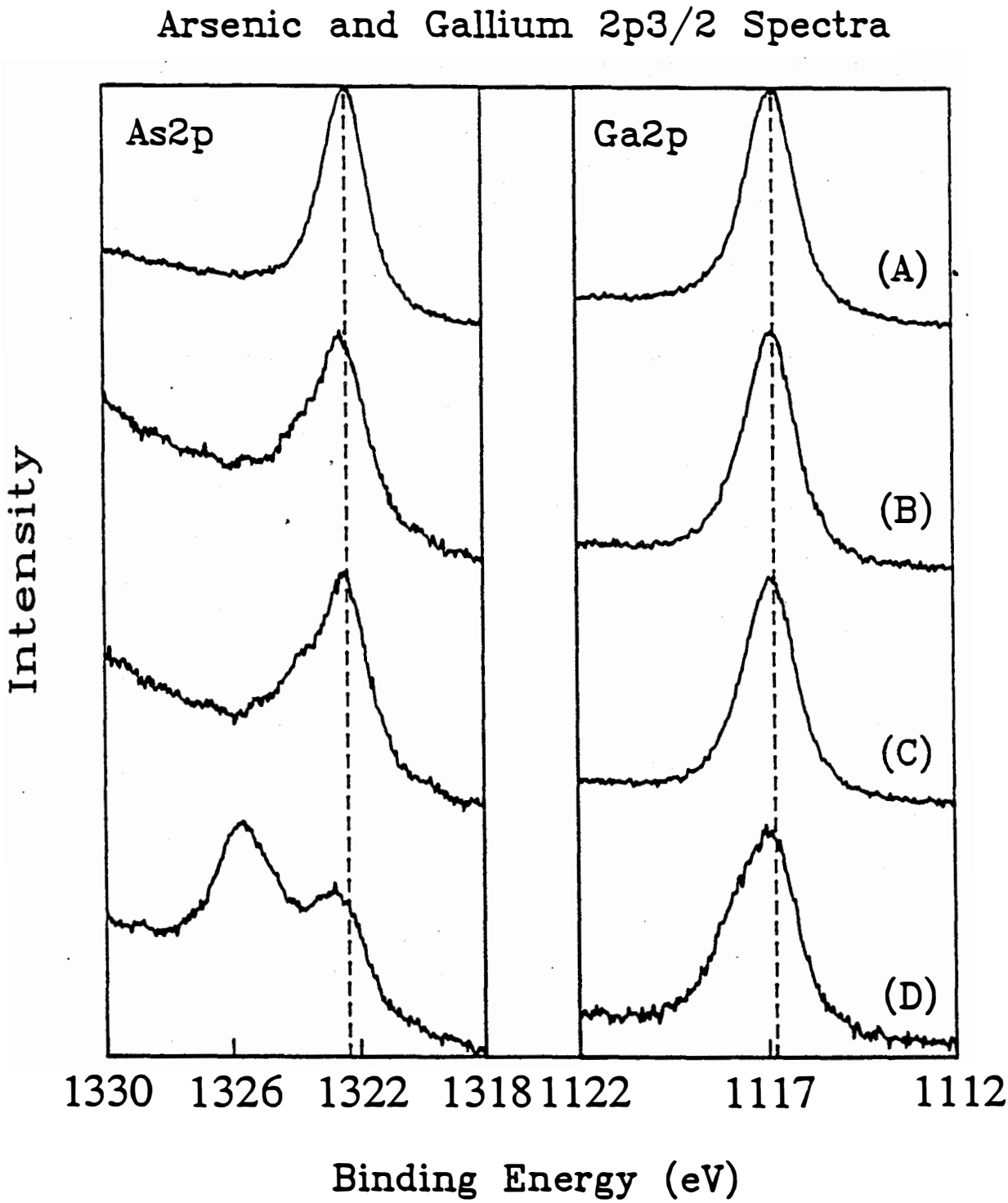

Fig. 6.1 Arsenic and gallium $2p_{3/2}$ core level spectra for (A) Ar^+ ion sputtered, (B) unsaturated ammonium sulfide etched, (C) saturated ammonium sulfide etched, and (D) ammonium hydroxide etched surfaces taken at an electron take-off angle of 15 degrees.

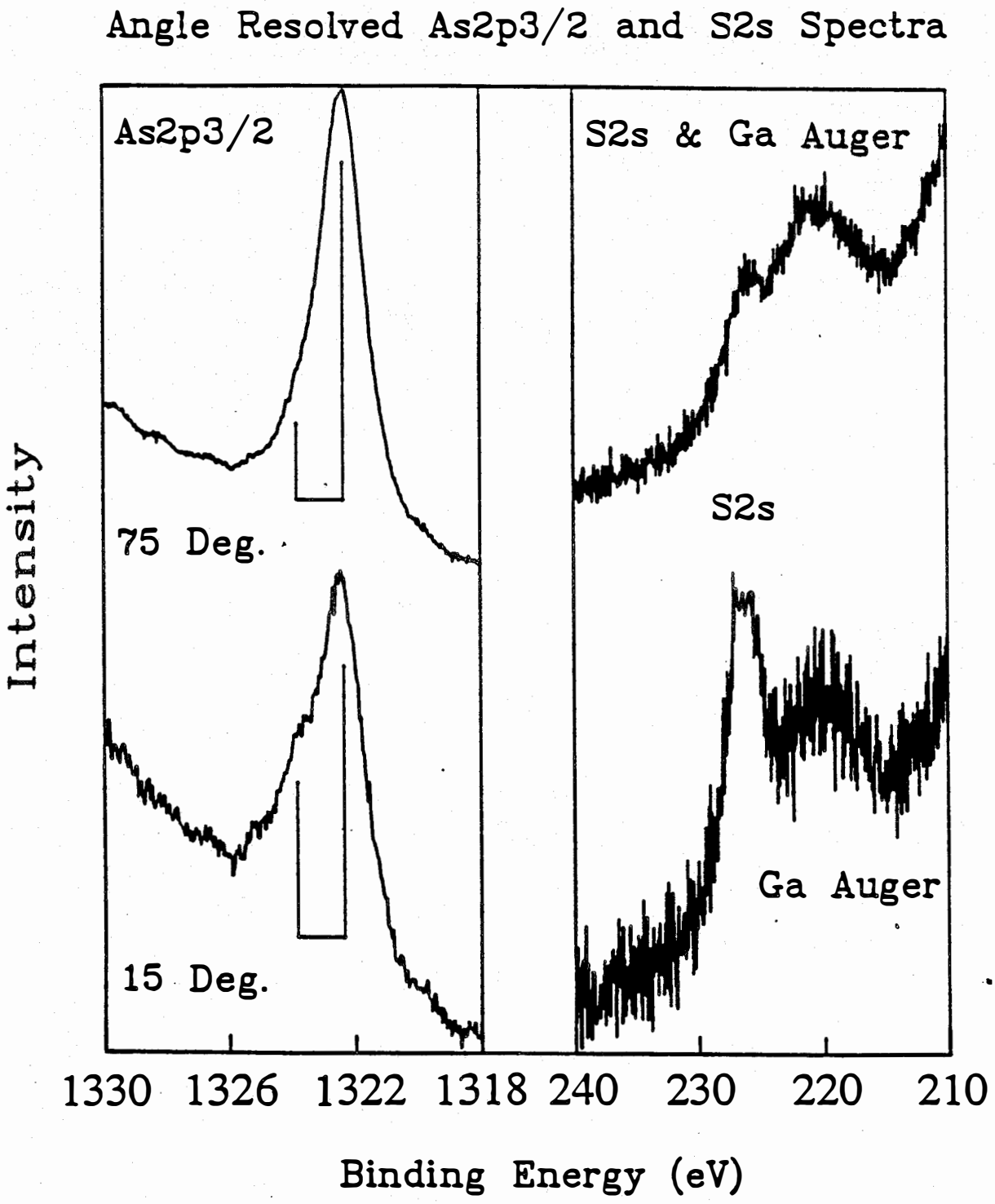

Fig. 6.2 High and low angle arsenic $2p_{3/2}$ (Al anode) and sulfur 2s (Mg anode) core level phootoelectron spectra for a GaAs surface etched with a saturated ammonium sulfide solution.

Table 6.1 Experimental photoelectron intensity ratios for As3d/Ga3d and S2s/(Ga3d + As3d) normalized by Scofield's differential photoelectron cross section (Mg radiation).

Sample	Saturated Sulfide		Unsaturated Sulfide	
Angle	As/Ga	S/(Ga + As)	As/Ga	S/(Ga + As)
15	0.67	0.16	0.78	0.16
30	0.66	0.11	0.83	0.11
45	0.65	0.09	0.82	0.09
60	1.08	0.06	0.60	0.06
75	0.71	0.05	0.92	0.06

and discussed in Section III. The sulfur to total (Ga3d + As3d) metal ratios are exactly the same for both saturated and unsaturated treatments at all angles. This is consistent with the relative ratios observed for the $2p_{3/2}$ levels and indicates that the sulfur coverage, as discussed below, is the same for both treatments.

The GaAs crystal is composed of alternating layers of Ga and As atoms which are parallel to the (100) plane. The fractional coverage of sulfur is calculated assuming the Ga and As layers are complete up to the surface [12,13], which is terminated with a uniform but not necessarily complete sulfur layer. If we assume that the mean free paths for As 3d and Ga 3d are equal and that the separated atomic layer densities for Ga and As are also equal, then the normalized ratio of sulfur to Ga + As intensities is given by,

$$\frac{J_S}{J_{Ga}+J_{As}}=\frac{a_o}{4\lambda\sin\Theta}\exp\left(\frac{d}{\lambda\sin\Theta}\right)\frac{\eta_S}{\eta_{GaAs}} \tag{6.1}$$

where J is the intensity normalized by Scofield's photoelectron cross section [14], η_S is the density of the sulfur layer (atoms/cm^2), η_{GaAs} is the density of one complete Ga or As (100) layer (atoms/cm^2), a_o is the GaAs crystal lattice constant, λ is the photoelectron mean free path [15], d is the thickness of the sulfide layer, and Θ is the electron take-off angle, i.e. the angle between the sample surface and the electron path to the entrance slit to the analyzer. The inelastic mean free path values for Ga and As are assumed to be 23.5 Å [15]. The fractional sulfur coverage is η_S/η_{GaAs} by definition. For a sulfide layer thickness of 3.68 Å, the diameter of a sulfide ion, the sulfur coverage is calculated to be 0.86 monolayers for both saturated and unsaturated sulfide treatments. For a sulfide layer thickness of 2.25 Å, the As-S bond length in As_2S_3 [9,16], the sulfur coverage is calculated to be 0.94 monolayers. For reasons stated above [11], these coverages were calculated using intensity ratios measured at 45 degrees.

6.3 REFLECTION HIGH ENERGY ELECTRON DIFFRACTION

The samples to be treated were prepared by growing 1.5μm of undoped GaAs in a Varian GEN II molecular beam epitaxy (MBE) system. The samples were 2-inch round (100) undoped wafers which were prepared with a standard MBE cleaning procedure before placement in a non-indium wafer mount. The non-indium wafer mounting facilitated easy removal and reinsertion of the sample in the MBE and also eliminates any need for heating the sample when remounting.

After growth of the 1.5μm GaAs film, the sample was removed from the MBE and placed in a laminar-flow clean bench. The sample was left for one hour to insure a pinned surface. The sample was then placed in deionized water while an etch of 1:1:250 H_2SO_4:H_2O_2:H_2O was prepared. The sample was then etched for 30 seconds followed by a de-ionized water rinse for 30 seconds. The sample was then placed in either a saturated or unsaturated ammonium sulfide solution for 20 minutes. The ammonium sulfide solution was removed by adding deionized water and decanting. This step is critical to keep excess sulfur from depositing on the GaAs

surface. The sample was then blown dry with nitrogen and reloaded into the MBE system. It was approximately 13 minutes from the end of the ammonium sulfide soak to placement of the sample in the MBE entry chamber.

Since our XPS measurements indicated less than a monolayer of sulfur coverage and no other contaminants, we were not concerned about contamination of our MBE growth chamber. However, we outgassed the sample at 350°C for one hour in a high vacuum buffer chamber before insertion in the growth chamber which contains the RHEED analysis apparatus.

The RHEED images for the saturated and unsaturated ammonium sulfide treated GaAs samples were observed as the substrate was heated and are displayed in Fig. 6.3 and 6.4. (The sample was under an arsenic flux during the RHEED observations.) Initially for the saturated ammonium sulfide treated sample, the RHEED pattern was somewhat spotty with only a hint of surface reconstruction. At 540°C there was a dramatic change in the RHEED pattern. The main RHEED lines become streaks followed by an appearance of a 2-fold surface reconstruction in the [110] azimuth. It is possible the sub-monolayer of sulfur is starting to evaporate at this temperature, allowing the GaAs surface to reconstruct. (This interpretation is consistent with the observations of Oigawa et al. [17] who determined that the sulfur atoms are removed by heat treatments above 530°C using low-energy electron energy loss spectroscopy (LEELS).) Above 580°C the 4-fold reconstruction lines in the [$\bar{1}$10] azimuth became clearly visible, with the 2-fold reconstruction lines in the [110] azimuth dimming somewhat in comparison to the main lines. This RHEED behavior was observed on three separate wafers which were treated with the saturated ammonium sulfide solution.

The RHEED behavior of the GaAs surface treated with the unsaturated ammonium sulfide solution was considerably different from that described above for the saturated ammonium sulfide treatment. The initial RHEED pattern exhibited a (2x2) surface reconstruction. At 500°C the surface reconstruction started to change to a (4x2) structure, although all the 4-fold reconstruction lines in the [$\bar{1}$10] azimuth were not visible. At 540°C the 4-fold reconstruction lines in the [$\bar{1}$10] azimuth are clearly visible.

Upon initializing growth on the ammonium sulfide treated samples at a substrate temperature of 600°C, the reconstruction lines in the [110] azimuth brightened, but the pattern was not unlike the pattern of the saturated ammonium sulfide treated surface at a substrate temperature near or slightly higher than 540°C as shown in Fig. 6.5. The use of the ammonium sulfide treatment may be a promising approach for MBE regrowth applications.

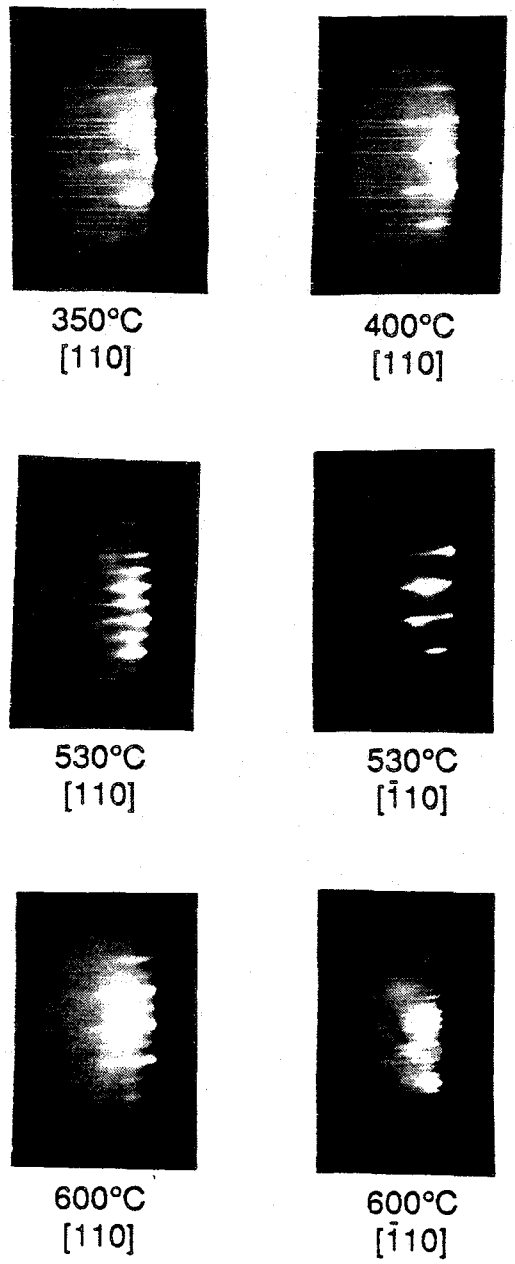

Fig. 6.3 Reflection high energy electron diffration pattern of a GaAs surface treated with a saturated ammonium sulfide solution.

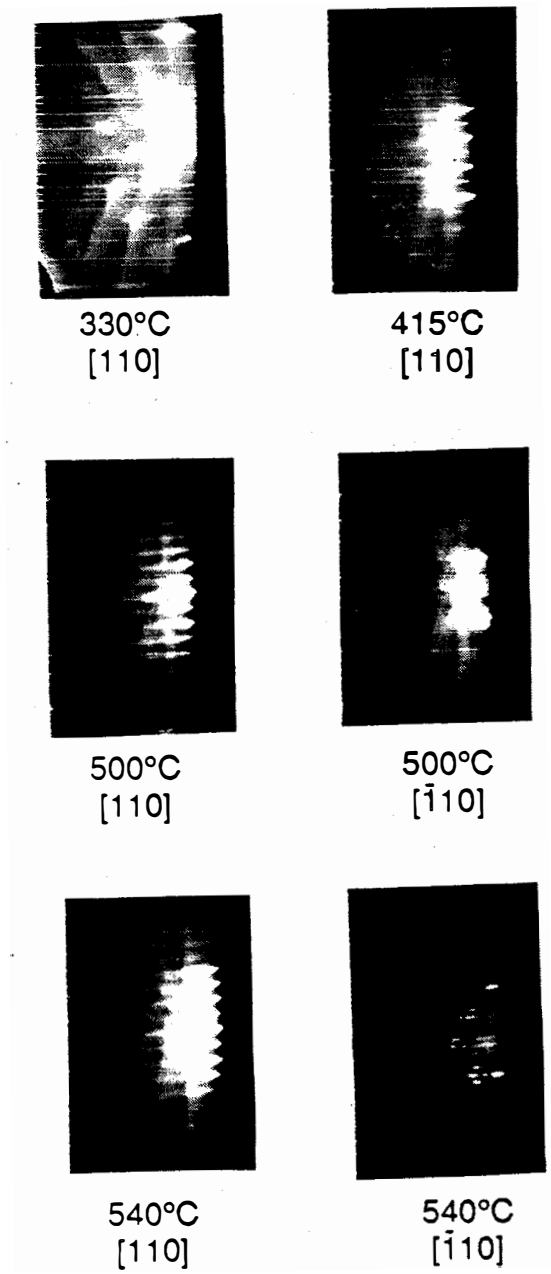

Fig. 6.4 Reflection high energy electron diffraction pattern of a GaAs surface treated with an unsaturated ammonium sulfide solution.

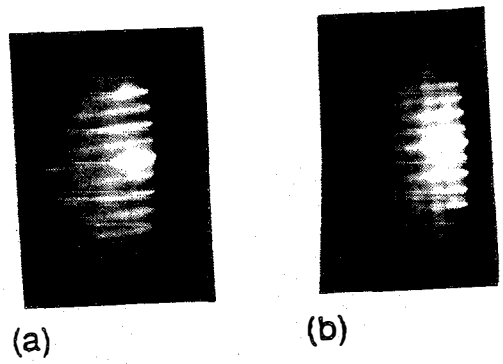

Fig. 6.5 Reflection high energy electron diffraction pattern of a growing film on a GaAs surface which was treated with (a) a saturated solution and (b) an unsaturated ammonium sulfide solution.

6.4 SCHOTTKY BARRIER FORMATION

The devices used in this study were fabricated from two (100) GaAs wafers. The first wafer was an n-type molecular beam epitaxially grown 1.25μm thick epilayer on an n^+ substrate. The second was similar except it was p-type. The doping of the epilayers was approximately $1x10^{17}$ cm^{-3}. The wafers were then cleaved into small samples and soldered on stainless steel mounts with indium. On each mount both n and p-type samples were placed side by side. Each mount was then prepared for evaporation. The ammonium sulfide treated mounts were prepared as previously described for the RHEED measurements. The control devices were etched in the same batch of etchant as the treated samples and just before loading into the deposition system they were soaked in 1:1 NH_4OH:H_2O. Three mounts were loaded into the deposition system for each evaporation, two treated and one control. One treated sample was placed beside the control sample and the other on a cooling stage which was cooled to 77 K during the metal evaporation. Metals were then thermally evaporated on all three mounts simultaneously. The devices were then fabricated using normal photolithographic processes and wet chemical etching.

The forward bias current-voltage (I-V) characteristics of the devices are shown in Fig. 6.6a,b and 6.7a,b. Fig. 6.6a shows the drastic change induced by the ammonium sulfide treatment on gold Schottky barriers to n-type GaAs. The upper curve is for the control or NH_4OH treated devices. The middle curve is for the ammonium sulfide treated devices and the lower curve is again a treated device but with the metal deposition done at a substrate temperature of 77 K. As can readily be seen there is over a three order of magnitude change in the current density. Shown in Fig. 6.6b is the same family of curves for gold Schottky barriers to p-type GaAs. Again the chemical treatment changes the I-V characteristics however, this time there is more current in the treated devices, with additional current in the cooled treated sample. The I-V characteristics in Fig. 6.6 indicate that the gold Schottky barrier has been raised on the n-type treated sample and lowered on the p-type treated sample. Shown in Fig. 6.7a and 6.7b are similar curves for aluminum. For aluminum the trend is reversed, more current is observed for the treated n-type samples and less for the p-type, indicating the barrier height is lowered for the n-type and raised for the p-type.

To determine barrier heights, the I-V characteristics were analyzed in terms of a thermionic emission model of current transport: [18]

$$J=J_s\exp\left(\frac{qV}{nkT}\right)\left[1 - \exp\left(\frac{-qV}{kT}\right)\right] \tag{2}$$

where J_s is the saturation current density and n is the ideality factor. The saturation current density was calculated by a least squares fit to equation 2. The effective barrier heights were determined from the following relation for saturation current density:

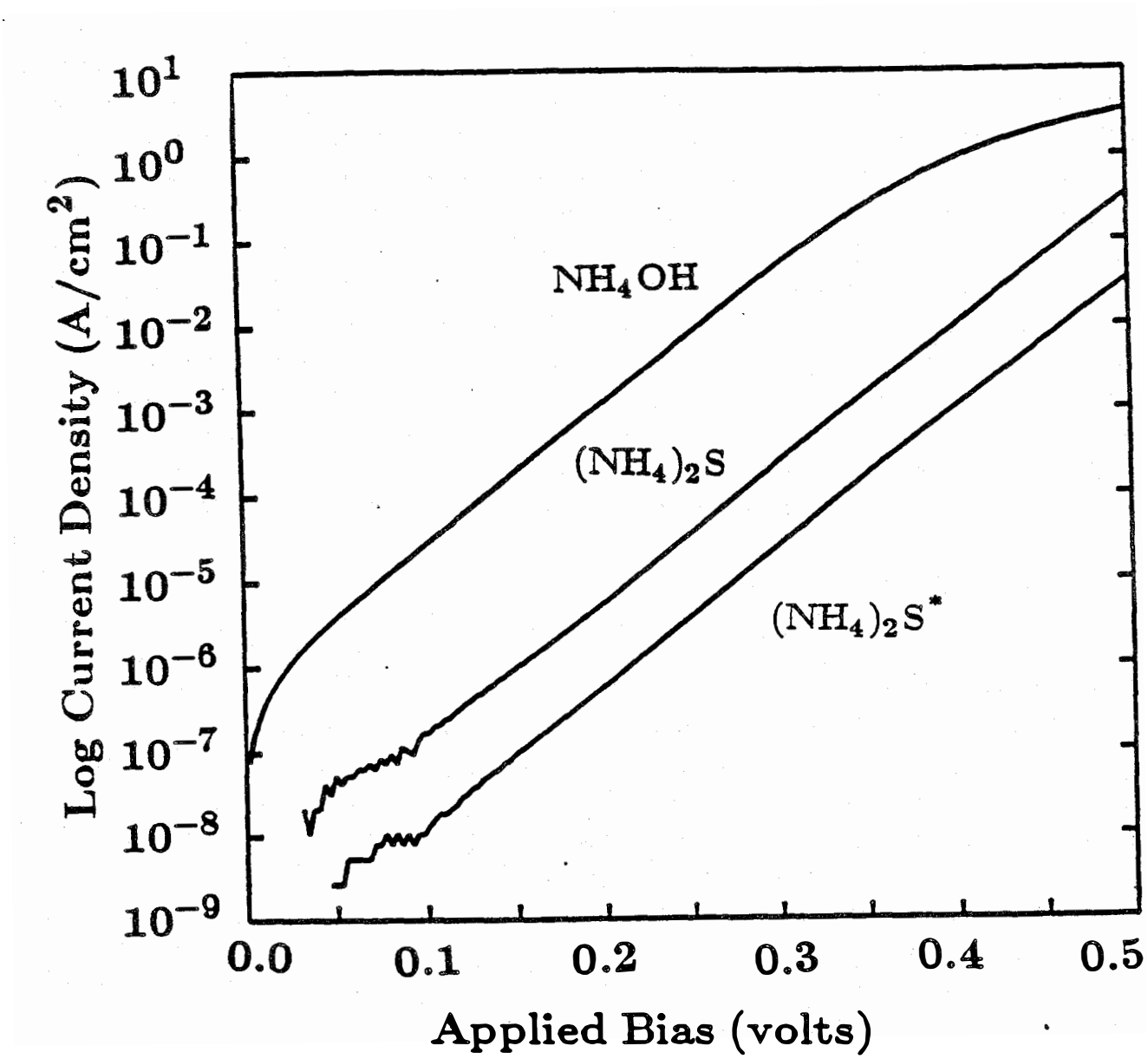

Fig. 6.6a Forward bias current-voltage characteristics measured at 300 K for gold Schottky barriers on n-type GaAs. The $(NH_4)_2S^*$ curve represents samples which were cooled to 77 K during the metal deposition.

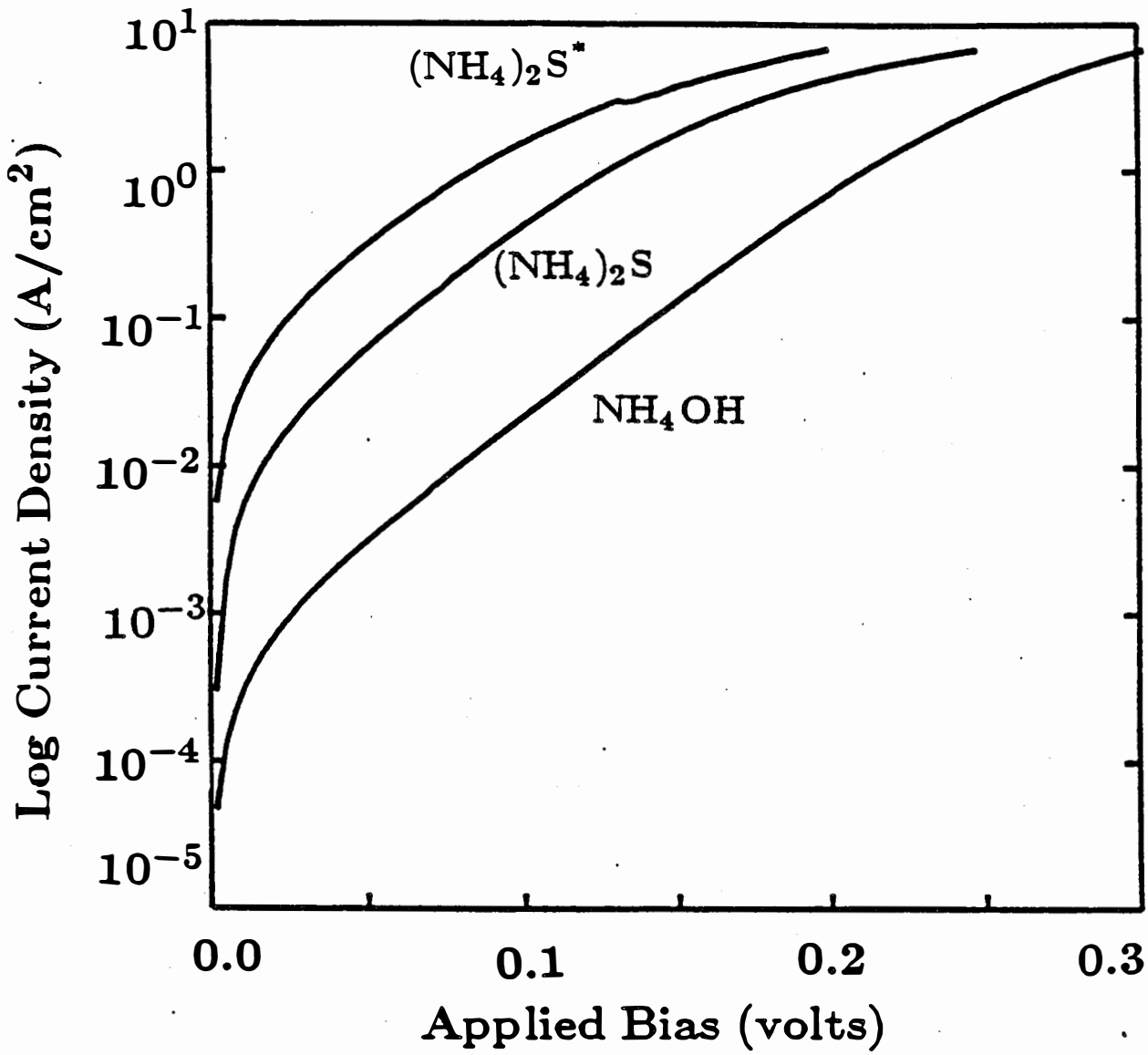

Fig. 6.6b Forward bias current-voltage characteristics measured at 300 K for gold Schottky barriers on p-type GaAs. The $(NH_4)_2S^*$ curve represents samples which were cooled to 77 K during the metal deposition.

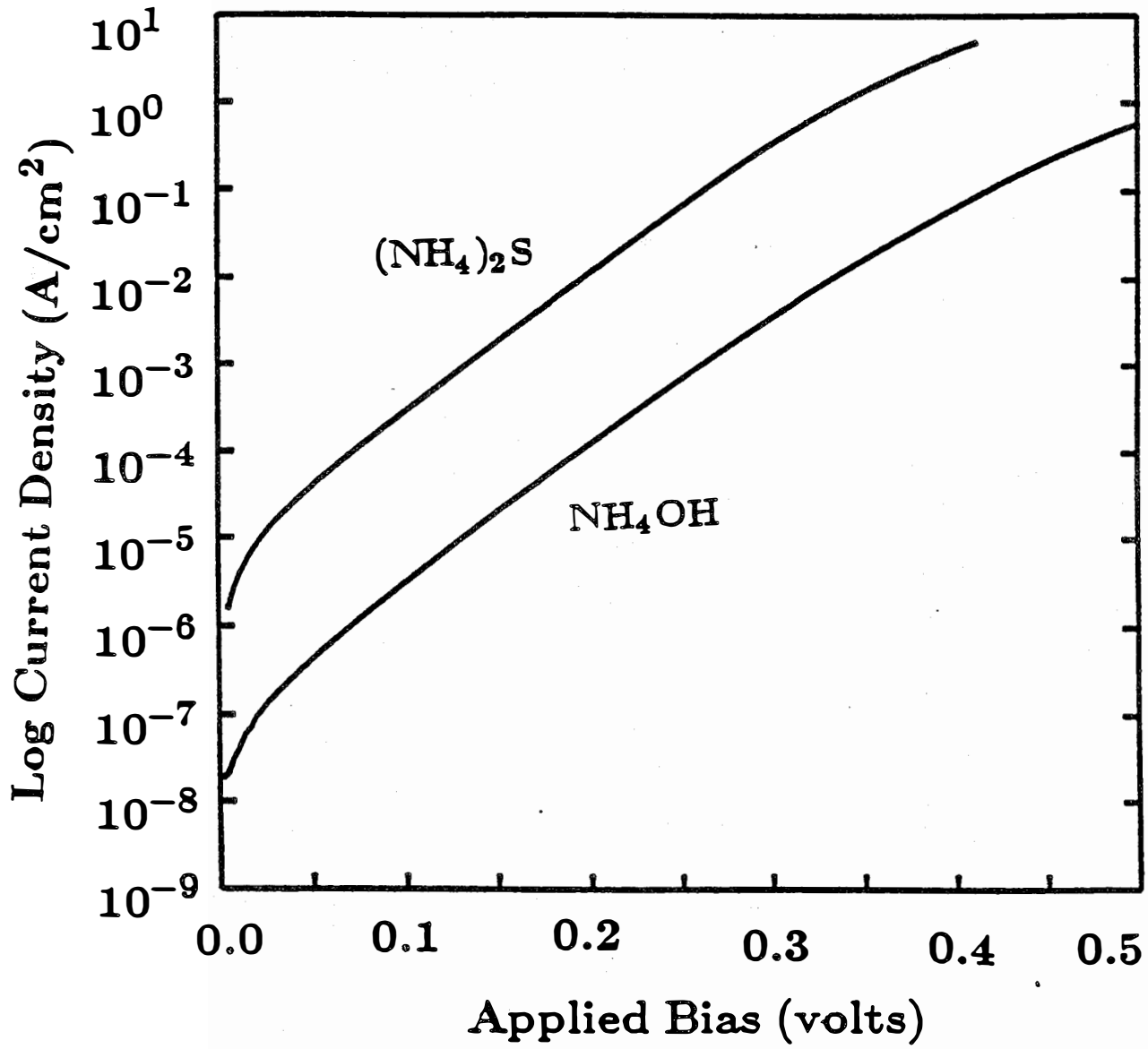

Fig. 6.7a Forward bias current-voltage characteristics measured at 300 K for aluminum Schottky barriers on n-type GaAs. The $(NH_4)_2S^*$ represents samples which were cooled to 77 K during the metal deposition.

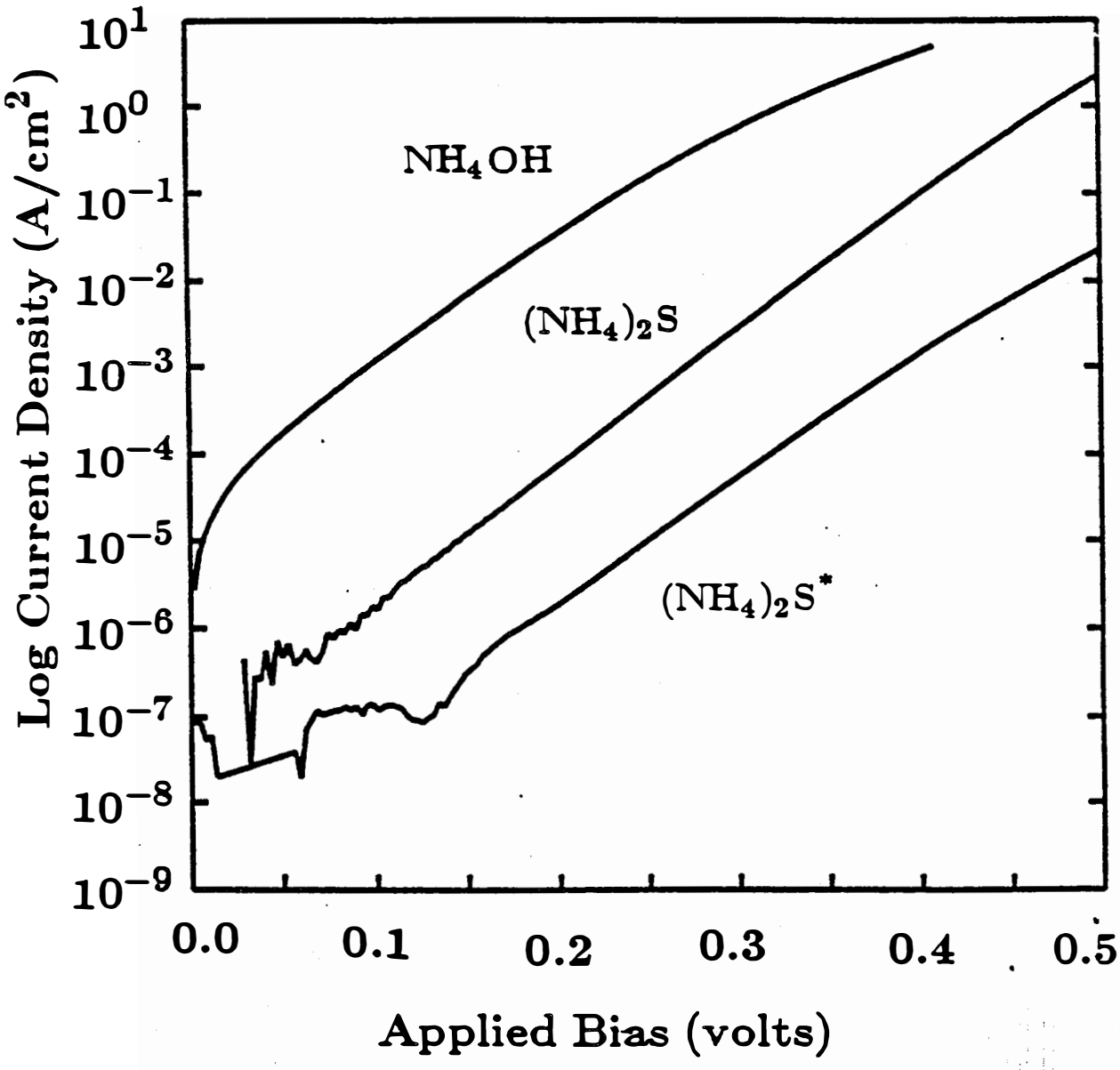

Fig. 6.7b Forward bias current-voltage characteristics measured at 300 K for aluminum Schottky barriers on p-type GaAs. The $(NH_4)_2S^*$ represents samples which were cooled to 77 K during the metal deposition.

$$J_s = A^* T^2 \exp\left[\frac{-q}{kT}(\phi_{bn}-\Delta\phi)\right] \quad (3)$$

where A^* is the effective Richardson constant and $\phi_{bn} - \Delta\phi$ is the effective barrier height, and $\Delta\phi$ is the image force correction term at zero bias. A summary of barrier heights and saturation current densities is given in Table 6.2. The data given in Figs. 6.6 and 6.7 and Table 6.2 are quite representative of the devices on each film. Not only were numerous devices measured, but numerous devices with varying area and perimeter were measured. Since the RHEED patterns for this type of treatment were spotty to begin with, it was possible there are islands of sulfur on the surface. To rule out the possibility that the observed change in barrier height was due to a change in effective device area, activation energy measurements were conducted on selected samples. The barrier heights obtained from activation energy measurements were in good agreement with those obtained from equations 2 and 3.

The barrier height we obtained for gold on ammonium sulfide treated n-type GaAs is similar to the Schottky barrier height obtained by Waldrop for gold on sulfur exposed n-type GaAs [19]. However the barrier height we obtained for aluminum on ammonium sulfide treated GaAs is much higher than that observed by Massies et al. on n-type GaAs exposed to H_2S [20]. This indicates that the full potential for the barrier shift for aluminum may not have been achieved by our method.

6.5 DISCUSSION AN CONCLUSIONS

Although various groups have suggested that the sulfide treatments result in the Fermi[livel being repinned at a new position [21-23], there is now considerable evidence to support the claim that the sulfide treatments reduce the GaAs surface state density and unpin the Fermi-level. The metal/insulator/GaAs work of Oigawa et al. has shown a definite measurable reduction in the surface state density with the incorporation of an ammonium sulfide treatment [17]. The surface recombination velocity has been shown to be reduced by sulfide treatments from both rf induction [8] and photoluminescence measurements [1]. the reduction in surface recombination velocity is the only explanation consistent with the results of Sandroff et al. and Carpenter et al. for sulfide treatments of etched edges of bipolar devices [1-3,7].

Recently, Brillson et al. have demonstrated that metals deposited on a pristine GaAs surface, such as an as-grown MBE surface, produce Schottky barriers which are more sensitive to the metal work function than previously demonstrated [24]. Furthermore, Viturro et al. have shown if in addition to having such a pristine GaAs surface, the metals are deposited with the substrate at low temperatures nearly ideal Schottky barriers are obtained [25]. Our aluminum and gold Schottky barriers formed on ammonium sulfide treated GaAs show similar Schottky barrier trends to those of Viturro et al. [25]. It is intriguing to speculate that our result is due to a low surface state density after deposition of aluminum and gold on the ammonium sulfide treated

Table 6.2 Summary of saturation current densities, Schottky barrier heights, and ideality factors for various surface treatments. All measurements were performed at room temperature. Note $(NH_4)_2S^*$ represents samples which were cooled to 77 K during metal deposition.

Surface treatment	metal	n-type J_s	n-type $\phi_{bn} - \Delta\phi$	n-type n	p-type J_s	p-type $\phi_{bp} - \Delta\phi$	p-type n
NH_4OH	au	7.3×10^{-7}	.781	1.06	5.7×10^{-4}	.585	1.09
$(NH_4)_2S$	au	2.1×10^{-9}	.841	1.08	6.1×10^{-3}	.523	1.19
$(NH_4)_2S^*$	au	1.8×10^{-10}	.917	1.09	1.9×10^{-2}	.461	1.21
NH_4OH	al	1.1×10^{-7}	.767	1.03	5.7×10^{-5}	.592	1.02
$(NH_4)_2S$	al	1.7×10^{-5}	.632	1.04	6.3×10^{-8}	.794	1.09
$(NH_4)_2S^*$	al	-	-	-	5.9×10^{-9}	.894	1.16

GaAs surface. However, Waldrop has investigated Schottky barrier formation when metals are deposited on a GaAs surface which had prior exposure to elemental sulfur [26]. Waldrop observed a large decrease in Schottky barrier heights for Al and Mn due to a contact metal-chalcogen chemical reaction. Waldrop also observed an increase in Schottky barrier heights with some nonreactive noble metal-chalcogen interfaces. In spite of the cause of the Schottky barrier variation, it appears that the ammonium sulfide treatment is a very easy processing step which can be used to obtain a wide range of Schottky barrier heights for metals deposited on GaAs.

CHAPTER 6 REFERENCES

1. C. J. Sandroff, R. N. Nottenburg, J.-C. Bishoff, and R. Bhat, Appl. Phys. Lett. 51, 33 (1987).
2. R. N. Nottenburg, C. J. Sandroff, D. A. Humphrey, T. H. Hollenbeck, and R. Bhat, Appl. Phys. Lett. 52, 218 (1988).
3. M. S. Carpenter, M. R. Melloch, M. S. Lundstrom, and S. P. Tobin, Appl. Phys. Lett. 52, 2157 (1988).
4. M. S. Carpenter, M. R. Melloch, and T. E. Dungan, Appl. Phys. Lett. 53, 66 (1988).
5. M. S. Carpenter and M. R. Melloch, 1988 International Symposium on GaAs and Related Compounds, Atlanta, Georgia, Sept. 11-14, 1988.
6. Jia-Fa Fan, Haruhiro Oigawa, and Yasuo Nannichi, Japanese J. Appl. Phys. 27, L2125 (1988).
7. E. Yablonovitch, C. J. Sandroff, R. Bhat, and T. Gmitter, Appl. Phys. Lett. 51, 439 (1987).
8. E. Yablonovitch, H. M. Cox, and T. J. Gmitter, Appl. Phys. Lett. 52, 1002 (1988).
9. C. J. Sandroff, M. S. Hegde, L. A. Farrow, C. C. Chang, and J. P. Harbison, Appl. Phys. Lett. 54, 362 (1989).
10. B. A. Cowans, Z. Dardas, W. N. Delgass, M. S. Carpenter, and M. R. Melloch, Appl. Phys. Lett. 54, 365 (1989).
11. P. Alnot, J. Olivier, F. Wyczisk, and C.S. Fadley, J. Electron Spectro. Rel. Phen. 43, 263 (1987).
12. W. Ranke and K. Jacobi, Surface Science 63, 33 (1977).
13. W. Ranke and K. Jacobi, Surface Science 47, 525 (1975).
14. J. H. Scofield, J. Electron Spectro. Rel. Phen. 8, 129 (1976).
15. C. M. Kwei and L.W. Chen, Surface and Interface Analysis 60 (1988).
16. J. Massies, F. Dezaly, and N. T. Linh, J. Vac. Sci. Tech B17, 1134 (1980).
17. H. Oigawa, J. Fan, Y. Nannichi, K. Ando, K. Saiki, and A. Koma, Extended Abstracts of the 20th (1988 International) Conference on Solid State Devices and Materials, 263 (1988).
18. E. H. Rhoderick, IEE Proc 129, Pt. I, 1 (1982).
19. J. R. Waldrop, J. Vac. Sci. Technol. B 3 1197 (1985).
20. J. Massies, J. Chaplart, M. Laviron, and N.T. Linh, Appl. Phys. Lett. 38 693 (1981).
21. R. S. Besser and C. R. Helms, Appl. Phys. Lett. 52 1707 (1988).
22. H. Hasegawa. T. Sawada, H. Ishii, S. Konishi, Y. Liu, T. Saitoh, and H. Ohno, Extended Abstracts of the 20th (1988 International) Conference on Solid State Devices and Materials, 263 (1988).
23. D. Liu, T. Zhang, R. A. LaRue, J.S. Harris, Jr., and T.W. Sigmon, Appl. Phys. Lett. 53 1059 (1988).

24. L. J. Brillson, R. E. Viturro, C. Mailhiot, J. L. Shaw, N. Tache, J. McKinley, G. Margaritondo, J. M. Woddall, P. D. Kirchner, G. D. Pettit, and S. L. Wright, J. Vac. Sci. Technol. B6, 1263 (1988).

25. R. E. Viturro, S. Chang, J. L. Shaw, C. Mailhiot, L. J. Brillson, R. Zanoi, Y. Hwu, G. Margaritondo, P. D. Kirchner, and J. M. Wooda II, Sixteenth Annual Conference on the Physics and Chemistry of Semiconductor Interfaces, Bozeman, Montana, Feb. 7-9, 1989.

26. J. R. Waldrop, Appl. Phys. Lett. 47, 1301 (1985).

APPENDIX 1: REPRINTS OF 1988-1989 PUBLICATIONS

This appendix contains reprints of the publications which resulted from the work conducted during the past year.

[1] M. S. Carpenter, M. R. Melloch, and T. E. Dungan, "Schottky barrier formation on $(NH_2)_2S$-treated n- and p-type (100) GaAs," *Appl. Phys. Lett.* 53 (1), pp. 66-68, 4 July 1988,

[2] M. E. Klausmeier-Brown, P. D. DeMoulin, H. L. Chuang, M. S. Lundstrom, and M. R. Melloch, S. P. Tobin, "Influence of Bandgap Narrowing Effects in p^+-GaAs on Solar Cell Performance," Conf. Rec., 20th IEEE Photovoltaic Specialists Conference, Las Vegas, NV, pp. 503-507, Sept. 1988.

[3] M. S. Carpenter and M. R. Melloch, "Formation of Schottky barriers on reduced surface state gallium arsenide," Inst. Phys. Conf. Ser. No. 96: Chapter 6, paper presented at Int. Symp. GaAs and Related Compounds, Atlanta, GA, 1988, pp. 381-386.

[4] H. L. Chuang, P. D. DeMoulin, M. E. Klausmeier-Brown, M. R. Melloch, and M. S. Lundstrom, "Evidence for band-gap narrowing effects in Be-doped, p-p^+ GaAs homojunction barriers," *J. Appl. Phys.* 64 (11), pp. 6361-6364, 1 December 1988.

[5] B. A. Cowans, Z. Dardas, W. N. Delgass, M. S. Carpenter and M. R. Melloch, "X-ray photoelectron spectroscopy of ammonium sulfide treated GaAs (100) surfaces," *Appl. Phys. Lett.* 54 (4), pp. 365-367, 23 January 1989.

[6] H.L. Chuang, M.E. Klausmeier-Brown, M.R. Melloch, and M.S. Lundstrom, ''Effective Minority Carrier Hole Confinement of Si-Doped, n^+–n GaAs Homojunction Barriers,'' *J. Appl. Phys.*, Vol. 66, pp. 273-277, 1989.

Schottky barrier formation on $(NH_4)_2S$-treated *n*- and *p*-type (100)GaAs

M. S. Carpenter, M. R. Melloch, and T. E. Dungan
Purdue University, School of Electrical Engineering, West Lafayette, Indiana 47907

(Received 7 March 1988; accepted for publication 3 May 1988)

Because of a large surface state density, which effectively pins the Fermi level at the surface, metals with vastly different work functions and chemistry produce very similar Schottky barriers when deposited on GaAs. We have investigated the effects of a $(NH_4)_2S$ surface treatment on the formation of Schottky barriers on *n*- and *p*-type GaAs. Samples which have undergone the $(NH_4)_2S$ treatment show a reduced pinning of the Fermi level at the surface and hence Schottky barriers which are more sensitive to the metal work function.

Metals with vastly different work functions and chemistry produce very similar Schottky barriers when deposited on GaAs.[1-3] This is due to the large surface state density which effectively pins the Fermi level at the surface. Surface Fermi levels are pinned near 0.75 eV above the valence-band edge for *n*-type samples and 0.5 eV above the valence-band edge for *p*-type samples. Massies *et al.*[4] have formed aluminum/*n*-type Schottky barriers by depositing aluminum *in situ* in a molecular beam epitaxy (MBE) system on a MBE-grown (100)GaAs epilayer exposed to hydrogen sulfide. These Schottky barriers were much lower than the barriers formed by depositing aluminum directly on an as-grown epilayer. It would be highly desirable to find a simpler process than *in situ* MBE processing for obtaining Schottky barriers on GaAs which are more sensitive to the metal work functions. A higher barrier could then be obtained which would reduce gate leakage currents in GaAs metal-semiconductor field-effect transistors (MESFET's). If one could raise the Schottky barrier to *p*-GaAs, it would be feasible to implement a complementary logic MESFET technology. Currently, a double-implanted junction field-effect transistor (JFET) technology is required to implement complementary logic in GaAs.[5] Alternatively, the barrier could also be lowered, leading to easier formation of ohmic contacts.

Recent photochemical[6] and chemical[7-10] treatments have been used to reduce the GaAs surface state density. In room air the photochemical treatment lasts for about 20 min, whereas the most widely reported chemical treatments with Na_2S last for 18–48 h. The aging of the Na_2S treatment probably depends on the atmospheric humidity, since the Na_2S treatment can be removed with a de-ionized water rinse. A $(NH_4)_2S$ treatment produces a similar reduction in surface state density as the Na_2S treatment. We have been investigating $(NH_4)_2S$ passivation of GaAs *pn* diodes because dried $(NH_4)_2S$ does not rinse off in water.[11] In fact, a de-ionized water rinse is a final step of our passivation procedure described below. Because we have found the $(NH_4)_2S$ passivation to be more durable, we have investigated the formation of Schottky contacts on the $(NH_4)_2S$ passivated surface.

The devices used in this study were fabricated from two (100)GaAs wafers. The first wafer was an *n*-type molecular beam epitaxially grown 1-μm-thick epilayer on an n^+ substrate. The second was similar except that it was *p*-type. The dopings of the epilayers were 2.2×10^{16} cm^{-3} for the *n*-type and 1.6×10^{16} cm^{-3} for the *p*-type as determined by capacitance-voltage profiling. The two wafers were cleaved into samples of approximate area of 0.25 cm^2, and these samples were prepared for evaporation by etching in 1:1:250 H_2SO_4:H_2O_2:H_2O for 10 s followed by a 30 s de-ionized water rinse. The samples were then either soaked in $(NH_4)_2S$ for 5 min or in NH_4OH for 20 s. (The NH_4OH rinse removes the surface oxides and is a typical processing step before depositing metals on GaAs.[12]) The samples were then rinsed in de-ionized water and quickly loaded into an evaporator. Either gold or aluminum was evaporated across the entire sample. (The metal was always evaporated at the same time on both an *n*- and *p*-type sample which had undergone similar surface treatment.) Schottky diodes were then defined by usual photolithographic processes and wet chemical etching.

The Schottky diodes were contacted by probes on a model 6000 micromanipulator test station, and the current voltage (*I-V*) characteristics were measured using a Hewlett–Packard 4145A semiconductor parameter analyzer. *I-V* data were obtained from -1 to 0.5 V.

Figures 1(a) and 1(b) show forward-bias *I-V* data for Schottky diodes formed from aluminum and gold on $(NH_4)_2S$-treated *n*- and *p*-GaAs, respectively. The figures also include a characteristic for aluminum on GaAs rinsed only in NH_4OH for comparison. This curve is typical of diodes formed from any metal on the pinned GaAs surface. Figure 1(a) shows that incorporation of the $(NH_4)_2S$ treatment significantly increases the aluminum-to-*n*-GaAs diode current while decreasing the gold-to-*n*-GaAs current. By comparison, Fig. 1(b) shows that the treatment significantly suppresses the aluminum-to-*p*-GaAs current while increasing the gold-to-*p*-GaAs current.

To determine the barrier heights, the *I-V* data were analyzed in terms of a thermionic emission model of current transport[13]:

$$\qquad (1)$$

where J_s is the saturation current density and n is the ideality factor which represents the voltage dependence of the barrier. This particular representation includes the image force correction for both reverse as well as forward bias. Plots of $\log\{J/[1-\exp(-qV/kT)]\}$ vs V were linear from a re-

 0003-6951/88/270066-03$01.00 © 1988 American Institute of Physics

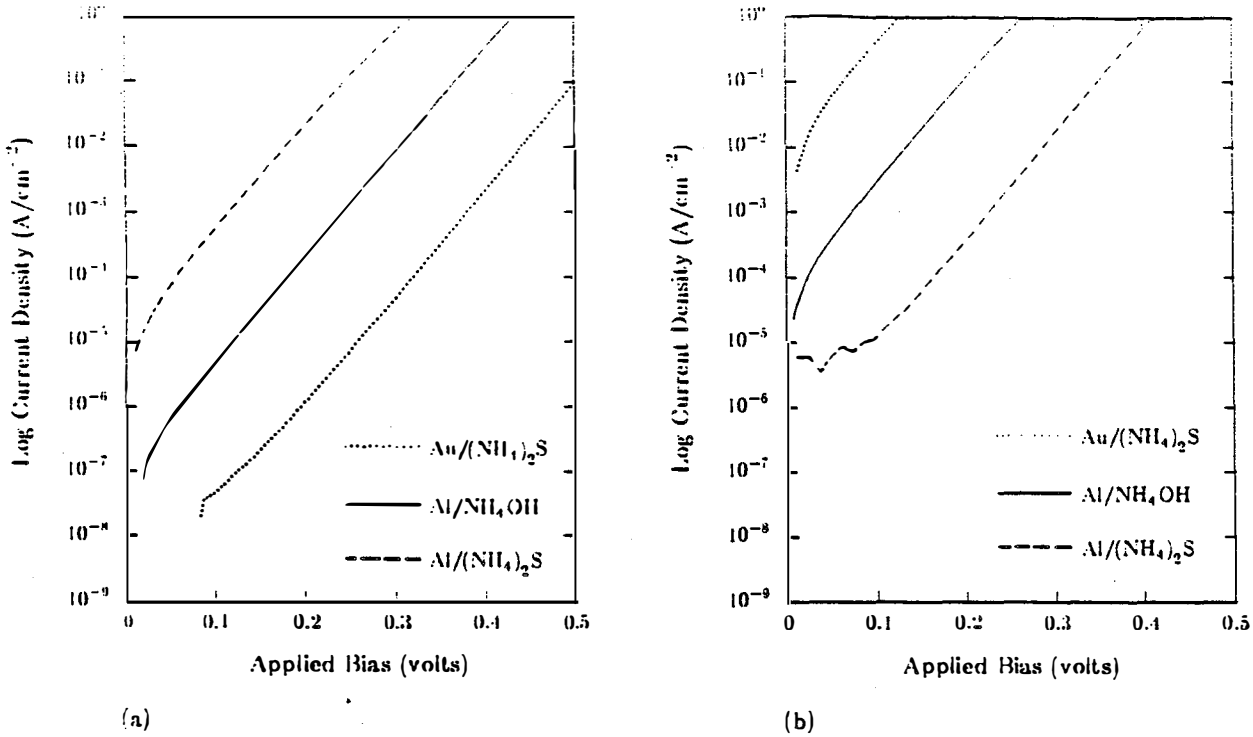

FIG. 1. (a) Schottky diode I-V characteristics for aluminum and gold deposited on $(NH_4)_2S$-treated n-GaAs and for aluminum deposited on n-GaAs wi only had a standard NH_4OH rinse. (b) Schottky diode I-V characteristics for aluminum and gold deposited on $(NH_4)_2S$-treated p-GaAs and for alumir deposited on p-GaAs which only had a standard NH_4OH rinse.

verse bias of -1 V to a forward bias of 0.5 V, except for series resistance effects at high forward currents. From a least-squares fit to the linear portion of these plots, we determined the saturation current densities and the ideality factors for our Schottky diodes. The effective barrier heights were then determined from the following relation for the saturation current density:

$$J_s = A^* T^2 \exp\left(\frac{-q}{kT}(\phi_{bn} - \Delta\phi)\right), \qquad (2)$$

where A^* is the effective Richardson constant (8.16 A cm^{-2} K^{-2} for n-type and 74.4 A cm^{-2} K^{-2} for p-type), $\phi_{bn} - \Delta\phi$ is the effective barrier height, and $\Delta\phi$ is the image force correction term at zero bias. The effective barrier heights, the current densities, and the ideality factors are summarized in Table I. (Measurements were made on diodes ranging in area from 2.5×10^{-5} to 1.6×10^{-3} cm^2 for each prepared sample. The current densities were independent of the areas and were very uniform across each sample, varying in the most extreme case by less than a factor of 2.) It should be noted that we have exposed our samples to room atmosphere for two weeks with no change in the Schottky diode I-V characteristics.

As can be seen from Table I, the $(NH_4)_2S$-treated a minum diodes have lower effective barriers to n-type Ga than to p-type GaAs. The $(NH_4)_2S$-treated gold diodes h higher effective barriers to n-type GaAs than to p-t GaAs. These results indicate that the Fermi level has been repinned at a new energy level since the treated samp shift in different directions for different metals. This in cates that there is a reduced number of surface states. T surface state density can be estimated by the following re tion developed by Cowley and Sze[14]:

$$\phi_{bn} = \gamma(\phi_m - \chi_s) + (1-\gamma)(E_g - \phi_0)\,, \qquad ($$

where ϕ_m is the metal function, χ_s is the semiconductor el tron affinity, ϕ_0 is the neutral level for the surface states, a γ is given by

$$\gamma = \epsilon_i/(\epsilon_i + q^2\delta D_s)\,, \qquad ($$

where ϵ_i is the permittivity of any interface layer, δ is width of the interface layer, and D_s is the surface state d sity. If the density of surface states is assumed to be unifo and if the interface layer is assumed to be about a monola (5 Å), then using numerical estimates for γ, we find density of surface states to be 1.9×10^{13} cm^{-2} for

TABLE I. Summary of Schottky diode current densities, ideality factors, and effective barrier heights.

Surface treatment	Metal	n-type J_s (A/cm^2)	$\phi_{bn} - \Delta\phi$	n	p-type J_s (A/cm^2)	$\phi_{bp} - \Delta\phi$	n
NH_4OH	Al	1.1×10^{-7}	0.767	1.03	5.7×10^{-5}	0.662	1.02
$(NH_4)_2S$	Al	2.2×10^{-5}	0.632	1.04	6.4×10^{-7}	0.780	1.03
$(NH_4)_2S$	Au	1.9×10^{-9}	0.871	1.08	2.5×10^{-3}	0.563	1.05

$(NH_4)_2S$-treated samples. Crowley and Sze found the density of states to be 1.2×10^{14} cm^{-2} for the same calculations and assumptions for untreated films.[14]

In conclusion, we have investigated the effects of a $(NH_4)_2S$ surface treatment on the formation of Schottky barriers on *n*- and *p*-type GaAs. The Schottky barriers formed on the $(NH_4)_2S$-treated GaAs surfaces show an order of magnitude reduction in surface state density. This reduction in surface density results in Schottky barriers which are more sensitive to the metal work functions.

This work was supported by the Solar Energy Research Institute under subcontract No. XL-5-05018-1 and the Office of Naval Research under grant No. N00014-86-K-0350.

[1]C. A. Mead and W. G. Spitzer, Phys. Rev. A **134**, 713 (1964).
[2]W. E. Spicer, I. Lindau, P. Skeath, and C. Y. Su, J. Vac. Sci. Technol. **17**, 1019 (1980).
[3]J. R. Waldrop, Appl. Phys. Lett. **44**, 1002 (1984).
[4]J. Massies, J. Chaplart, M. Laviron, and N. T. Linh, Appl. Phys. Lett. 693 (1981).
[5]R. Zuleeg, J. K. Notthoff, and G. L. Troeger, IEEE Electron Device 5, 21 (1984).
[6]S. D. Offsey, J. M. Woodall, A. C. Warren, P. D. Kirchner, T. I. Chapp and G. D. Pettit, Appl. Phys. Lett. **48**, 475 (1986).
[7]C. J. Sandroff, R. N. Nottenburg, J. C. Bischoff, and R. Bhat, Appl. Lett. **51**, 33 (1987).
[8]E. Yablonovitch, C. J. Sandroff, R. Bhat, and T. J. Gmitter, Appl. Ph Lett. **51**, 493 (1987).
[9]B. J. Skromme, C. J. Sandroff, E. Yablonovitch, and T. J. Gmitter, Phys. Lett. **51**, 2022 (1987).
[10]R. N. Nottenburg, C. J. Sandroff, D. A. Humphrey, T. H. Hollenbe and R. Bhat, Appl. Phys. Lett. **52**, 218 (1988).
[11]M. S. Carpenter, M. R. Melloch, M. S. Lundstrom, and S. P. Tobin, Phys. Lett. **52**, 2157 (1988).
[12]Ralph E. Williams, *Gallium Arsenide Processing Techniques* (Art House, Dedham, MA, 1984).
[13]E. H. Rhoderick, IEE Proc. **129**, Pt. I, 1 (1982).
[14]A. M. Cowley and S. M. Sze, J. Appl. Phys. **46**, 3212 (1965).

INFLUENCE OF BANDGAP NARROWING EFFECTS IN p^+-GaAs ON SOLAR CELL PERFORMANCE

M. E. Klausmeier-Brown, P. D. DeMoulin, H. L. Chuang, M. S. Lundstrom, and M. R. Melloch
School of Electrical Engineering, Purdue University, West Lafayette, IN 47907

S. P. Tobin
Spire Corporation, Patriots Park, Bedford, MA 01730

ABSTRACT

In this paper we review the first electrical measurements of bandgap narrowing effects in p^+-GaAs and assess their influence on solar cell performance. It is found that these effects degrade solar cell performance by increasing the dark current associated with electron injection in p^+-n cells, and by degrading the performance of p-p^+ back-surface fields. We describe an experiment which directly measures the electron recombination velocity, S, for a p-p^+ back-surface field, and show that the high value of S can be explained by bandgap narrowing. Computer simulation is employed to assess the influence of bandgap narrowing on realistic solar cells.

INTRODUCTION

It is well known that changes in the energy band structure of silicon due to heavy p-type impurity doping strongly enhance electron injection currents in silicon p^+-n junctions. These enhanced electron injection currents have a profound effect on the efficiency of silicon solar cells [1]. We review the first electrical measurements of bandgap narrowing effects in p^+-GaAs [2] and assess their influence on solar cell performance. A sequential etch technique [3] was employed to measure electron injection currents in p^+-n GaAs heteroface solar cells for impurity concentrations in the range $\simeq 10^{18}$-$10^{19}\,cm^{-3}$. Results show that $n_{ie}^2 D_n$ increases greatly with doping just as it does in p^+-Si. These effects degrade solar cell performance by increasing the dark current associated with electron injection in p^+-n cells and by degrading the performance of p-p^+ back-surface fields.

We first review our electrical measurements of bandgap narrowing effects in p^+-GaAs, and consider the importance of such effects in n^+-GaAs. Next, the influence of bandgap narrowing effects on the performance of p-p^+ back-surface fields is examined. Finally, we assess the influence of these effects on the efficiency of optimized p^+-n and n^+-p heteroface solar cells.

BANDGAP NARROWING IN HEAVILY DOPED GaAs

The p^+-n GaAs heteroface solar cells used in the study of bandgap narrowing effects were high quality devices grown in a Spire Model MO-450 MOCVD reactor. The measurement technique used consists essentially of characterizing J_{01e}, the component of the n=1 saturation current density due to electrons injected in the p-type emitter, as a function of the width of the emitter. After etching away the p^+-GaAs cap and AlGaAs heteroface layers, J_{01e} dominated the n=1 dark current [3]. The emitter was then thinned by successive etches in a weak etchant. After each etch, J_{01e} was extracted from the measured dark current versus voltage characteristic by curve fitting. The inverse of the electron injection current is a linear function of emitter etch time, t:

$$J_{01e}^{-1} = \left[\frac{pW_{E0}}{qn_{ie}^2 D_n} + \frac{p}{qn_{ie}^2 S}\right] - \left[\frac{pR}{qn_{ie}^2 D_n}\right] t, \qquad (1)$$

where p is the emitter hole concentration, R is the etch rate, and D_n is the electron diffusion coefficient in the p^+-emitter. The product $n_{ie}^2 D_n$ can be determined from the slope of the line, $pR/qn_{ie}^2 D_n$, without knowledge of the surface recombination velocity, S.

Conf. Rec., 20th IEEE Photovoltaic Specialists Conference, Las Vegas, NV, Sept. 1988.

0160-8371/88/0000-0503 $1.00 © 1988 IEEE

The influence of bandgap shrinkage effects on the equilibrium np product is illustrated by the definition

$$n_{ie}^2 \equiv n_o p_o \equiv n_{io}^2 \, e^{\frac{\Delta E_G^{app}}{k_B T}} \times \left[\frac{\mathcal{F}_{1/2}(\eta)}{e^{\eta}} \right], \qquad (2)$$

where n_{ie} is the effective intrinsic carrier concentration, ΔE_G^{app} is the apparent shrinkage of the bandgap, n_{io} is the intrinsic carrier concentration for lightly doped GaAs, and the term $\mathcal{F}_{1/2}(\eta)/e^{\eta}$ accounts for degeneracy of the hole gas. Equation (2) results from a simple, rigid band model. Fig. 1 is a plot of the measured $n_{ie}^2 D_n$ versus hole concentration. A theoretical curve, calculated using (2) with $\Delta E_G^{app}=0$, taking n_{io} from Blakemore [4], and D_n from Walukiewicz et al. [5] for zero compensation, is also plotted. Measured values of D_n [6-8] are significantly lower than the theoretical zero compensation values of Walukiewicz et al., meaning that the lower curve in Fig. 1 represents an upper limit for $n_{ie}^2 D_n$. Therefore, the comparison in Fig. 1 represents a *conservative* estimate of the importance of bandgap narrowing in p^+-GaAs. Still, the difference in the two $n_{ie}^2 D_n$ curves is a factor of ten just above $p = 10^{19}\,\mathrm{cm}^{-3}$, demonstrating the importance of considering bandgap narrowing.

This increase in $n_{ie}^2 D_n$ degrades solar cell performance by increasing the dark current associated with electron injection into the p-type active layer of the cell. The result is that the electron injection component, J_{01e}, for a p^+-n GaAs heteroface cell may be quite significant, even for an emitter doping of $10^{19}\,\mathrm{cm}^{-3}$. J_{01e} would be nearly a factor of ten higher than the value expected assuming no bandgap narrowing at $p = 10^{19}\,\mathrm{cm}^{-3}$, becoming comparable to the hole injection component of the dark current. The increase in dark current could be even more pronounced in cell designs for which the top metal grid directly contacts the p-type emitter, or if the front surface is not well passivated.

We expect bandgap narrowing to be much less important in heavily doped n-type GaAs. Use of the correct Fermi-Dirac statistics in calculating the position of the Fermi level in n^+-GaAs shows that the Fermi level penetrates quite far into the conduction band, due to the small density of states in GaAs. The minority carrier hole concentration in n-type GaAs, described by

$$p_o = N_V \, e^{\frac{-(E_F - E_V)}{k_B T}}, \qquad (3)$$

is reduced by the effects of this strong electron degeneracy. The term $\mathcal{F}_{1/2}(\eta)/e^{\eta}$ in (2) accounts for this degeneracy, and can be thought of as an effective bandgap *widening* which opposes the effect of bandgap shrinkage, represented by the term $e^{\Delta E_G^{app}/k_B T}$ in (2).

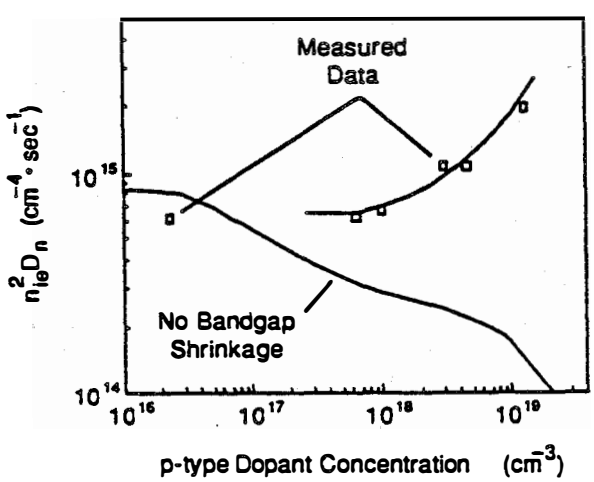

Fig. 1. Measured $n_{ie}^2 D_n$ product versus hole concentration in GaAs at 300 K. Also shown is a fit to the measured data, and a theoretical curve which assumes no bandgap shrinkage.

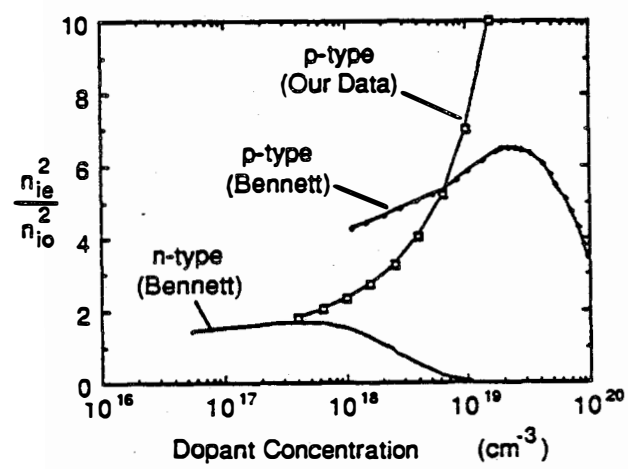

Fig. 2. Effective intrinsic carrier concentration ($n_{ie}^2 \equiv n_o p_o$) in n- and p-type GaAs. The curve representing our data (from electrical measurements) is a lower limit, because we assumed the "upper limit" values of D_n of Walukiewicz et al. in deducing n_{ie}^2 from the measured $n_{ie}^2 D_n$ (see text).

Detailed band structure calculations by Bennett and Lowney [9] confirm that the degeneracy (or effective bandgap widening) dominates any bandgap narrowing effects in n^+-GaAs at a fairly low doping level relative to p^+-GaAs. Fig. 2 shows that the equilibrium np product ($\equiv n_{ie}^2$) in n^+-GaAs is much lower than in p^+-GaAs above $10^{18}\,cm^{-3}$. Since bandgap narrowing in p^+-GaAs is expected to be so much more important than in n^+-GaAs, this paper will focus on the effects of bandgap narrowing in p^+-GaAs on solar cell performance.

EFFECTS OF BANDGAP NARROWING ON HOMOJUNCTION BACK-SURFACE FIELDS

This enhanced $n_{ie}^2 D_n$ product in p^+-GaAs also reduces the effectiveness of p-p^+ low-high junctions employed as back-surface fields to improve collection efficiency in n^+-p cell designs. The effectiveness of these low-high junctions in reducing back-surface recombination can be characterized in terms of an interface recombination velocity:

$$S_{LH} = \frac{(n_{ie}^2 D_n)^+}{W^+(n_{ie}^2)^-}\left(\frac{p^-}{p^+}\right), \qquad (4)$$

where the "−" and "+" superscripts refer to the low- and high-doped sides of the junction, respectively [10]. This expression assumes that the minority carrier diffusion length is much greater than the width of the barrier layer, W^+. The measured $n_{ie}^2 D_n$ products were used in (4) to calculate S_{LH} versus hole concentration for a p-p^+ barrier, for barrier width $W^+ = 0.5\,\mu m$, and $p^- = 10^{17}\,cm^{-3}$. The results are displayed in Fig. 3. Also shown is the corresponding curve for an n-n^+ barrier, calculated using n_{ie} in n-type GaAs from [9], and the measured mobility of holes as majority carriers. Fig. 3 shows that for the p-p^+ barrier, $S_{LH} > 10^4$ cm/sec, even for the highest barrier doping levels. In contrast, the n-n^+ barrier recombination velocity is less than 10^4 cm/sec for barrier dopings greater than $10^{18}\,cm^{-3}$.

We now describe an experiment which directly measures the recombination velocity for a p-p^+ back-surface field, and show that the high recombination velocity can be explained by bandgap narrowing. The structure shown in Fig. 4 was grown by MBE. In this structure the barrier layers to be studied, p^+-GaAs and p^+-$Al_{0.2}Ga_{0.8}As$, were situated near the top surface of the diode so that their effectiveness as minority carrier mirrors could be probed by a successive etch experiment. Note that the p-type active layer is doped much lighter than the n-GaAs, so the n=1 dark current is very sensitive to the top-surface recombination velocity.

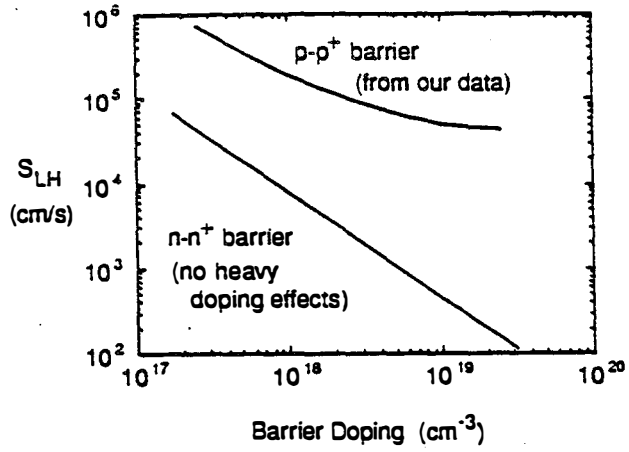

Fig. 3 Back-surface recombination velocity for p-p^+ and n-n^+ low-high doping junctions as a function of the doping of the barrier. The barrier layer (heavily doped side of the junction) was 0.5 μm thick.

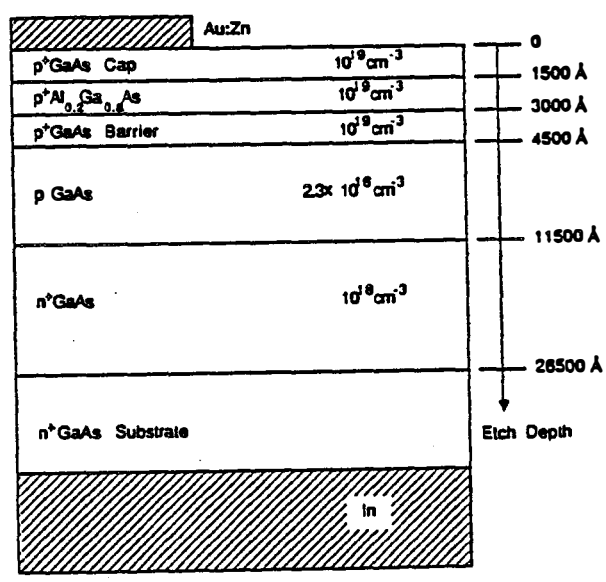

Fig. 4 Epitaxial layer structure of the diode used to study back-surface field barrier layers.

The measured J_{01} was roughly constant until the p^+-$Al_{0.2}Ga_{0.8}As$ was removed; it then increased as the p^+-GaAs barrier layer was thinned. From the value of J_{01} measured after removing the p^+-$Al_{0.2}Ga_{0.8}As$ layer, it was possible to deduce the recombination velocity at the p-p^+ GaAs junction as a function of the thickness of the p^+-barrier. The result is shown in Fig. 5. For a barrier thickness of 1500 Å (etch depth = 3000 Å) the measured surface recombination velocity was 6×10^4 cm^{-3}.

As the p^+-barrier was etch-thinned, the surface recombination velocity deduced from the measured dark current increased until the etch depth reached 4500 Å, at which point the barrier had been completely removed, exposing the lighter doped p-GaAs. The fact that the recombination velocity depended on the barrier thickness shows that the high recombination velocities were *not* due to defects or charge present at the p-p^+ interface. Once the p^+-barrier was removed, the surface recombination velocities deduced were $\simeq 10^7$ cm/sec, in agreement with the value expected for a bare GaAs surface [11]. Also shown in Fig. 5 is the barrier recombination velocity for the p^+-barrier calculated using (4), assuming no bandgap shrinkage in the p^+-GaAs. The high observed recombination velocities appear to be due to significant bandgap narrowing in the p^+-GaAs.

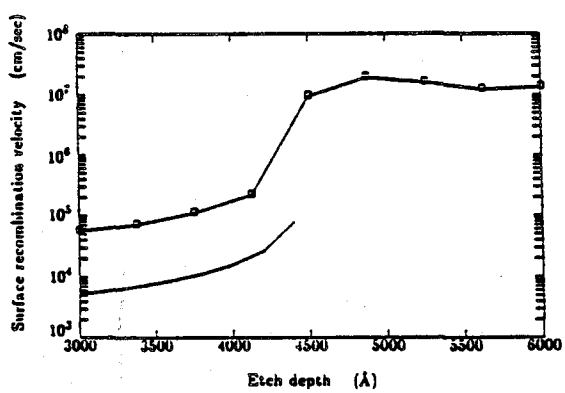

Fig. 5 Recombation velocity vs. etch depth starting from the p^+-GaAs barrier layer. The top curve represents measured data, while the bottom curve represents theoretical calculations which neglect bandgap narrowing effects.

EFFECTS OF BANDGAP NARROWING ON HETEROFACE SOLAR CELL EFFICIENCY

Complete two-dimensional drift-diffusion simulations of optimized heteroface solar cells were performed to test the effects of bandgap narrowing on overall cell performance. The structures studied are shown in Fig. 5. All simulations were conducted with a 500-sun (AM1.5, direct, 100 mW/cm^2/sun) illumination. The assumed cell temperature was 25 °C. With bandgap narrowing in p^+-GaAs "turned off" the simulations found efficiencies of 31.5% for the p^+-n cell and 31.0% for the n^+-p cell.

Both cells were simulated again, this time with bandgap narrowing in the p^+-GaAs "turned on". Bandgap shrinkage effects had an adverse effect on the efficiencies of both cells, as shown in Table 1.

Table 1 Effects of bandgap narrowing on optimized cell performance.

Parameter	p^+-n	n^+-p
ΔV_{OC}	- 23 mV	- 25 mV
ΔJ_{SC}	0.0 A/cm^2	- 0.18 A/cm^2
$\Delta \eta$	- 0.7%	- 1.1%

The decreased open-circuit voltage was in both cases due to increased injection of electrons into the p^+-GaAs due to bandgap shrinkage. The short-circuit current of the n^+-p cell was reduced because of the ineffectiveness of the p-p^+ back-surface field, again due to bandgap shrinkage in the p^+-GaAs barrier layer. It was found that use of a p^+-AlGaAs heterojunction barrier as a back-surface field increased the efficiency of the n^+-p cell to 31.4%, with bandgap narrowing turned on. This figure is even higher than the 30.8% efficiency of the p^+-n cell, which used an n-n^+ homojunction as a back-surface field. Note that the short-circuit current of the p^+-n cell was not reduced at all by inclusion of bandgap narrowing effects in the simulation.

SUMMARY

Our results show that bandgap narrowing is quite significant in p^+-GaAs, and has important effects on the performance of conventional GaAs heteroface cell designs. The open-circuit voltage in both p^+-n and n^+-p configurations was reduced because of increased electron injection into p^+-GaAs, due to bandgap narrowing effects. In addition, performance of n^+-p designs incorporating a p-p^+ GaAs homojunction as a back-surface field was found to be degraded as a result of bandgap shrinkage in the p^+-GaAs barrier layer.

ACKNOWLEDGEMENTS

This work was supported by the Solar Energy Research Institute, sub-contract XL-5-05018-1. M. E. Klausmeier-Brown was supported by the Eastman-Kodak Company. The authors wish to thank Staney Vernon of Spire Corporation for providing the MOCVD films used in the experimental studies of bandgap narrowing.

REFERENCES

[1] J. A. del Alamo and R. M. Swanson, Solid-State Electron. **30**, 1127 (1987).

[2] M. E. Klausmeier-Brown, M. S. Lundstrom, M. R. Melloch and S. P. Tobin, Appl. Phys. Lett. **52**, 2255 (1988).

[3] M. E. Klausmeier-Brown, C. S. Kyono, P. D. DeMoulin, S. P. Tobin, M. S. Lundstrom and M. R. Melloch, IEEE Trans. Electron Devices **ED-35**, 1159 (1988).

[4] J. S. Blakemore, J. Appl. Phys. **53**, R123 (1982).

[5] W. Walukiewicz, J. Lagowski, L. Jastrzebski, and H. C. Gatos, J. Appl. Phys. **50**, 5040 (1979).

[6] R. K. Ahrenkiel, D. J. Dunlavy, D. Greenberg, J. Schlupmann, H. C. Hamaker and H. F. MacMillan, Appl. Phys. Lett. **51**, 776 (1987).

[7] M. I. Nathan, W. P. Dumke, K. Wrenner, S. Tiwari, S. L. Wright and K. A. Jenkins, Appl. Phys. Lett. **52**, 654 (1988).

[8] H. L. Chuang, P. D. DeMoulin, M. E. Klausmeier-Brown, M. R. Melloch and M. S. Lundstrom, to appear in J. Appl. Phys. (1988).

[9] H. S. Bennett and J. R. Lowney, J. Appl. Phys. **62**, 521 (1987).

[10] P. D. DeMoulin, M. S. Lundstrom, and R. S. Schwartz, Solar Cells **20**, 229 (1987).

[11] R. P. Leon, Proc. of the 19th Photovoltaic Spec. Conf. (New Orleans, LA, 1987), 808.

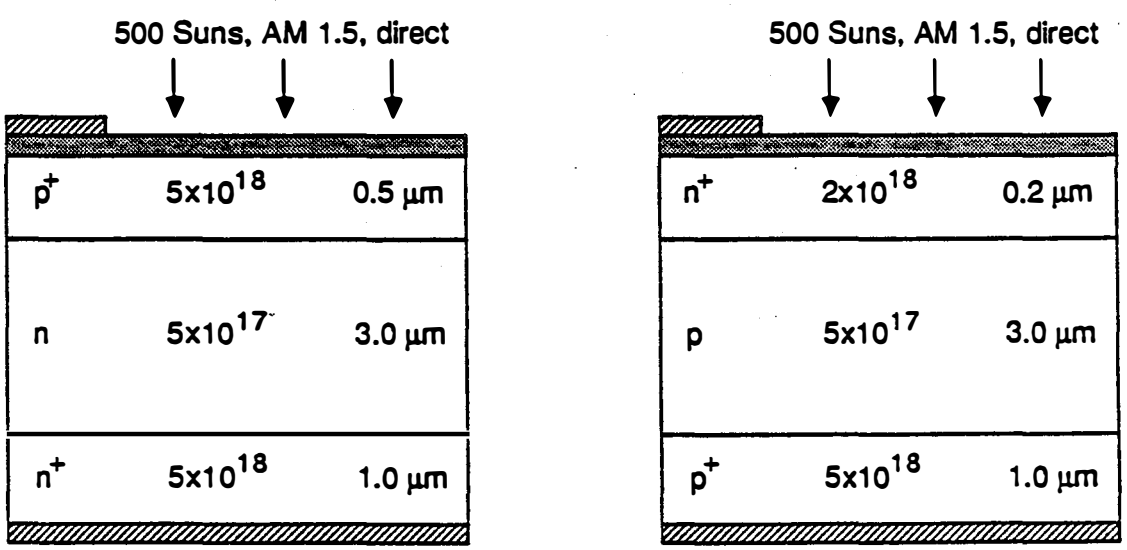

Fig. 6 Cell structure for the optimized (a) p^+-n and (b) n^+-p cells. The shaded region in each figure represents the AlGaAs window layer.

Inst. Phys. Conf. Ser. No 96: Chapter 6
Paper presented at Int. Symp. GaAs and Related Compounds, Atlanta, Georgia, 1988

Formation of Schottky barriers on reduced surface state gallium arsenide

M.S. Carpenter and M.R. Melloch

Purdue University, School of Electrical Engineering, West Lafayette, Indiana 47907

ABSTRACT: The large surface state density exhibited by gallium arsenide effectively pins the Fermi level at the surface. Due to this pinning Schottky barriers exhibit similar behavior even though the chemical properties and work functions vastly differ. We have used a $(NH_4)_2S$ treatment, which has been shown to unpin the surface, to prepare the surface for Schottky barrier formation. We have found the treatment to reduce the surface state density by an order of magnitude and provide barriers which are sensitive to the metal work function.

Metals with various work function and chemical properties produce Schottky barriers which behave similarly when deposited on GaAs [Mead, Spicer, Waldrop]. This phenomenon is due to the large surface state density which effectively pins the Fermi level. The Fermi level at the surface is pinned at 0.75 eV below the conduction band minimum for n-type material and at 0.50 eV above the valence band maximum for p-type material. Spicer and co-workers have shown great similarities between Fermi level pinning due to oxygen uptake and metal deposition. They conclude that the pinning mechanism for both is essentially the same. With this in mind, one may conclude that mechanisms which unpin an oxygen pinned surface may be helpful in modifying a pinned Schottky barrier.

Recently photochemical and chemical treatments have been shown to be effective at reducing the surface state density and recombination velocity of GaAs surfaces. The photochemical treatment consists of washing the sample in deionized water while it is being illuminated [Offsey]. The treated surface has been examined and was found to leave a GaAs surface terminated by gallium oxide. No elemental arsenic or arsenic oxide has been detected [Ives]. However, the treatment lasts for only 20 to 30 minutes in atmospheric conditions.

Chemical treatments usually consist of soaking the sample in an aqueous solution of inorganic sulfides. The most widely reported solution is Na_2S [Carpenter 1988a, Sandroff, Yablonovitch]. A Na_2S treatment usually consist of soaking a sample in a Na_2S solution for up to 20 minutes and then spin drying. The spin dry leaves approximately a micron of slightly conducting $Na_2S{\cdot}9H_2O$ on the

© 1989 IOP Publishing Ltd

surface. While this treatment has been shown to be almost as effective as an AlGaAs layer in reducing the surface recombination velocity [Yablonovitch], it last for only 18-36 hours. Another compound which is gaining popularity is $(NH_4)_2S$ [Carpenter, Oigawa]. Treatment with this sulfide is similar except the solution is rinsed off in water and the sample is blown dry with nitrogen. The $(NH_4)_2S$ treatment has been shown to be as effective as Na_2S in reducing perimeter current as shown in figure 1.

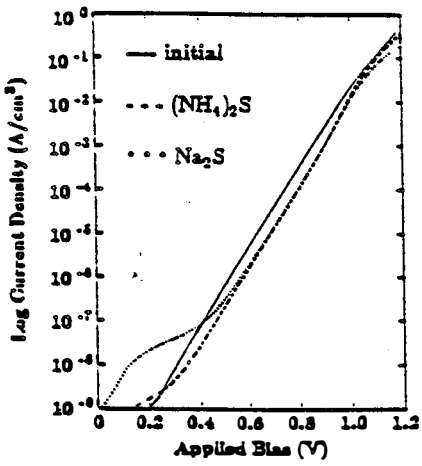

Figure 1 I-V for pn junction

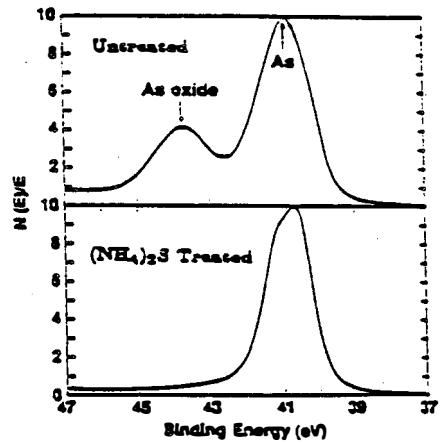

Figure 2 XPS spectra for As3d line [Cowans]

In figure 1 the forward bias current vs voltage is plotted for a GaAs pn junction. The recombination current (n=2 current) is directly related to the surface recombination velocity in the exposed depletion region [Demoulin]. Figure 1 contains plots of current density for an exposed pn junction and for the same junction with both surface treatments. As shown the two treatments behave similarly in reducing the recombination current except at low bias where the Na_2S treated sample exhibits a shunt current. Another consequence of rinsing the $(NH_4)_2S$ off is that no visible layer is left behind, only chemically bonded sulfur, as will be discussed below. With no excessive layer on the GaAs surface, a number of surface analysis techniques such as Raman scattering, X-ray photoemission spectroscopy (XPS) and low energy electron loss spectroscopy (LEELS) can be used to probe the unpinning mechanism. In our lab XPS was used to analyze the surface and we found that the treatment produced only 0.6 of a monolayer of sulfur on the surface [Cowans]. This layer inhibited the initial oxidation of the GaAs when exposed to atmospheric conditions, as shown in figure 2. Shown in figure 2 is the XPS spectra of the arsenic 3d line. the lower spectra is for the $(NH_4)_2S$ treated sample and the upper spectra is for an etched sample. Easily noticed is the lack of a well defined peak corresponding to the arsenic oxide, in the treated sample. More detailed presentation of the XPS work will be published at a later date. Since the $(NH_4)_2S$ treatment unpins the surface and

leaves an abrupt interface, it provides a suitable surface for Schottky barrier formation [Carpenter 1988b].

Experimental Schottky diodes were fabricated from two (100) GaAs wafers. The first wafer was an n-type MBE grown epilayer approximately 1 μm thick. The second was similar except it was p-type. The dopings of the epilayers were 2.2 x $10^{16}cm^{-3}$ for the n-type and 1.6 x $10^{16}cm^{-3}$ for the p-type as determined by capacitance - voltage profiling. The two wafers were cleaved into samples of approximately 0.25 cm^2. These samples were prepared for evaporation by etching in 1:1:250 H_2SO_4:H_2O_2:H_2O followed by a deionized water rinse for 30 seconds. The samples were then either soaked for 5 minutes in $(NH_4)_2S$ or for 20 seconds in NH_4OH. The samples were then rinsed and immediately loaded into an evaporator. Metal for both n and p type samples as well as for treated and untreated samples was evaporated at the same time. The process was done for both gold and aluminum. The diodes were defined by usual photolithography and wet chemical etching.

The Schottky diodes were electrically contacted by a model 6000 Micromanipulator test station. The current voltage characteristics were obtained from a Hewlett Packard 4145A semiconductor parameter analyzer. I-V data was collected from -1 to 0.5 volts.

Figure 3a and 3b show forward bias I-V data for Schottky diodes formed from aluminum and gold on n and p type GaAs respectively. Each figure contains a control sample as well as both $(NH_4)_2S$ treated samples. Figure 3a shows that the treated aluminum sample has more current than the control sample and the gold sample has less current than the control sample. The trend is reversed on the p-type samples shown in figure 3b.

To determine barrier heights, the I-V data was analyzed according to the thermionic emission model of current transport [Rhoderick].

$$J=J_s\exp\left(\frac{qV}{nkT}\right)\left[1-\exp\left(\frac{-qV}{kT}\right)\right] \tag{1}$$

Where J_s is the saturation current density and n is the ideality factor which represents the voltage dependence of the barrier. This model includes image force lowering for both forward and reverse bias. The saturation current density and ideality factor were determined by curve fitting the linear portion of plots of $\log\left\{J/\left[1-\exp\left(\frac{-qV}{kT}\right)\right]\right\}$ vs V. The linear region extended from a forward bias to a reverse bias of greater than 1 volt. This linearity suggests that the reverse current is due to the bulk and not leakage at the perimeter of the devices. The curve fitting was done by a least squares fit from -1 V to a forward bias where series resistance became significant, typically 0.4 V. The effective barrier heights ($\Phi_{bn}-\Delta\Phi$) were determined by the thermionic emission model where the

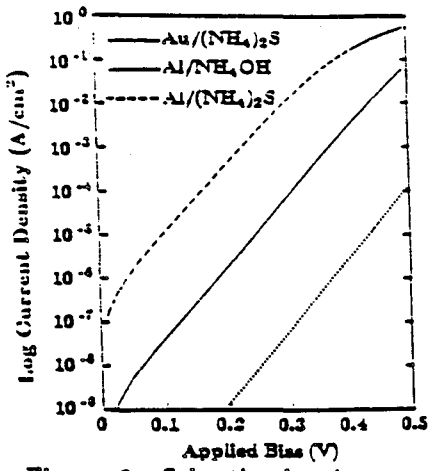

Figure 3a Schottky barriers on n-GaAs

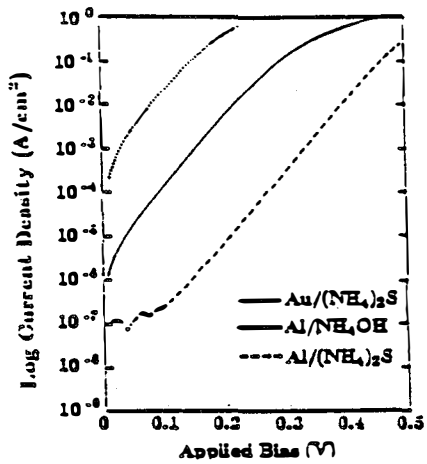

Figure 3b Schottky barriers on p-GaAs

saturation current density is given by:

$$J_s = A^* T^2 \exp\left(\frac{-q}{kT}(\Phi_{bn} - \Delta\Phi)\right), \qquad (2)$$

where A^* is the effective Richardson constant (8.16 A $cm^{-2}K^{-2}$ for n-type and 74.4 A $cm^{-2}K^{-2}$ for p-type), $\Delta\Phi$ is the image force correction term at zero bias. Table 1 presents a summation of the barrier heights, saturation current density and ideality factor. The barrier heights were also determined by activation energy plots. The activation energy method produced similar results as the current voltage method.

The current densities were uniform across the samples, the worst case variation was less than a factor of 2 with more than 10 devices measured per sample. No correlation was found between perimeter and current density. Since diodes of various areas (2.5×10^{-5} to 1.6×10^{-3} cm^2) and perimeter were measured, we conclude that the I-V characteristics are not influenced by the edges of the devices and that the barrier heights represent true bulk values. The thermal stability of the devices has been demonstrated by the constant characteristics before and after the activation energy measurements. During the activation energy measurements the samples were heated to 180 °C. The long term stability has yet to be determined since the devices have only been observed for 9 months. During these 9 months no change has been observed.

From table 1 it is readily seen that the barrier height for the $(NH_4)_2S$ treated gold n-type sample is higher than the barrier for p-type sample as is usually

Surface treatment	metal	n-type J_s	n-type $\phi_{bn}-\Delta\phi$	n-type n	p-type J_s	p-type $\phi_{bp}-\Delta\phi$	p-type n
NH_4OH	al	$1.1X\ 10^{-7}$	.767	1.03	$5.7X\ 10^{-5}$	.662	1.02
$(NH_4)_2S$	al	$2.2X\ 10^{-5}$	.632	1.04	$6.4X\ 10^{-7}$	.780	1.03
	au	$1.9X\ 10^{-9}$	.871	1.08	$2.5X\ 10^{-3}$	.563	1.05

found for untreated devices. However, the reverse is true for the $(NH_4)_2S$ treated aluminum samples where the p-type sample has a higher barrier than for n-type. Since the barrier heights go in different directions for different metals, it is apparent that the Fermi level has not been repinned at a new level by the $(NH_4)_2S$ treatment. The increased sensitivity of barrier height to metal work function can be interpreted as a reduction in surface state density. This reduction can readily be seen and calculated by the following relation developed by Cowley [1964] and Sze:

$$\Phi_{bn}=\gamma(\Phi_M-\chi_s)+(1-\gamma)(E_g-\Phi_0), \tag{3}$$

where Φ_m is the metal work function, χ_s is the semiconductor electron affinity, Φ_0 is the neutral level for surface states and γ is given by the following relation:

$$\gamma=\epsilon_i/(\epsilon_i+q^2\delta D_s) \tag{4}$$

where ϵ_i is the permittivity of the interface layer, δ is the layer thickness, and D_s is the density of surface states. Since the interface layer has been shown to be of the order of a monolayer, δ is about 5 Å. If the density of states is assumed to be uniform in the region of the Fermi level, then we can estimate the density of surface states. From the numerical estimate for γ ($\frac{\Delta\Phi_{bn}}{\Delta\Phi_M}$ = 0.30) the surface state density is found to be $1.9 \times 10^{13} cm^{-2}eV^{-1}$ for the $(NH_4)_2S$ treated devices. Cowley and Sze found the density of states to be $1.2 \times 10^{14} cm^{-2}eV^{-1}$ for untreated devices and similar assumptions.

In conclusion, we have investigated the effect of Na_2S and $(NH_4)_2S$ treatments on GaAs surfaces. We find the surface recombination velocity to be reduced. From this reduction we propose the surface state density is indeed reduced. This proposition has been shown to be correct by the four fold increase observed in the Schottky barrier height sensitivity parameter γ. This increase in γ is directly related to the reduction of the surface state density by an order of magnitude.

We would like to thank Brett Cowans and Nick Delgass for providing the XPS data and allowing us to present it before publication. We would also like to acknowledge the assistance provided by Tom Dungan in the fabrication of these devices. This work was supported by the Office of Naval Research under grant No. N00014-86-K-0350 and by the Solar Energy Research Institute under subcontract No. XL-5-05018-1.

References

Carpenter M.S. Melloch M.R. Lundstrom M.S. Tobin S.P. 1988a Appl. Phys. Lett. **52**,2157
Carpenter M.S Melloch M.R. Dungan T.E. 1988b Appl. Phys. Lett. **53**.66
Cowans B. Delgass N. Carpenter M.S. Melloch M.R. To Be Published
Cowley A.M. Sze S.M. 1965 J. Appl. Phys. **46**,3212
Demoulin P.D. Tobin S.P. Lundstrom M.S. Carpenter M.S. Melloch M.R. 1988 IEEE Electron Dev. Lett. **9**,368
Ives N.A. Stupian G.W. Leung M.S. 1987 Appl. Phys. Lett. **50**,256
Mead C.A., Spitzer W.G. 1964 Phys. Rev. A **134**,713
Offsey S.D. Woodall J.M. Warren A.C. Kirchner P.D. Chappel T.I. Pettit G.D. 1986 Appl. Phys. Lett. **48**,475
Oigawa H. Fan J. Nanichi Y. Ando K. Saiki K. Koma A. 1988 Inter. Conf. on Solid State Dev. and Mat. Tokyo, pp 263-266
Rhoderick E.H. 1982 IEE Proc. **129**,Pt.I,1
Sandroff C.J. Nottenburg R.N. Bischoff J.C. Bhat R. Gmitter T.J. 1987 Appl. Phys. Lett. **51**,33
Spicer W.E. Lindau I. Skeath P. Su C.Y. 1980 J. Vac. Sci. Technol. **17**,1019
Waldrop J.R. 1984 Appl. Phys. Lett. **44**,1002
Yablonovitch E. Sandroff C.J. Bhat R. Gmitter T.J. 1987 Appl. Phys. Lett. **51**,493

Evidence for band-gap narrowing effects in Be-doped, p-p^+ GaAs homojunction barriers

H. L. Chuang, P. D. DeMoulin, M. E. Klausmeier-Brown, M. R. Melloch, and M. S. Lundstrom
School of Electrical Engineering, Purdue University, West Lafayette, Indiana 47907

(Received 20 June 1988; accepted for publication 28 July 1988)

The electrical performance of Be-doped, p-p^+ GaAs homojunction barriers is characterized and analyzed. The results of the analysis show that minority-carrier electrons, at 300 K, have a mobility of 4760 cm^2/V s at a hole concentration of 2.3×10^{16} cm^{-3}, and that the effective recombination velocity for these homojunction barriers is about 6×10^4 cm/s. We present evidence that this unexpectedly high recombination velocity is a consequence of an effective reduction in band gap due to the heavy impurity doping. The effective band-gap shrinkage in this Be-doped material grown by molecular-beam epitaxy appears to be comparable to that already observed for Zn-doped GaAs grown by metalorganic chemical vapor deposition. This work demonstrates that so-called band-gap narrowing effects significantly influence the electrical performance of GaAs devices.

I. INTRODUCTION

Strong heavy doping effects have recently been reported for Zn-doped GaAs grown by metalorganic chemical vapor deposition (MOCVD).[1] In this paper we present evidence that comparable effects of similar magnitude also occur in Be-doped GaAs grown by molecular-beam epitaxy (MBE). The experiments utilized p-p^+ homojunction barriers commonly used to confine minority carriers in GaAs solar cells. Previous work showed that the effective recombination velocity associated with such a barrier was much too high for effective minority-carrier confinement.[2] Significantly better performance has been achieved by replacing the isotype homojunction barrier with an isotype heterjunction barrier in n-p GaAs solar cells.[3] The work we report suggests that the poor confinement of minority carriers by these homojunction barriers is due to an effective reduction in the band gap associated with heavy Be doping.

A successive etch technique[4] was employed to estimate the recombination velocity of a p-p^+ homojunction barrier. The barrier recombination velocity was found to be about 6×10^4 cm/s, and it increased as the width of the p^+-barrier layer decreased. Recombination through defects at the p-p^+ interface cannot explain these results, but the occurrence of band-gap narrowing effects[5] in p^+-GaAs can. The amount of band-gap narrowing deduced from the measurements is consistent with that measured for Zn-doped GaAs grown by MOCVD.[1] These results demonstrate that band-gap narrowing effects significantly influence the electrical performance of devices containing p^+-GaAs regions. They underscore the need to characterize such effects for Be-doped GaAs grown by MBE.

II. EXPERIMENTAL TECHNIQUE

The epitaxial layer structure for the solar cells used in this study is shown in Fig. 1. The films were grown in a Perkin–Elmer PHI-400 MBE system. The starting substrate was cleaved from a (100)-oriented, n-type GaAs wafer, and the thicknesses of the epitaxial layers were determined by counting oscillations in the intensity of the reflection high-energy electron diffraction pattern. Silicon was used as the n-type dopant and beryllium as the p-type dopant. Solar cells of dimension 0.1×0.1 cm^2 were defined by photolithography and subsequent wet etching. The p-type contact was a Au:Zn metal finger pattern which covered 18.4% of the cell area and formed a nonalloyed contact to the p^+-GaAs cap layer. The back contact metal was indium. The doping density of the P layer was measured as 2.3×10^{16} cm^{-3} by capacitance versus voltage profiling. Doping densities of the other layers were estimated from the growth rate of the film and the temperature of the dopant oven.

The completed cells were characterized by current versus voltage (I-V) measurements performed with a Hewlett–Packard 4145A semiconductor parameter analyzer. All measurements were performed in the dark at about 23.3 The measured current density versus applied voltage can described by

$$J = J_{01}(e^{qV/kT} - 1) + J_{02}(e^{qV/2kT} - 1)\,, \qquad (1$$

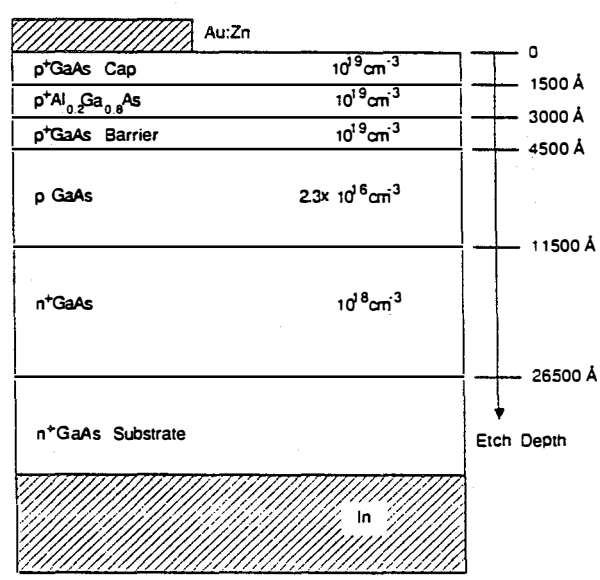

FIG. 1. Epitaxial layer structure of the solar cells used in this study.

 0021-8979/88/236361-04$02.40 © 1988 American Institute of Physics

where J_{01} and J_{02} are the saturation current densities associated with carrier recombination in the quasineutral and space-charge regions, respectively. The dark I-V characteristics were fitted to Eq. (1) to determine the two saturation current densities.

A successive etch technique was used to characterize the electron injection current.[4] The metal grid pattern was protected with photoresist, and the exposed semiconductor was removed in a series of short etches. Each etch was 20 s long in a solution of $[8H_2SO_4:4H_2O_2:400H_2O]$ at 26 °C and removed 375 Å of material as measured by step profiling. After each etch, the forward-biased dark I-V characteristic was measured.

III. ANALYSIS AND DISCUSSION

The dark I-V characteristic was measured after each etch step, and the resulting $n = 1$ saturation current density J_{01} is plotted in Fig. 2. J_{01} was roughly constant until the $Al_{0.2}Ga_{0.8}As$ layer was removed; it then increased as the p^+-GaAs barrier layer was thinned. When the p^+-barrier layer was completely removed, J_{01} increased sharply. This result clearly demonstrates that the heterojunction barrier is more effective than the homojunction barrier in minority-carrier confinement.

In a p-n^- GaAs diode, the major component of J_{01} is due to electron injection in the p-GaAs and is given by

$$J_{01e} = \frac{qn_{io}^2}{N_A}\left(\frac{S + (D_n/L_n)\tanh(W_p/L_n)}{1 + S(L_n/D_n)\tanh(W_p/L_n)}\right), \quad (2)$$

where D_n and L_n are the minority-carrier electron diffusion coefficient and length, respectively, n_{io} is the intrinsic carrier concentration of lightly doped GaAs, W_p is the width, and S is the surface recombination velocity of the lightly doped p layer. If the p layer is thin ($W_p \ll L_n$) and the surface is unpassivated ($S \gg W_p/\tau_n$), then Eq. (2) can be simplified as

$$J_{01e} = \frac{qn_{io}^2 D_n}{N_A W_p}\frac{S}{S + D_n/W_p}. \quad (3)$$

Equation (3) should describe the electron injection current after the p^+-GaAs cap, the p^+-$Al_{0.2}Ga_{0.8}As$, and the p^+-GaAs barrier layers have been removed.

Since the measured $n = 1$ current component increased by more than a factor of 30 after the top three layers were removed, the measured J_{01} can be equated to Eq. (3). The width of the p-GaAs layer varied with time according to $W_p(t) = W_{p0} - Rt$, where W_{p0} is the width of the lightly doped thin p layer at $t = 0$, and R is the etch rate. Equation (3) can then be rearranged as

$$J_{01}^{-1} \simeq J_{01e}^{-1} = \left(\frac{N_A W_{p0}}{qn_{io}^2 D_n} - \frac{N_A}{qn_{io}^2 S}\right) - \left(\frac{N_A R}{qn_{io}^2 D_n}\right)t. \quad (4)$$

Figure 3 shows that a plot of J_{01}^{-1} versus etch time was linear with a slope of $N_A R/qn_{io}^2 D_n$, from which the product, $n_{io}^2 D_n$ at 23.3 °C, was determined to be 2.9×10^{14} cm^{-4} s^{-1}. From the intercept, a surface recombination velocity of 9.4×10^6 cm/s was deduced.

The measured surface recombination velocity agrees well with the value expected for a bare GaAs surface.[6] From the measured $n_{io}^2 D_n$ product and the data of Blakemore for n_{io},[7] a minority-carrier electron diffusion coefficient of $D_n = 123$ cm^2/s was deduced. This value corresponds to a minority-carrier electron mobility of 4760 cm^2/V s at 300 K and is 25% lower than the mobility of minority-carrier electrons in uncompensated GaAs as predicted by Walukiewicz *et al.*[8] Low minority-carrier mobilities have also been reported in p-GaAs doped much more heavily than that employed here.[9,10]

Consider next the situation in which the p^--GaAs barrier layer was present. A theoretical expression relating the barrier recombination velocity, S_{pp^-}, to the structural parameters of the barrier, valid for both homojunction and heterojunction barriers, has been given by DeMoulin, Lundstrom, and Schwartz[11] as

$$S_{pp^-} = \frac{D_n^- N_A^-}{L_n^+ N_A^+}\frac{n_{ie}^2}{n_{io}^2}\coth\left(\frac{W_p^+}{L_n^+}\right), \quad (5)$$

where the $-$ and $+$ superscripts refer to the lightly and heavily doped sides of the junction, respectively, and n_{ie} is the effective intrinsic carrier concentration of the heavily

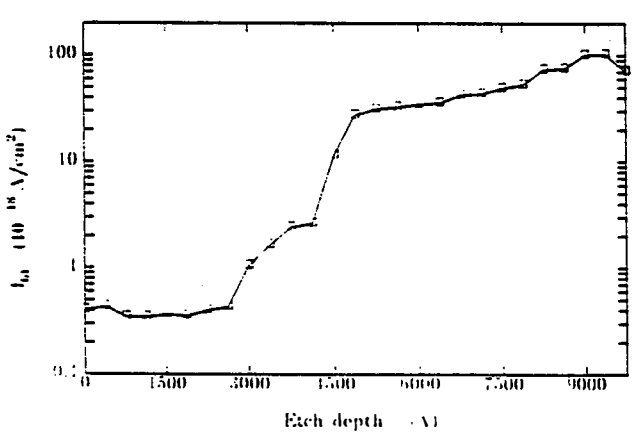

FIG. 2. $n = 1$ saturation current density J_{01} extracted from the measured dark current-voltage characteristic after each etch.

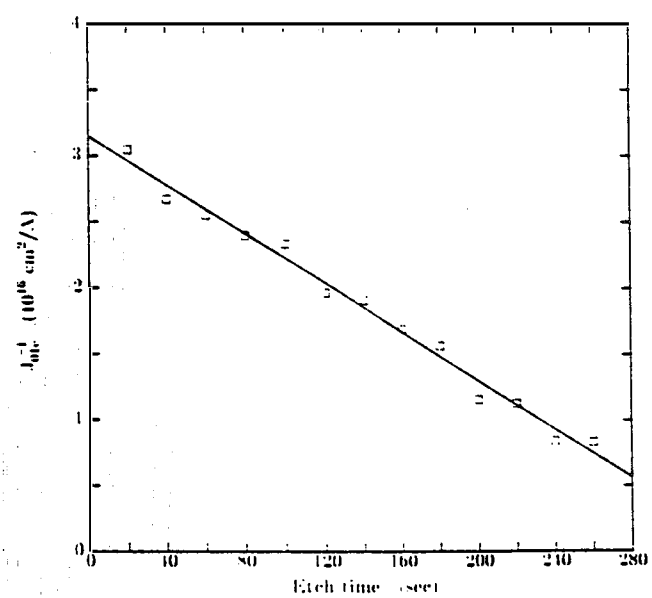

FIG. 3. J_{01e}^{-1} vs etch time was linear with a slope of $N_A R/qn_{io}^2 D_n$, from which D_n and μ_n were deduced.

doped side that accounts for the effective reduction in band gap associated with heavy impurity doping and for the influence of Fermi–Dirac statistics. In this case, since the p^+-GaAs barrier layer was only 0.15 μm thick, the assumption $W_p^+ \ll L_n^+$ is valid; Eq. (5) can thus be simplified as

$$S_{pp^-} = (D_n^+ N_A^- / W_p^+ N_A^+)(n_{ie}^2/n_{io}^2) . \quad (6)$$

Thus, S_{pp^-} is expected to be inversely proportional to W_p^+.

S_{pp^-} can be related to the measured $n = 1$ component of the dark current; since $W_p \ll L_n$ and S_{pp^-} may be comparable to W_p/τ_n, Eq. (2) is simplified as

$$J_{01e} = \frac{qn_{io}^2}{N_A} \frac{S_{pp^-} + W_p/\tau_n}{1 + (W_p/D_n)S_{pp^-}} , \quad (7)$$

which can be solved for

$$S_{pp^-} = \frac{1 - (qn_{io}^2/N_A J_{01e})(W_p/\tau_n)}{(qn_{io}^2/N_A J_{01e}) - (W_p/D_n)} . \quad (8)$$

Since J_{01e} is very nearly the measured J_{01}, and D_n has been determined as described above, with an appropriate τ_n, Eq. (8) can be employed to estimate S_{pp^-}; values of S_{pp^-} versus etch depth were calculated for a few different values of τ_n. By plotting S_{pp^-} vs $1/W_p^+$ (see Fig. 4), it is found that the relationship is linear, and that a τ_n of 1.1 ns caused the straight line to pass through the origin, thus satisfying Eq. (6). This implies that a minority-carrier electron in our MBE-grown material of doping $N_A = 2.3\times10^{16}$ cm^{-3} has a lifetime of 1.1 ns. Taking the square root of the product $D_n\tau_n$, the minority-carrier electron diffusion length L_n was determined to be 3.7 μm; thus, the assumption $W_p \ll L_n$ used in Eqs. (3) and (7) is valid. Using Eq. (6) and the slope of the straight line that passes through the origin in Fig. 4, $n_{ie}^2 D_n^+$ was determined to be 1.8×10^{15} cm^{-4} s^{-1}, which agrees with the data measured by Klausmeier-Brown, Lundstrom, Melloch, and Tobin.[1] They found $n_{ie}^2 D_n^+ = 1.8\times10^{15}$ cm^{-4} s^{-1} for MOCVD-grown GaAs, Z doped at 1×10^{19} cm^{-3}. They reported that the prod $n_{ie}^2 D_n^+$ was affected by band-gap narrowing through an crease in n_{ie}. This implies that the effective band-gap shrin age in Be-doped GaAs grown by MBE is comparable to th observed for Zn-doped GaAs grown by MOCVD.

A plot of measured S_{pp^-} versus etch depth is display in Fig. 5, which shows that S_{pp^-} is about 6×10^4 cm/s an that it increases as the thickness of the p^+-layer decreas Since S_{pp^-} was found to depend on the thickness of the layer, it cannot be controlled by recombination at the dopin junction but must be related to the properties of the barr Assuming no band-gap narrowing effects, theoretical val of S_{pp^-} were calculated using Eq. (6), in which n_{ie} equals n from Blakemore[7] corrected for hole degeneracy, and usin D_n given by Walukiewicz *et al.* for uncompensated p-GaA Figure 5 compares the theoretical estimate of S_{pp^-} with t measured value computed from Eq. (8). The figure show that when band-gap narrowing effects were not consider the theoretical estimate of S_{pp^-} was about 10 times lo than the value deduced from the measurements. The result clearly suggest that the high barrier recombination veloci is a consequence of an effective narrowing of the band gap p^+-GaAs.

Lower values of S_{pp^-} may be achieved by making th p^+-GaAs barrier layer thicker. Suppose the p^+-barrier lay is so thick that W_p^+ is several times greater than L_n^+. Equ tion (5) can then be simplified as

$$S_{pp^-} = (D_n^+ N_A^- / L_n^+ N_A^+)(n_{ie}^2/n_{io}^2) . \quad (9$$

Using the product $n_{ie}^2 D_n^+$ determined above, our dopin densities, and n_{io} from Blakemore,[7] S_{pp^-} was estimated to b $\lesssim 10^4$ cm/s, provided that L_n^+ is greater than 0.82 μ However, because it is very difficult to determine the value L_n^+, the possibility of achieving such a low value of S_{pp^-} b increasing the thickness is uncertain.

IV. CONCLUSIONS

In this paper we employed a successive etch technique study electron injection currents in GaAs p-n^+ diod grown by molecular-beam epitaxy. The results show that the

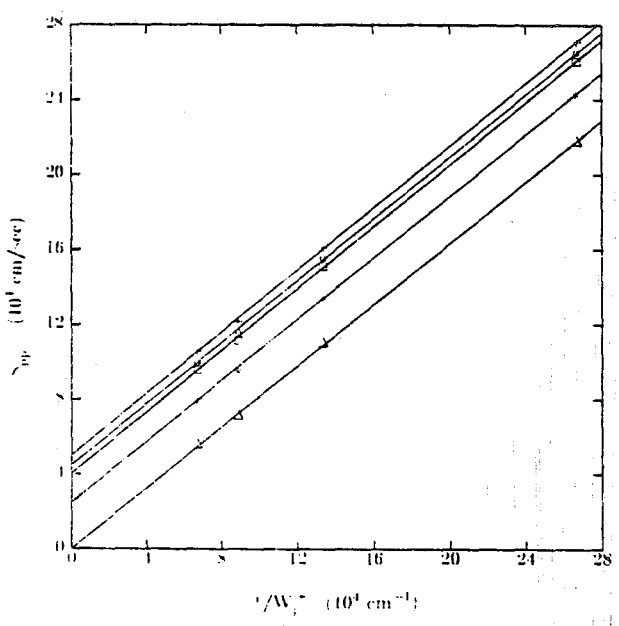

FIG. 4. Barrier recombination velocity S_{pp^-} vs thickness of the p^+-GaAs barrier layer plotted, from top to bottom, for minority-carrier electron lifetimes of 100, 10, 5, 2, and 1.1 ns, respectively.

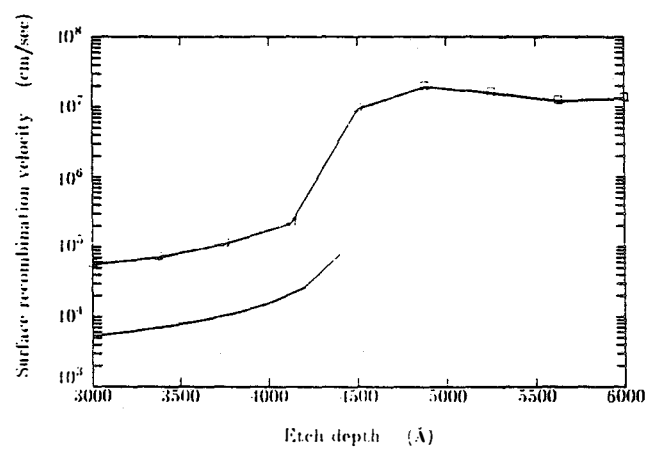

FIG. 5. Surface recombination velocity vs etch depth starting from the p^+-GaAs barrier layer. Top curve represents measured data. Bottom curve represents theoretical data without band-gap narrowing effects.

effective recombination velocity of the p-p^+ homojunction barriers in these diodes is about 6×10^4 cm/s. Analysis of these results strongly suggests that the high barrier recombination velocity is a consequence of an effective reduction in band gap caused by heavy Be doping. These effects appear to be comparable in magnitude to those reported for Zn-doped GaAs grown by metalorganic chemical vapor deposition.[1] The results also show that minority-carrier electrons, at 300 K, have a mobility of 4760 cm^2/V s at a hole concentration of 2.3×10^{16} cm^{-3}, thus confirming that the minority-carrier electron mobility in this moderately doped p-GaAs is lower than the majority-carrier mobility in comparably doped, uncompensated n-GaAs.

The results reported in this paper demonstrate that heavy doping effects significantly influence the performance of GaAs bipolar devices. This work helps to explain the substantial increase in solar cell performance that was observed when a homojunction p-p^+ barrier was replaced with an isotype heterojunction barrier.[3] We conclude that heterojunction barriers are essential for maximizing the efficiency of n-p GaAs solar cells.

ACKNOWLEDGMENTS

This work was supported by the Solar Energy Research Institute under Subcontract No. XL-5-05018-1. H. L. Chuang, P. D. DeMoulin, and M. E. Klausmeier-Brown were supported by the Indiana Corporation for Science and Technology, Sandia National Laboratories, and the Eastman-Kodak Corporation, respectively.

[1] M. E. Klausmeier-Brown, M. S. Lundstrom, M. R. Melloch, and S. P. Tobin, Appl. Phys. Lett. **52**, 2255 (1988).
[2] M. E. Klausmeier-Brown, C. S. Kyono, D. P. Rancour, M. S. Carpenter, M. R. Melloch, M. S. Lundstrom, and R. F. Pierret, Conf. Rec. 19th IEEE Photovoltaic Specialists Conference, 1174 (1987).
[3] R. P. Gale, J. C. C. Fan, G. W. Turner, and R. L. Chapman, Conf. Rec. 17th IEEE Photovoltaic Specialists Conference, 1422 (1984).
[4] M. E. Klausmeier-Brown, C. S. Kyono, P. D. DeMoulin, S. P. Tobin, M. S. Lundstrom, and M. R. Melloch, IEEE Trans. Electron Devices **ED-35**, 1159 (1988).
[5] J. Wagner and J. A. del Alamo, J. Appl. Phys. **63**, 425 (1988).
[6] R. P. Leon, Conf. Rec. 19th IEEE Photovoltaic Specialists Conference, 808 (1987).
[7] J. S. Blakemore, J. Appl. Phys. **53**, R123 (1982).
[8] W. Walukiewicz, J. Lagowski, L. Jastrzebski, and H. C. Gatos, J. Appl. Phys. **50**, 5040 (1979).
[9] R. K. Ahrenkiel, D. J. Dunlavy, D. Greenberg, and J. Schlupmann, Appl. Phys. Lett. **51**, 776 (1987).
[10] M. I. Nathan, W. P. Dumke, K. Wrenner, S. Tiwari, S. L. Wright, and K. A. Jenkins, Appl. Phys. Lett. **52**, 654 (1988).
[11] P. D. DeMoulin, M. S. Lundstrom, and R. J. Schwartz, Sol. Cells **20**, 229 (1987).

X-ray photoelectron spectroscopy of ammonium sulfide treated GaAs (100) surfaces

B. A. Cowans, Z. Dardas, and W. N. Delgass
School of Chemical Engineering, Purdue University, West Lafayette, Indiana 47907

M. S. Carpenter and M. R. Melloch
School of Electrical Engineering, Purdue University, West Lafayette, Indiana 47907

(Received 6 September 1988; accepted for publication 26 September 1988)

The effect of an ammonium sulfide treatment on the GaAs (100) surface has been investigated by x-ray photoelectron spectroscopy. The treatment produces a slight Ga enrichment on the surface and leaves roughly 0.6 of a monolayer of sulfide which inhibits initial oxidation of the surface. The sulfide is not lost as the surface becomes oxidized but appears to remain near the GaAs/oxide interface. Furthermore, in the oxidized layer, As oxide is preferentially drawn to the surface relative to Ga oxide.

The electrical quality of the GaAs surface has imposed performance constraints upon nearly all GaAs devices[1] and prevented the development of a GaAs-based metal-insulator-semiconductor technology.[2] The surface state density exhibited by a GaAs surface is on the order of 10^{13} $cm^{-2}\,eV^{-1}$ and the surface recombination velocity is on the order of 10^7 cm/s. Recently, the electrical quality of the GaAs surface has been dramatically improved by various sulfide chemical treatments.[3–8] Sandroff *et al.* obtained a 60-fold increase in the current gain of a heterojunction bipolar transistor (HBT) by treating the edges of the emitter-base junction with $Na_2S\cdot 9H_2O$.[3] The gain improvement in the HBT was due to a reduction in the perimeter recombination current of the emitter-base junction. Carpenter *et al.* found similar reductions in the perimeter recombination current of GaAs*pn* diodes following treatment of the edges with either a $Na_2S\cdot 9H_2O$ or an ammonium sufide solution.[6] Yablonovitch *et al.*[4] and Nottenberg *et al.*[5] found that improvements in the surface recombination velocity of $Na_2S\cdot 9H_2O$-treated GaAs approach that of the nearly ideal AlGaAs/GaAs interface.

One limitation of the sulfide treatment is aging. Sandroff *et al.* found that improvements in the gain of the $Na_2S\cdot 9H_2O$-treated HBT would persist for a few days.[3] The ammonium sulfide treatment also ages when exposed to air, but appears to be more durable than the $Na_2S\cdot 9H_2O$ treatment.[6] Carpenter *et al.* investigated Schottky barriers formed on ammonium sulfide treated *n*- and *p*-type GaAs and found an order of magnitude reduction in the surface state density at the ammonium sulfide treated metal-GaAs interface relative to an untreated film.[7] The Schottky diodes show no apparent aging after several months of room air exposure.

In order to determine how the sulfide treatment causes such improvements in the electrical quality of the surface, x-ray photoelectron spectroscopy (XPS) was used to examine GaAs (100) surfaces following either an acid etch or an etch and sulfide treatment. All samples were cut from MaCom undoped (100) GaAs wafers to roughly 16 mm×20 mm and etched in 1:1:250 H_2SO_4:H_2O_2:H_2O for 10 s followed by a 30 s running de-ionized water rinse. Sulfide-treated samples were then soaked in a saturated ammonium sulfide solution for 5 min, followed by another de-ionized water rinse, and dried under a stream of nitrogen.[6,7] Samples were stored in dust-free containers and exposed to air at room temperature for measured lengths of time before being loaded into the spectrometer.

Spectra were recorded on a Perkin–Elmer PHI 5300 spectrometer. The Mg (1253.6 eV)/Al (1486.6 eV) dual anode x-ray source was operated at 15 kV and 300 or 400 W, respectively. The spectrometer was calibrated by setting the binding energies of the Au $4f_{7/2}$ and Cu $2p_{3/2}$ levels to 84.0 and 932.7 eV, respectively. The full width at half maximum for Ag $3d_{5/2}$ level (368.4 eV) was 0.86 eV at 489 kHz for the pass energy at which all data were collected. The C 1*s* binding energy was recorded at 284.3 eV for all GaAs samples. A low-energy electron gun, operated at either 2.0 mA emission current with 1.0 eV bias (Mg radiation) or 5.0 mA emission current with 1.5 eV bias (Al radiation), was used to control charging on the undoped samples. Background pressure in the analysis chamber was always less than 1×10^{-9} Torr. Data accumulation times were roughly 5 h (Ref. 9) and data reduction was accomplished using Perkin–Elmer software.

Photoelectron spectra of the As 3*d* core level are shown in Fig. 1. The upper spectrum shows an etched sample following a 15 min air exposure while the lower spectrum shows a sulfide-treated sample following a 20 min air expo-

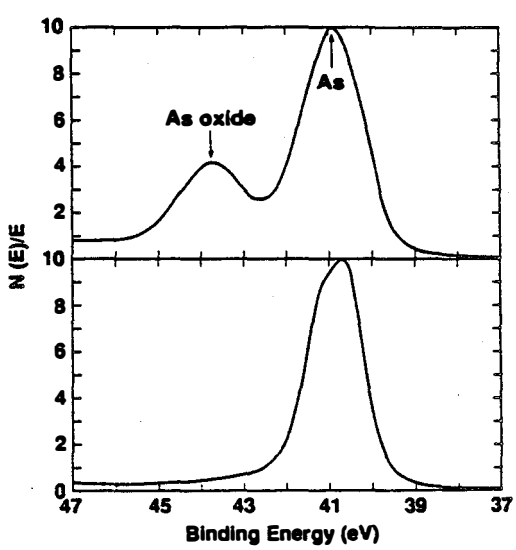

FIG. 1. Upper spectrum: Etched sample following a 15 min air exposure. Lower spectrum: ammonium sulfide treated sample following a 20 min air exposure.

 0003-6951/89/040365-03$01.00 © 1989 American Institute of Physics

sure. The absence of the large As oxide peak from the spectrum of the sulfide-treated sample clearly demonstrates that the As atoms are oxidized much less on that sample.

The XPS spectra observed for the different core levels were fit as follows. The As $3d$ level was fit by four peaks assigned as: As (of bulk GaAs) $3d_{5/2}$ and $3d_{3/2}$ peaks at 40.6 eV and 41.3 eV,[10,11] an As-sulfide species at 42.5 eV,[12] and an As oxide at 44.1 eV.[10,11] The spin orbit splitting is not resolved for the sulfide and oxide peaks, and the sulfide and oxide species are not specifically defined, since at these low coverages, *vide infra*, a bulk-type stoichiometric compound probably does not exist. The As $2p_{3/2}$ level was fit by three peaks also assigned as metal, sulfide, and oxide at 1323.1, 1324.6, and 1326.3 eV, respectively. Both Ga $3d$ and $2p_{3/2}$ levels were composed of metal peaks at 19.0 and 1117.2 eV and oxide peaks at 20.0 and 1118.3 eV. Due to the smaller spin orbit splitting and binding energy shift of Ga, we cannot resolve the Ga $3d_{5/2}$ and $3d_{3/2}$ levels or a clear sulfide peak.

The binding energies of the sulfur $2s$ and $2p$ levels were observed at 226.0 and 161.9 eV, suggesting that the sulfur atoms which form this layer are in the sulfide (2 −) state. The position of the S $2p$ level for most metal sulfides is normally in the range 160.0–163.0 eV, while that of an oxidized sulfur species is 166–170 eV.[13] The binding energies of the sulfide did not shift with time, leading us to believe that the chemical nature of the sulfur does not change significantly with exposure to air. The sulfur to total metal intensity ratios are listed in Table I. The magnitude of these ratios shows little change with time, indicating that the sulfur is not lost as the surface becomes oxidized. However, the angular dependence of these ratios is more pronounced initially than after long exposure to air, which indicates that Ga and As may be diffusing through the sulfide as the surface becomes oxidized. The angular dependence of the sulfur to oxidized Ga and As intensity ratios further suggests that oxidized As lies above the sulfur while oxidized Ga covers the sulfur with increasing time of exposure.

The fractional coverage of sulfur was calculated from the standard equation relating the sulfur to gallium intensity ratio at a given electron take-off angle assuming a uniform layer model[14,15]

$$\frac{I_S}{I_{Ga}} = \frac{S_S \sigma_S \eta_S \lambda_S [1 - \exp(-d/\lambda_S \sin\Theta)]}{S_{Ga} \sigma_{Ga} \eta_{Ga} \lambda_{Ga} \exp(-d/\lambda_{S,Ga} \sin\Theta)}, \quad (1)$$

where I is the intensity, S is the spectrometer transmission function, σ is the photoelectron cross section,[16] η is the atomic density, λ is the photoelectron mean free path, d is the thickness of the sulfide layer, and Θ is the angle between the sample surface and the entrance slit to the analyzer. The energy dependence of the spectrometer transmission function was calculated according to Hanke *et al.*[17] and photoelectron mean free paths were taken from Kwei and Chen.[18] Assuming the sulfide layer thickness equals the diameter of the sulfide ion (3.68 Å), a sulfur coverage of 3.6×10^{14} atoms/cm^2 can then be determined from the atomic density of sulfur. Since an ideal GaAs (100) surface contains approximately 6.3×10^{14} atoms/cm^2, the surface is covered by approximately 0.6 monolayer of sulfur.

TABLE I. Relative atomic ratios calculated from O 1s, S 2s, and Ga and As 3d level intensities taking into account only the photoelectron cross section (Mg radiation).

Sample	Angle	S/O	S/Ga_{ox}	S/As_{ox}	$S/(Ga+As)_{total}$
Treated	30	1.08	1.98	4.69	0.10
0.33 h	60	1.04	0.73	7.80	0.05
Treated	30	0.19	0.35	0.75	0.07
116 h	60	0.22	0.40	1.21	0.05
Treated	30	0.17	0.29	0.76	0.06
264 h	60	0.26	0.44	1.74	0.06

The (100) GaAs surface can have phases with As coverages ranging from roughly 0.2 to 1 monolayer.[19] Massies *et al.*[20] have shown that the sticking coefficient of H_2S on the (100) GaAs surface is dependent upon the As coverage and is greatest on an As-depleted surface. They also determined the saturation coverage of H_2S to be between 0.7 and 1 monolayer. Furthermore, Sandroff *et al.*[3,4] stated from their preliminary Auger analysis that roughly half a monolayer of sulfur remains after washing the $Na_2S \cdot 9H_2O$-treated surface. These results are consistent with the 0.6 monolayer of sulfur and the slight Ga enrichment (as discussed below) observed on our sulfide-treated surfaces.

The peak intensity ratios of oxygen to total metal are shown in Table II. Initially, the oxygen to metal ratios are significantly higher for the etched surface than for the treated surface, confirming that the sulfide treatment limits initial oxidation on the GaAs (100) surface. The O/Ga_{total} ratio at 30° is greater than the O/As_{total} ratio for the etched sample and less than the O/As_{total} ratio for the treated sample, at short exposures. Furthermore, the As_{ox}/Ga_{ox} and the As_m/Ga_m ratios are larger for the etched surface than the treated one. These results suggest that the surface of the etched sample is enriched in As while the surface of the sulfide-treated sample is slightly enriched in Ga. Acid etched surfaces have indeed been found to be As-rich.[11] However, the effect of a basic sulfide solution on surface composition has not been previously reported. Higher values of the As_{ox}/Ga_{ox} ratios at low angle indicate that the relative amounts of As oxide to Ga oxide increase toward the outermost surface of both etched and sulfide-treated samples. This suggests that oxidized As migrates to the surface as the surface becomes oxidized.[11] For longer air exposures, we see that the O to total metal ratios are more nearly equivalent. Therefore, the total amount of surface oxidation reaches similar saturation values on both etched and treated samples.

In conclusion, we have obtained the following results from our XPS analysis. (i) The ammonium sulfide treatment produces a slight Ga enrichment on the surface and leaves approximately 0.6 of monolayer of sulfide, which severely restricts the initial oxidation of the GaAs (100) surface. (ii) The binding energies of the sulfur $2s$ and $2p$ levels at 226.0 and 161.9 eV respectively, suggest that the sulfur atoms which form this layer are in the sulfide (2 −) oxidation state and do not change chemical state with long exposure to air. (iii) The sulfide layer is not lost as the GaAs surface becomes oxidized and apparently remains near the oxide interface. Ga and As apparently diffuse through the sulfide layer as the surface becomes oxidized. (iv) The total

TABLE II. Relative atomic ratios calculated from O 1*s* and Ga and As 3*d* level intensities corrected for photoelectron cross section (Mg radiation).

Sample	Angle	As_m/Ga_m	As_{ox}/Ga_{ox}	O/Ga_{total}	O/As_{total}	$O/(Ga+As)_{total}$
Etched						
0.25 h	30	1.93	2.52	1.01	0.51	0.34
	60	1.00	1.38	0.42	0.41	0.21
145 h	30	1.21	0.95	1.01	0.96	0.49
	60	0.80	0.78	0.57	0.73	0.32
Treated						
0.33 h	30	0.86	0.42	0.16	0.21	0.09
	60	0.61	0.09	0.07	0.12	0.04
116 h	30	0.96	0.47	0.68	0.90	0.39
	60	0.67	0.33	0.37	0.63	0.23

oxidation on both etched and sulfide treated surfaces is nearly equivalent after long exposure to air. Furthermore, the angular dependence of the As_{ox}/Ga_{ox} ratios indicates that As oxide preferentially migrates to the surface of both etched and treated samples.

The authors are grateful to I. K. Means for assistance in preparing data for publication. This work was supported by the Solar Energy Research Institute under subcontract No. XL-5-05018-1 and the Office of Naval Research under contract No. N00014-86-K0350.

[1]D. L. Lile, J. Vac. Sci. Technol. B 2, 496 (1984).
[2]C. R. Zeisse, L. J. Messich, and D. L. Lile, J. Vac. Sci. Technol. 14, 957 (1977).
[3]C. J. Sandroff, R. N. Nottenberg, J.-C. Bischoff, and R. Bhat, Appl. Phys. Lett. 51, 33 (1987).
[4]E. Yablonovitch, C. J. Sandroff, R. Bhat, and T. Gmitter, Appl. Phys. Lett. 51, 439 (1987).
[5]R. N. Nottenberg, C. J. Sandroff, D. A. Humphrey, T. H. Hollenbeck, and R. Bhat, Appl. Phys. Lett. 52, 218 (1988).
[6]M. S. Carpenter, M. R. Melloch, M. S. Lundstrom, and S. P. Tobin, Appl. Phys. Lett. 52, 2157 (1988).
[7]M. S. Carpenter, M. R. Melloch, and T. E. Dungan, Appl. Phys. Lett. 53, 66 (1988).
[8]E. Yablonovitch, H. M. Cox, and T. Gmitter, Appl. Phys. Lett. 51, 439 (1988).
[9]R. P. Vasquez, B. F. Lewis, and F. J. Grunthaner, Appl. Phys. Lett. 42, 293 (1983).
[10]C. M. Demanet and M. A. Marais, Surf. Interface Anal. 7, 13 (1985).
[11]J. Massies and J. P. Contour, J. Appl. Phys. 58, 806 (1985).
[12]W. J. Stec, W. E. Morgan, R. G. Albridge, and J. R. Van Wazer, Inorg. Chem. 11, 219 (1972).
[13]C. D. Wagner, W. M. Riggs, L. E. Davis, J. F. Moulder, and G. E. Muilenberg, *Handbook of X-ray Photoelectron Spectroscopy* (Perkin–Elmer, Eden Prairie, MN, 1979).
[14]W. A. Fraser, J. V. Florio, W. N. Delgass, and W. D. Robertson, Surf. Sci. 36, 661 (1973).
[15]C. S. Fadley, Prog. Solid State Chem. 11, 265 (1974).
[16]J. H. Scofield, J. Electron Spectro. Rel. Phen. 8, 129 (1976).
[17]W. Hanke, H. Ebel, and M. Ebel, J. Electron Spectro. Rel. Phen. 40, 241 (1986).
[18]C. M. Kwei and L. W. Chen, Surf. Interface Anal. 10, 60 (1988).
[19]W. Ranke and K. Jacobi, Prog. Surf. Sci. 10, 1 (1981).
[20]J. Massies, F. Dezaly, and N. T. Linh, J. Vac. Sci. Technol. B 17, 1134 (1980).

Effective minority-carrier hole confinement of Si-doped, n^+-n GaAs homojunction barriers

H. L. Chuang, M. E. Klausmeier-Brown, M. R. Melloch, and M. S. Lundstrom
School of Electrical Engineering, Purdue University, West Lafayette, Indiana 47907

(Received 6 February 1989; accepted for publication 7 March 1989)

The electrical performance of Si-doped n^+-n GaAs homojunction barriers grown by molecular-beam epitaxy (MBE) is characterized and analyzed. We employed a successive etch technique to study hole injection currents in GaAs n^+-n-p^+ solar cells. The results of the analysis show that minority-carrier holes in our MBE-grown material have a mobility of 293 cm^2/V s for an n-type Si-doping level of 1.5×10^{16} cm^{-3} at 300 K. The interface recombination velocity for these homojunction barriers is estimated to be less than 1×10^3 cm/s, and it appears to be comparable to that recently observed for Si-doped n^+-n GaAs homojunction barriers grown by metalorganic chemical vapor deposition. We present evidence that these n^+-n GaAs homojunctions, unlike p^+-p GaAs homojunctions, are almost as effective as AlGaAs heterojunctions in minority-carrier confinement, and that their electrical performance is not degraded by heavy doping effects.

I. INTRODUCTION

High-efficiency GaAs solar cells routinely employ high–low junctions for confining minority carriers.[1,2] Depending on whether the cell is n^+-p or p^+-n, the high–low junction (also known as back-surface field or minority-carrier mirror) is either a p^+-p or n^+-n homojunction. Recent work has demonstrated that p^+-p GaAs homojunctions are not effective minority-carrier mirrors.[3] The poor confinement was attributed to strong effective band-gap narrowing in p^+-GaAs which lowers the confining potential for minority carriers. In this paper we examine n^+-n GaAs homojunction barriers and demonstrate that, in contrast with p^+-p homojunction barriers, they are effective minority-carrier mirrors. The interface recombination velocity of these homojunctions is quite comparable to that of heterojunction barriers, and is sufficient for most solar cell applications. These results suggest that the strong effective band-gap narrowing which occurs in p^+-GaAs is absent in n^+-GaAs.

Both the experiment conducted and the techniques employed are similar to those we recently described for p^+-p GaAs homojunctions.[3,4] The experiment itself and the results obtained are briefly described in Sec. II. These results are analyzed in Sec. III in order to deduce the interface recombination velocity of the n^+-n gallium arsenide homojunctions. In Sec. IV we compare the interface recombination velocity deduced from electrical measurements with that computed theoretically. Finally, our conclusions are summarized in Sec. V.

II. EXPERIMENTAL TECHNIQUE AND RESULTS

The epitaxial layer structure for the solar cells used in this study is shown in Fig. 1. The films were grown in a Varian GEN II molecular-beam epitaxy (MBE) system. The starting substrate was cleaved from a (100)-oriented, p-type GaAs wafer, and the thicknesses of the epitaxial layers were determined by counting oscillations in the intensity of the reflection high-energy electron diffraction pattern. Silicon was used as the n-type dopant and beryllium as the p-type dopant. Solar cells of dimension 0.1×0.1 cm^2 were de fined by photolithography and subsequent wet etching. Th ohmic contact to the n^+-GaAs cap layer was a AuGe/Ni Ti/Au metal finger pattern fabricated using a low-tempera ture annealing process. The back contact metal was indium The doping density of the n layer was measured as 1.5×10^1 cm^{-3} by capacitance versus voltage profiling. Doping densi ties of the other layers were determined from the calibrate temperatures of the dopant ovens.

A successive etch technique was used to characterize th hole injection current.[4] The metal grid pattern was protecte with photoresist, and the exposed semiconductor was re moved in a series of short etches. Each etch was 20 s long in solution of $[6H_2SO_4{:}3H_2O_2{:}400H_2O]$ at 27 °C and remove 250 Å of material, as measured by step profiling. After eacl etch, the short-circuit current I_{sc} under constant illumina tion through a 546-nm narrow-band filter, and the forward biased dark I-V characteristics were measured. All I-V mea surements were performed with a Hewlett-Packard 4145A semiconductor parameter analyzer at 23.3 °C.

The dark I-V characteristic measured after each etch step was analyzed to extract the $n=1$ saturation curren density J_{01}; the results are plotted in Fig. 2. J_{01} did not increase until the n^+-GaAs barrier layer was completely removed. It is important to note that J_{01} remained fairly constant as the n^+-AlGaAs heteroface and n^+-GaAs barrier layers were being etched away. This result clearly demonstrates that the homojunction barrier is as effective as the heterojunction barrier in minority-carrier hole confinement. This is in sharp contrast with the results that we obtained from a similar experiment for Be-doped, p^+-p GaAs homojunction barriers grown by MBE.[3] In that experiment, we employed p^+-p-n^+ solar cells of similar structure and comparable doping densities (see Fig. 3), and found that J_{01} increased significantly as the p^+-GaAs barrier layer was being etched away (see Fig. 4).

The fact that the n^+-n GaAs homojunction appears to be a good minority-carrier mirror is further substantiated by the short-circuit current I_{sc} versus etch depth plot, as shown

 0021-8979/89/130273-05$02.40 © 1989 American Institute of Physics

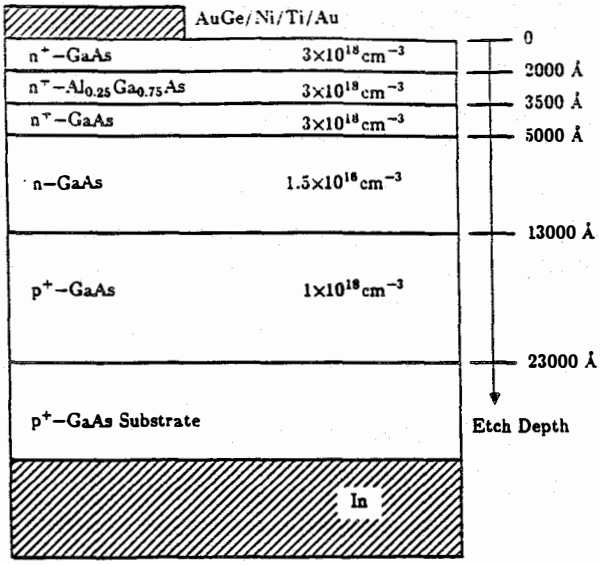

FIG. 1. Epitaxial layer structure of the solar cells used in this experiment.

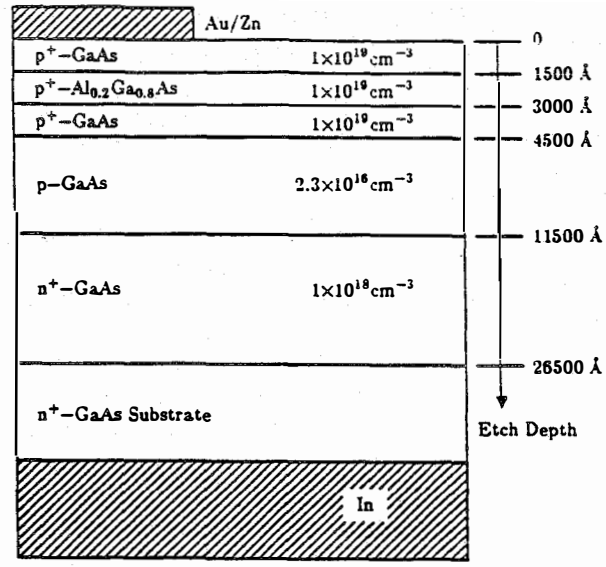

FIG. 3. Epitaxial layer structure of the solar cells used in a similar experiment for Be-doped, p^+-p GaAs homojunction barriers (see Ref. 3).

in Fig. 5. I_{sc} rose as the n^+-GaAs cap layer was etched away and more photons passed through the AlGaAs layer, generating electron-hole pairs. I_{sc} rose at a faster rate after the AlGaAs layer was exposed, due to the different absorption coefficients of the AlGaAs and GaAs layers. When the AlGaAs layer was completely removed, I_{sc} plummeted because some carriers generated in the n^+-GaAs barrier layer recombined at the front surface. I_{sc} again rose as the barrier layer was etched away and more carriers were generated behind the barrier where they were collected. When the n^+-GaAs barrier layer was completely removed, I_{sc} plummeted to the lowest point due to the very high surface recombination velocity of the bare GaAs surface. As the n-GaAs layer was thinned and more carriers were generated closer to the n-p^+ junction, I_{sc} rose gradually. Notice that the two peaks that occurred just before the complete removal of the heterojunction and homojunction barriers have nearly equal heights. This indicates that these two different types of barriers are almost equally effective.

III. ANALYSIS

In an n-p^+ GaAs diode, the component of J_{01} due to hole injection in the n-GaAs is given by

$$J_{01p} = \frac{qn_{i0}^2}{N_D}\left(\frac{S_n + (D_p/L_p)\tanh(W_n/L_p)}{1 + S_n(L_p/D_p)\tanh(W_n/L_p)}\right), \quad (1$$

where D_p and L_p are the minority-carrier hole diffusion coefficient and length, respectively, n_{i0} is the intrinsic carrier

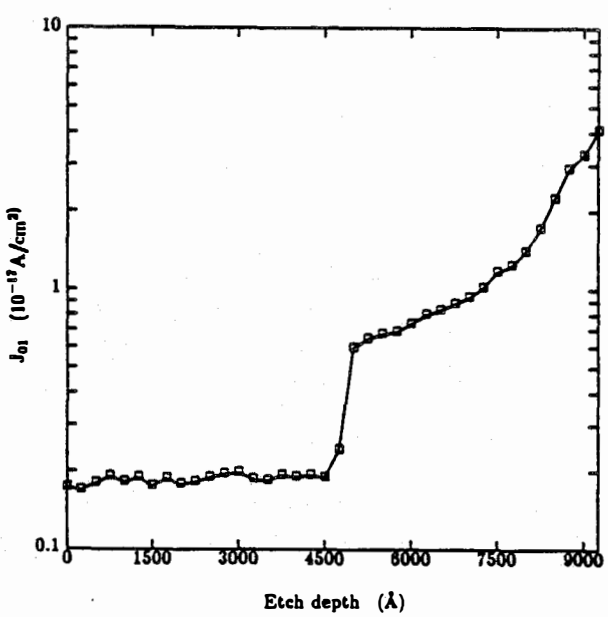

FIG. 2. J_{01} measured in this experiment.

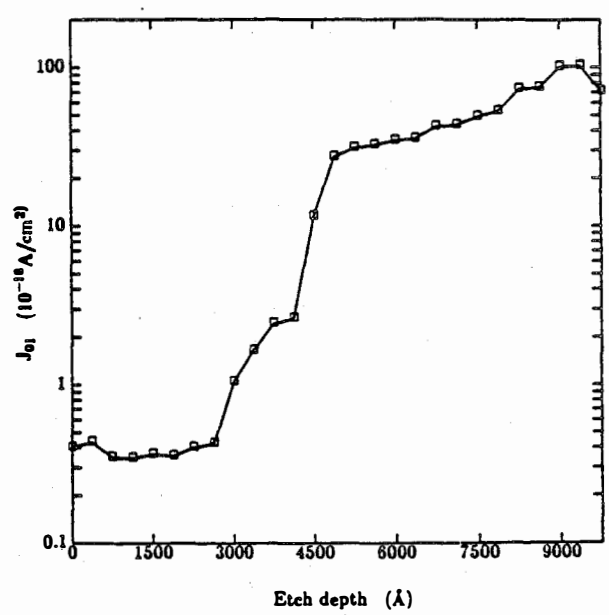

FIG. 4. J_{01} measured in a similar experiment for Be-doped, p^+-p GaAs homojunction barriers (see Ref. 3).

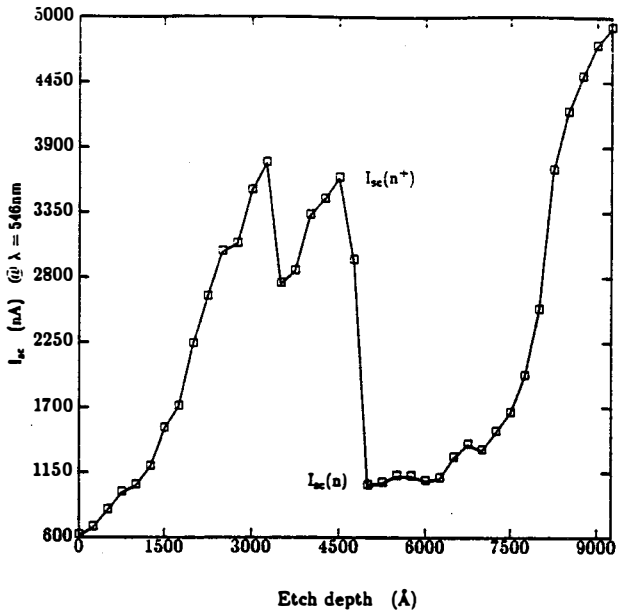

FIG. 5. Short-circuit current measured under constant illumination through a 546-nm narrow-band filter.

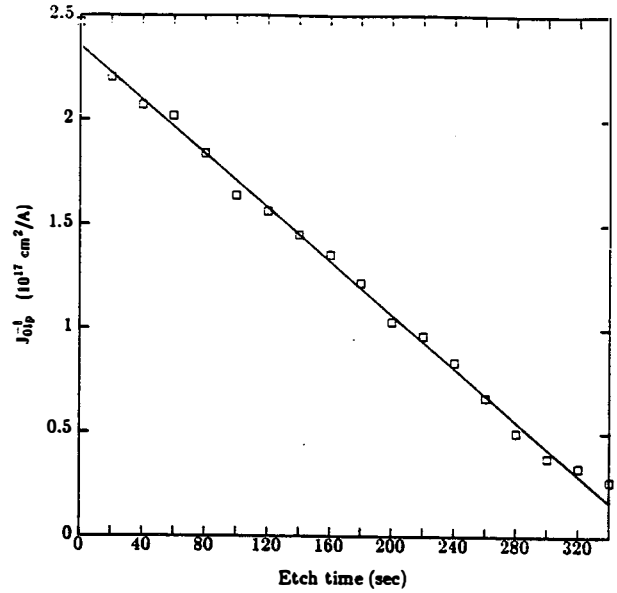

FIG. 6. J_{01p}^{-1} vs etch time was linear with a slope of $N_D R/qn_{i0}^2 D_p$, from which D_p and μ_p were deduced.

concentration of lightly doped GaAs, W_n is the width, and S_n is the recombination velocity at the surface of the lightly doped n layer. If the n layer is thin ($W_n \ll L_p$) and the surface is unpassivated ($S_n \gg W_n/\tau_p$), then Eq. (1) can be simplified as

$$J_{01p} = \frac{qn_{i0}^2 D_p}{N_D W_n} \frac{S_n}{S_n + D_p/W_n}. \tag{2}$$

Equation (2) should describe the hole injection current after the n^+-GaAs cap, the n^+-AlGaAs, and the n^+-GaAs barrier layers have been removed. Before these layers are completely removed, S_n is low and J_{01} is dominated by electron injection into the p^+-GaAs. This implies that J_{01p} of Eq. (2) is the difference between the J_{01} measured after the top three layers were removed and that measured initially, which we denote by J_{01e}.

The width of the n-GaAs layer varied with the etch time according to $W_n(t) = W_{n0} - Rt$, where W_{n0} is the undepleted width of the n layer at $t = 0$, and R is the etch rate. Equation (2) can then be rearranged as

$$J_{01p}^{-1} = (J_{01} - J_{01e})^{-1}$$
$$= \left(\frac{N_D W_{n0}}{qn_{i0}^2 D_p} + \frac{N_D}{qn_{i0}^2 S_n}\right) - \left(\frac{N_D R}{qn_{i0}^2 D_p}\right) t. \tag{3}$$

Figure 6 shows that a plot of J_{01p}^{-1} versus etch time was linear with a slope of $N_D R/qn_{i0}^2 D_p$, from which the product, $n_{i0}^2 D_p$ at 23.3 °C, was determined to be 1.82×10^{13} cm^{-4} s^{-1}. From the intercept, the surface recombination velocity, S_n, was deduced to be 1.1×10^7 cm/s, which agrees well with the value expected for a bare GaAs surface.[3,5]

From the measured $n_{i0}^2 D_p$ product and the data of Blakemore[6] for n_{i0} (which is 1.55×10^6 at 23.3 °C), a minority-carrier hole diffusion coefficient of $D_p = 7.6$ cm^2/s was deduced. This value corresponds to a minority-carrier hole mobility of 293 cm^2/V s at 300 K. Venkatsubramanian *et al.*[7] have reported somewhat lower minority-carrier hole diffusion coefficients in n-GaAs material grown by metalorganic chemical vapor deposition (MOCVD). They measured diffusion coefficients of 6.5 and 2.5 cm^2/s for doping densities of 3×10^{15} and 4×10^{16} cm^{-3}, respectively.

The interface recombination velocity $S_{n^+\text{-}n}$ of the n^+-GaAs homojunction barrier can be estimated from the ratio $I_{sc}(n^+)/I_{sc}(n)$, where $I_{sc}(n^+)$ and $I_{sc}(n)$ represent the short-circuit currents measured just before and after the complete removal of the n^+-GaAs barrier layer, respectively. Using a theoretical expression for short-circuit current derived by Sze[8] with the S_n and D_p measured here, we calculated the ratio $I_{sc}(n^+)/I_{sc}(n)$ for a series of minority-carrier hole lifetimes and interface recombination velocities. The results, $I_{sc}(n^+)/I_{sc}(n)$ vs $S_{n^+\text{-}n}$, are shown in Fig. 7. The actual $I_{sc}(n^+)/I_{sc}(n)$ measured from the short-circuit current plot (Fig. 5) is 3.51. From Fig. 7, an upper limit for the interface recombination velocity of 1×10^3 cm/s and a lower limit for the minority-carrier hole lifetime of 10 ns can be estimated. These estimates imply that the minority-carrier hole diffusion length L_p is greater than 2.75 μm. The low interface recombination velocity obtained here is at least 60 times lower than that of Be-doped, p^+-p GaAs homojunction barriers grown by MBE.[3] This clearly indicates that the n^+-n barrier is superior to the p^+-p barrier in minority-carrier confinement.

These results can be used to check our assumptions that were made in the derivations of Eqs. (2) and (3). Since the minority-carrier hole diffusion length L_p is greater than 2.7 μm and the hole lifetime τ_p is more than 10 ns, and the surface recombination velocity S_n of the bare GaAs surface is 1.1×10^7 cm/s, therefore the assumptions ($W_n \ll L_p$) and ($S_n \gg W_n/\tau_p$) used in Eq. (2) are valid. Since ($W_n \ll L_p$) and $S_{n^+\text{-}n}$ is comparable to W_n/τ_p, Eq. (1) can be simplified as

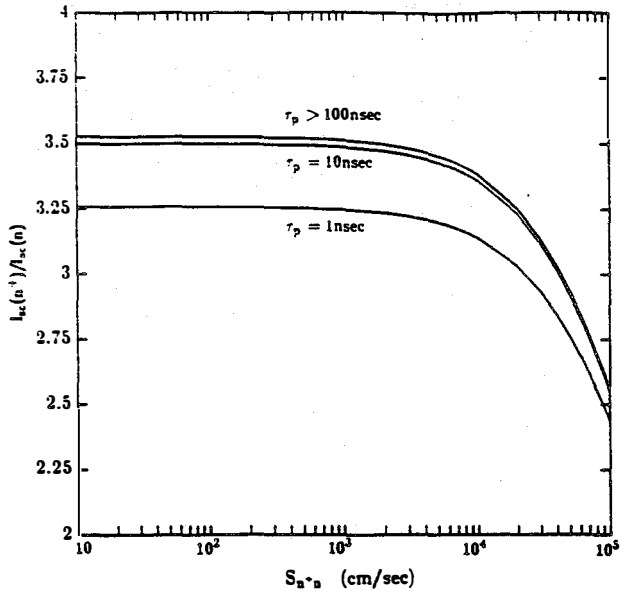

FIG. 7. Ratio of short-circuit currents calculated for a series of minority-carrier hole lifetimes and interface recombination velocities. $I_{sc}(n^+)$ and $I_{sc}(n)$ represent the short-circuit currents just before and after the complete removal of the n^+-GaAs barrier layer, respectively.

$$J_{01p} = \frac{qn_{i0}^2}{N_D} \frac{S_{n^+\text{-}n} + W_n/\tau_p}{1 + (W_n/D_p)S_{n^+\text{-}n}}. \quad (4)$$

By assuming an upper limit of 1×10^3 cm/s for $S_{n^+\text{-}n}$ and a lower limit of 10 ns for τ_p in Eq. (4), we estimated that the upper limit of J_{01p} only contributes less than 8% of the initial J_{01} measured before the lightly doped n layer is exposed. This implies that the initial J_{01} is dominated by electron injection current J_{01e} and that the assumption used in Eq. (3) is valid.

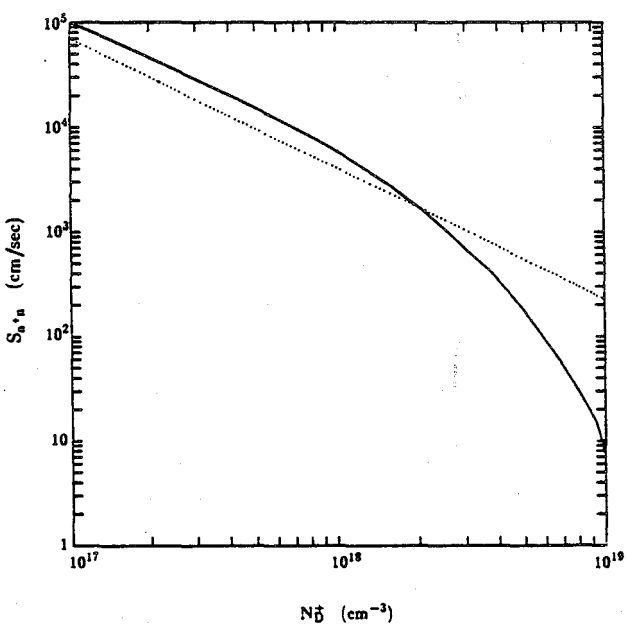

FIG. 8. Theoretical estimates of $S_{n^+\text{-}n}$ with and without heavy doping effects vs a range of heavy doping concentrations, N_D^+, represented by solid and dotted lines, respectively.

IV. DISCUSSION

The theoretical interface recombination velocity of the n^+-n GaAs homojunction[9] can be computed from

$$S_{n^+\text{-}n} = \frac{D_p^+ N_D^-}{L_p^+ N_D^+} \frac{n_{ie}^2}{n_{i0}^2} \coth\left(\frac{W_n^+}{L_p^+}\right), \quad (5)$$

where the $-$ and the $+$ superscripts refer to the lightly and heavily doped sides of the junction, respectively, n_{i0} is the intrinsic carrier concentration of lightly doped GaAs, and n_{ie} is the effective intrinsic carrier concentration of the heavily doped GaAs. Since the n^+-GaAs barrier layer is only 0.15 μm thick, $W_n^+ \ll L_p^+$, so Eq. (5) can be simplified as

$$S_{n^+\text{-}n} = \frac{D_p^+ N_D^-}{W_n^+ N_D^+} \frac{n_{ie}^2}{n_{i0}^2}. \quad (6)$$

Detailed band structure calculations by Bennett and Lowney[10] show that n_{ie} is much greater than n_{i0} due to strong effective band-gap shrinkage in p^+-GaAs, but for n^+-GaAs, majority-carrier degeneracy acts to reduce n_{ie} and should offset band-gap shrinkage effects. This implies that the strong increase in n_{ie} observed in p^+-GaAs is absent in n^+-GaAs. For very heavy n-type doping, n_{ie} may actually be less than n_{i0}.

Theoretical estimates of $S_{n^+\text{-}n}$ with and without heavy doping effects were calculated for a range of heavy doping concentrations, N_D^+, using Eq. (6) with the same W_n^+ and N_D^- from our device. For heavy doping effects, we used the theoretical calculations (n_{ie}^2/n_{i0}^2) of Bennett and Lowney.[10] In the absence of heavy doping effects, (n_{ie}^2/n_{i0}^2) is set to be one. The experimental values for majority-carrier hole mobility from Sze[8] were used to deduce D_p^+. Figure 8 shows the theoretical estimates of $S_{n^+\text{-}n}$ with and without heavy doping effects versus N_D^+. As expected, heavy doping effects have only a minor effect on the results. However, the improving characteristics for $N_D^+ > 2\times10^{18}$ cm^{-3} are attributed to an effective widening of the band gap caused by majority-carrier degeneracy. Note that at $N_D^+ = 3\times10^{18}$ cm^{-3}, the theoretical value of $S_{n^+\text{-}n}$ is approximately equal to 650 cm/s. This is consistent with our experimental estimate that $S_{n^+\text{-}n}$ is less than 1×10^3 cm/s, and with that recently reported for Si-doped, n^+-n GaAs homojunction barriers grown by MOCVD.[7]

V. CONCLUSIONS

In this paper, the electrical performance of Si-doped n^+-n GaAs homojunction barriers grown by MBE is characterized and analyzed. We employed a successive etch technique to study hole injection currents in GaAs n^+-n-p^+ solar cells. The results of the analysis show that minority-carrier holes in our MBE-grown material have a mobility of 293 cm^2/V-s for an n-type Si-doping level of 1.5×10^{16} cm^{-3} at 300 K. The interface recombination velocity for these n^+-n GaAs homojunction barriers is estimated to be less than 1×10^3 cm/s, and it appears to be comparable to that recently observed for Si-doped, n^+-n GaAs homojunction barriers grown by MOCVD.[7] We present evidence that these n^+-n GaAs homojunctions, unlike the p^+-p GaAs homojunctions, are almost as effective as AlGaAs heterojunctions.

minority-carrier confinement, and that their electrical performance is not degraded by heavy doping effects. This work helps to explain the superior performance of a p^+-n solar cell with an n^+-n back-surface field compared to an n^+-p solar cell with a p^+-p back-surface field.

ACKNOWLEDGMENTS

This work was supported by the Solar Energy Research Institute under Subcontract No. XL-5-05018-1. H. L. Chuang and M. E. Klausmeier-Brown were supported by the Indiana Corporation for Science and Technology, and the Eastman-Kodak Company, respectively.

[1]S. P. Tobin, C. Bajgar, S. M. Vernon, L. M. Goeffroy, C. J. Keavney, M. M. Sanfacon, V. E. Haven, M. B. Spitzer, and K. A. Emery, Proceedings of the 19th IEEE Photovoltaic Specialists Conference, May 4–8, 1987, 1492.

[2]H. F. MacMillan, N. R. Kaminar, M. S. Kuryla, M. J. Ladle, D. D. Li G. F. Virshup, J. M. Gee, in Proceedings of the 20th IEEE Photovolta Specialists Conference (IEEE, New York, 1988) (to be published).

[3]H. L. Chuang, P. D. DeMoulin, M. E. Klausmeier-Brown, M. R. Melloc and M. S. Lundstrom, J. Appl. Phys. **64**, 6361 (1988).

[4]M. E. Klausmeier-Brown, C. S. Kyono, P. D. DeMoulin, S. P. Tobin, M S. Lundstrom, and M. R. Melloch, IEEE Trans. Electron Devices ED-3 1159 (1988).

[5]R. P. Leon, Conference Recordings of the 19th IEEE Photovoltaic Sp cialists Conference, May 4–8, 1987, p. 808.

[6]J. S. Blakemore, J. Appl. Phys. **53**, R123 (1982).

[7]R. Venkatsubramanian, S. Bothra, S. K. Ghandhi, and J. M. Borrego, t be published in Proceedings of the 20th IEEE Photovoltaic Specialis Conference (IEEE, New York, 1988).

[8]S. M. Sze, *Physics of Semiconductor Devices*, 2nd ed. (Wiley, New York 1981).

[9]P. D. DeMoulin, M. S. Lundstrom, and R. J. Schwartz, Solar Cells **20**, 22 (1987).

[10]H. S. Bennett and J. R. Lowney, J. Appl. Phys. **62**, 521 (1987).

APPENDIX 2: BIBLIOGRAPHY OF SERI-SUPPORTED PUBLICATIONS

This appendix lists the various reports, theses, conference presentations, and journal publications that have resulted from research supported under this subcontract.

Reports:

[1] M. S. Lundstrom, M. R. Melloch, C. S. Kyono, C. P. McMahon, R. E. Noren, and D. P. Rancour, "Basic Studies of III-V High-Efficiency Cell Components," TR-EE-86-35, Aug. 1986, 163 pages.

[2] M. S. Lundstrom, M. R. Melloch, R. F. Pierret, P. D. DeMoulin, D. P. Rancour, C. S. Kyono, M. S. Carpenter, and M.E. Klausmeier-Brown, "Basic Studies of III-V, High-Efficiency Cell Components," TR-EE 87-33, Sept. 1987, 71 pages.

[3] M. S. Lundstrom, M. R. Melloch, R. F. Pierret, M. S. Carpenter, H. L. Chuang, P. D. DeMoulin, M. R. Klausmeier-Brown, G. B. Lush, D. P. Rancour, "Basic Studies of III-V High-Efficiency Cell Components," TR-EE 88-57, Dec. 1988, 109 pages.

Theses:

[1] Christian Paul McMahon, "A Quantum Efficiency Device for Solar Cells," MSEE thesis, August 1986.

[2] Robert E. Noren, "MBE Growth and Characterization of GaAs Heteroface Solar Cells," MSEE thesis, August 1986.

[3] Michael S. Carpenter, "Characterization and Passivation of Gallium Arsenide Surfaces," MSEE thesis, December 1987.

[4] David P. Rancour, "Investigation of GaAs Solar Cell Structures Using Deep Level Transient Spectroscopy," Ph.D. thesis, August 1988.

Conference Presentations:

[1] M. S. Lundstrom and M. R. Melloch, "Basic Studies of III-V High-Efficiency Cell Components," presented at the 7th SERI Photovoltaic Advanced Research and Development Project Review, Denver, CO, May 13-15, 1986.

[2] P. D. DeMoulin, C. S. Kyono, M. S. Lundstrom, and M. R. Melloch, "Dark I-V Characterization of GaAs P/N Heteroface Cells," 19th IEEE Photovoltaic Specialists Conf., New Orleans, LA, May 1987, pp. 93-97.

[3] M. E. Klausmeier-Brown, C-S. Kyono, M. S. Carpenter, M. R. Melloch, M. S. Lundstrom, and R. F. Pierret, "Experimental Characterization of Minority Carrier Mirrors for GaAs-Based Solar Cells," Proc. 19th IEEE Photovoltaic Specialist's Conf., New Orleans, May 1987, pp. 1174-1179.

[4] M. S. Lundstrom, "Device Physics of Crystalline Cells," presented at the 8th Photovoltaic Advanced Research and Development Project Review Meeting, Denver, Co, Nov. 16-18, 1987.

[5] M. E. Klausmeier-Brown, P. D. DeMoulin, M. S. Lundstrom, M. R. Melloch, and S. P. Tobin, "Measurement of Bandgap Narrowing Effects in p-GaAs and Implications for AlGaAs/GaAs HBT Performance," presented at the 46th Device Research Conference, Boulder, CO, June 20-22, 1988.

[6] M. E. Klausmeier-Brown, P. D. DeMoulin, H. L. Chuang, M. S. Lundstrom, M. R. Melloch, and S. P. Tobin, "Influence of Band Gap Narrowing Effects in p^+ GaAs on Solar Cell Performance," Conf. Rec., 20th IEEE Photovoltaic Specialists Conference, Las Vegas, NV, Sept. 26-30, 1988, pp. 503-507.

[7] M. S. Carpenter, M. R. Melloch, B. A. Cowans, and W. N. Delgass, "Investigations of $(NH_4)_2S$ Surface Treatments on GaAs," 16th Conference on Physics and Chemistry of Semiconductor Interfaces, Bozeman, Montana, February 7-9, 1989.

[8] M. S. Lundstrom, "Heavy Doping Effects in HBTs," presented at the Workshop on Compound Semiconductor Materials and Devices, WOCSEMMAD, Hilton Head, S.C., Feb.

20-22, 1989.

[9] M. E. Klausmeier-Brown, M. S. Lundstrom, and M. R. Melloch, "Electrical Measurements of Bandgap Shrinkage in Heavily Doped p-type GaAs," presented at the 1989 Electronic Materials Conference, June 21-23, 1989, Boston, MA.

[10] G. B. Lush, T. B. Stellwag, A. Keshavarzi, S. Venkatesan, M. R. Melloch, M. S. Lundstrom and R. F. Pierret, "Correlation of Material Properties and Recombination Losses in $Al_{0.2}Ga_{0.8}As$ Solar Cells," presented at the 9th Photovoltaic Advanced Research and Development Review Meeting, Lakewood, CO, May 24-26, 1989.

[11] M. R. Melloch, S. P. Tobin, C. Bajgar, T. B. Stellwag, A. Keshavarzi, M. S. Lundstrom, and K. Emery, "High-Efficiency GaAs Solar Cells Grown by Molecular Beam Epitaxy," Tenth Molecular Beam Epitaxy workshop, Raleigh, NC, September 13-15, 1989.

Journal Publications:

[1] M. R. Melloch, C. P. McMahon, M. S. Lundstrom, J. A. Cooper, Jr., Q-D. Qian, and S. Bandyopadhyay, "Bias-Dependent Photoresponse of p^+in GaAs/AlAs/GaAs Diodes," *Appl. Phys. Lett.,* Vol. 50, p. 161-163, Jan. 19, 1987.

[2] P. D. DeMoulin, M. S. Lundstrom, and R. J. Schwartz, "Back-Surface Field Design for n^+p GaAs Cells," *Solar Cells,* Vol. 20, pp. 229-236, March-April 1987.

[3] M. R. Melloch, C. P. McMahon, M. S. Lundstrom, J. A. Cooper, Jr., and Q-D. Qian, "Photocollection Efficiency of GaAs/AlAs/GaAs p^+in and n^+ip Photodiodes," *Solar Cells,* pp. 233-240, June-August 1987.

[4] D. Rancour, M. R. Melloch, R. F. Pierret, M. S. Lundstrom, M. E. Klausmeier-Brown and C. S. Kyono, "Recombination Current Suppression in GaAs P-N Junctions Grown on AlGaAs Buffer Layers by Molecular Beam Epitaxy," *J. Appl. Phys.,* Vol. 62, pp. 1539-1541, Aug. 15, 1987.

[5] M. S. Lundstrom, "Device Physics of Crystalline Solar Cells," *Solar Cells,* Vol. 24, pp. 91-102, May-June 1988.

[6] M. S. Carpenter, M. R. Melloch, M. S. Lundstrom, and S. P. Tobin, "Effects of Na_2S and $(NH_4)_2S$ Edge Passivation Treatments on the Dark Current-Voltage Characteristic of GaAs pn Diodes," *Applied Physics Letters,* Vol. 52, pp. 2157-2159, June 20, 1988.

[7] M. E. Klausmeier-Brown, M. S. Lundstrom, M. R. Melloch, and S. P. Tobin, "Effects of Heavy Impurity Doping on Electron Injection in p^+-n GaAs Diodes," *Applied Physics Letters,* Vol. 52, pp. 2255-2257, June 27, 1988.

[8] M. E. Klausmeier-Brown, C. S. Kyono, P. D. DeMoulin, S. P. Tobin, M. S. Lundstrom, and M. R. Melloch, "Sequential Etch Analysis of Electron Injection in P^+ GaAs," *IEEE Trans. Electron Devices,* Vol. ED-35, pp. 1159-1161, July 1988.

[9] M. S. Carpenter, M. R. Melloch, and T. E. Dungan, "Schottky Barrier Formation on $(NH_4)_2$ S-treated n- and p-type (100) GaAs," *Appl. Phys. Lett.* 53, pp. 66-68, July 4, 1988.

[10] P. D. DeMoulin, S. P. Tobin, M. S. Lundstrom, M. S. Carpenter, and M. R. Melloch, "Influence of Perimeter Recombination on High-Efficiency GaAs P/N Heteroface Solar Cells," *Electron Device Letters,* Vol. EDL-9, pp. 368-370, August 1988.

[11] H. L. Chuang, P. D. DeMoulin, M. E. Klausmeier-Brown, M. R. Melloch, and M. S. Lundstrom, "Evidence for Bandgap Narrowing Effects in Be-Doped, p-p^+ GaAs Homojunction Barriers," *Journal of Appl. Phys.,* Vol. 64, pp. 6361-6364, Nov. 1988.

[12] B. A. Cowans, Z. Dardas, W. N. Delgass, M. S. Carpenter, and M. R. Melloch, "X-ray Photoelectron Spectroscopy of Ammonium Sulfide Treated GaAs (100) Surfaces," *Appl. Phys. Lett.,* Vol. 54, pp. 365-367, January 23, 1989.

[13] D. P. Rancour, R. F. Pierret, M. S. Lundstrom and M. R. Melloch, "Application of Isothermal Current Deep Level Transient Spectroscopy to Solar Cells," *J. Appl. Phys.,* Vol. 65, pp.

2173-2176, March 1, 1989.

[14] P. D. DeMoulin and M. S. Lundstrom, "Projections of GaAs Solar Cell Performance Limits Based on 2-D Numerical Simulation," *IEEE Trans. Electron Devices,* Vol. 36, pp. 897-905, May 1989.

[15] H. L. Chuang, M. E. Klausmeier-Brown, M. R. Melloch, and M. S. Lundstrom, "Effective Minority Carrier Hole Confinement of Si-doped, n^+/n GaAs Homojunction Barriers," *J. Appl. Phys.,* Vol. 66, pp. 273-278, July 1989.

[16] M. S. Carpenter, M. R. Melloch, B. A. Cowans, Z. Dardas, and W. N. Delgass, "Investigations of Ammonium Sulfide Surface Treatments on GaAs," *Journal of Vacuum Science and Technology B,* Vol. 7, July-August 1989.

[17] M. S. Lundstrom, M. E. Klausmeier-Brown, and M. R. Melloch, "Effects of Heavy Impurity Doping on AlGaAs/GaAs Bipolar Transistors," *IEEE Trans. Electron Dev.,* Vol. 36, Oct. 1989.

[18] M. R. Melloch, S. P. Tobin, T. B. Stellwag, C. Bajgar, A. Keshavarzi, M. S. Lundstrom, and K. Emery, "High-Efficiency GaAs Solar Cells Grown by Molecular Beam Epitaxy," *Journal of Vacuum Science and Technology B,* Vol. 8, March-April 1990.

[19] S. P. Tobin, S. M. Vernon, C. Bajgar, S. J. Wojtczuk, M. R. Melloch, A. Keshavarzi, T. B. Stellwag, S. Venkatesan, M. S. Lundstrom, and K. A. Emery, "Assessment of MOCVD- and MBE-Grown GaAs for High-Efficiency Solar Cell Applications, submitted to *IEEE Trans. Electron Devices.*

[20] G. B. Lush, T. B. Stellwag, A. Keshavarzi, S. Venkatesan, M. R. Melloch, M. S. Lundstrom and R. F. Pierret, "Correlation of Material Properties and Recombination Losses in $Al_{0.2}Ga_{0.8}As$ Solar Cells," submitted to *Solar Cells,* Lakewood, CO, May 24-26, 1989.

Document Control Page	1. SERI Report No. SERI/TP-211-3904	2. NTIS Accession No. DE90000360	3. Recipient's Accession No.

4. Title and Subtitle
Basic Studies of III-V High Efficiency Cell Components, Annual Subcontract Report

5. Publication Date
July 1990

6.

7. Author(s)
M.S. Lundstrom and M.R. Melloch, Principal Investigators

8. Performing Organization Rept. No.

9. Performing Organization Name and Address
School of Electrical Engineering
Purdue University
West Lafayette, Indiana 47907

10. Project/Task/Work Unit No.

11. Contract (C) or Grant (G) No.
(C) XL-5-05018-1
(G)

12. Sponsoring Organization Name and Address
Solar Energy Research Institute
1617 Cole Boulevard
Golden, Colorado 80401-3393

13. Type of Report & Period Covered
Technical Report

14. 8/15/88 - 8/14/89

15. Supplementary Notes
SERI Technical Monitor: C. Leboeuf, (303) 231-1066

16. Abstract (Limit: 200 words)

This report describes activities during the fourth year of a project to improve the understanding of the generation, recombination, and transport of carriers within III-V homo- and heterostructures. Work in the fourth year concentrated on studying heavy doping effects in p^+-GaAs, assessing the importance of similar effects in n^+-GaAs, and characterizing, controlling, and passivating perimeter recombination currents. Work also began to identify the dominant loss mechanisms in $Al_{0.2}Ga_{0.8}As$ solar cells. A new molecular beam epitaxy growth facility was brought on line, and 23.8%-efficient one-sun solar cells were fabricated.

17. Document Analysis

a. Descriptors Photovoltaic cells ; high efficiency ; semi-conductor materials ; doped materials ; amorphous state

b. Identifiers/Open-Ended Terms

c. UC Categories 271

18. Availability Statement
National Technical Information Service
U.S. Department of Commerce
5285 Port Royal Road
Springfield, Virginia 22161

19. No. of Pages
120

20. Price
A06